



Fugro Airborne Surveys

**LOGISTICS AND PROCESSING REPORT
Airborne Magnetic and MEGATEM[®] Survey**

North Range Blocks 1,2,3 and Airport Property.

Sudbury, Ontario, Canada

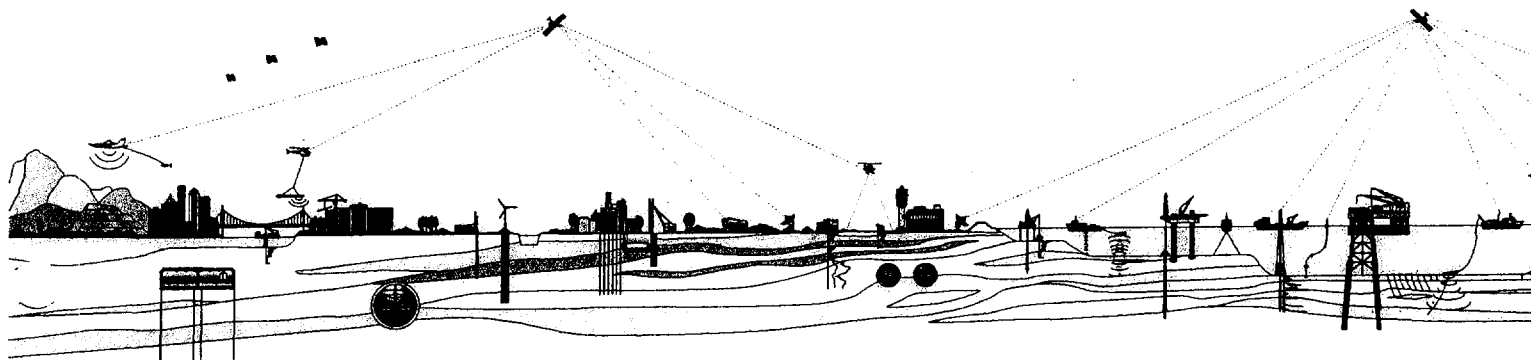
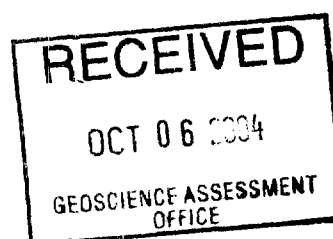
Job No. 04408

Crowflight Minerals Inc.



41I14SE2018 2.28573 HUTTON

010





**LOGISTICS AND PROCESSING REPORT
AIRBORNE MAGNETIC AND MEGATEM[®] SURVEY
NORTH RANGE BLOCKS 1,2,3 AND AIRPORT PROPERTY
ONTARIO, CANADA**

JOB NO. 04408

Client : Crowflight Minerals Inc.
65 Queen Street West, Suite #810
Toronto, Ontario
M5H 2Y2
Canada

Date of Report : June, 2004

SUPPLEMENTAL TABLE OF CONTENTS

Property Access and Supplemental Information	i
Topographic Map	ii
Claim Location Map	1
Claim Map with Flight Lines	2
Fugro Table of Contents	3
INTRODUCTION	5
QUALITY CONTROL AND COMPILATION PROCEDURES	12
DATA PROCESING	13
FINAL PRODUCTS	19
Maps	87
Statements of qualifications	97

Property Access and Supplemental Information

Additional information as required for the submission of assessment work by Crowflight Minerals Inc. for claims 1244500,1244495, 1244496.

- To accompany Fugro Airborne Report. 04408

1244495- Kitchener Twp.

1244496- Hutton Twp.

1244500- Kitchener Twp.

All claims are held by:

John G Brady Client # 111562

1227 Holland Rd.

Sudbury Ont.

P3A 3R1

Access

The property is located about 35 air miles northwest of Sudbury. One takes highway 85 north of Hanmer, then Highway 84 past the town of Capreol, towards the old Moose Mountain Mine. About 4 km west of Milnet and about 3 km west of the Moose Mountain open pit. At 499200 E, an old road heads west toward the Brady property. One then travels this road west for about 5km. to come to the most eastern claim, 1244496.

-The Fugro airborne survey was done between April 15 and May 12, 2004 and the report was written in June 2004.

-A total of 4558 line kilometers of data was collected in the entire survey, at a cost of \$585,200.

-The person who supervised the airborne survey is:

John Buckle

20 Segwun Rd.

Waterdown, Ont.

L0R2H6

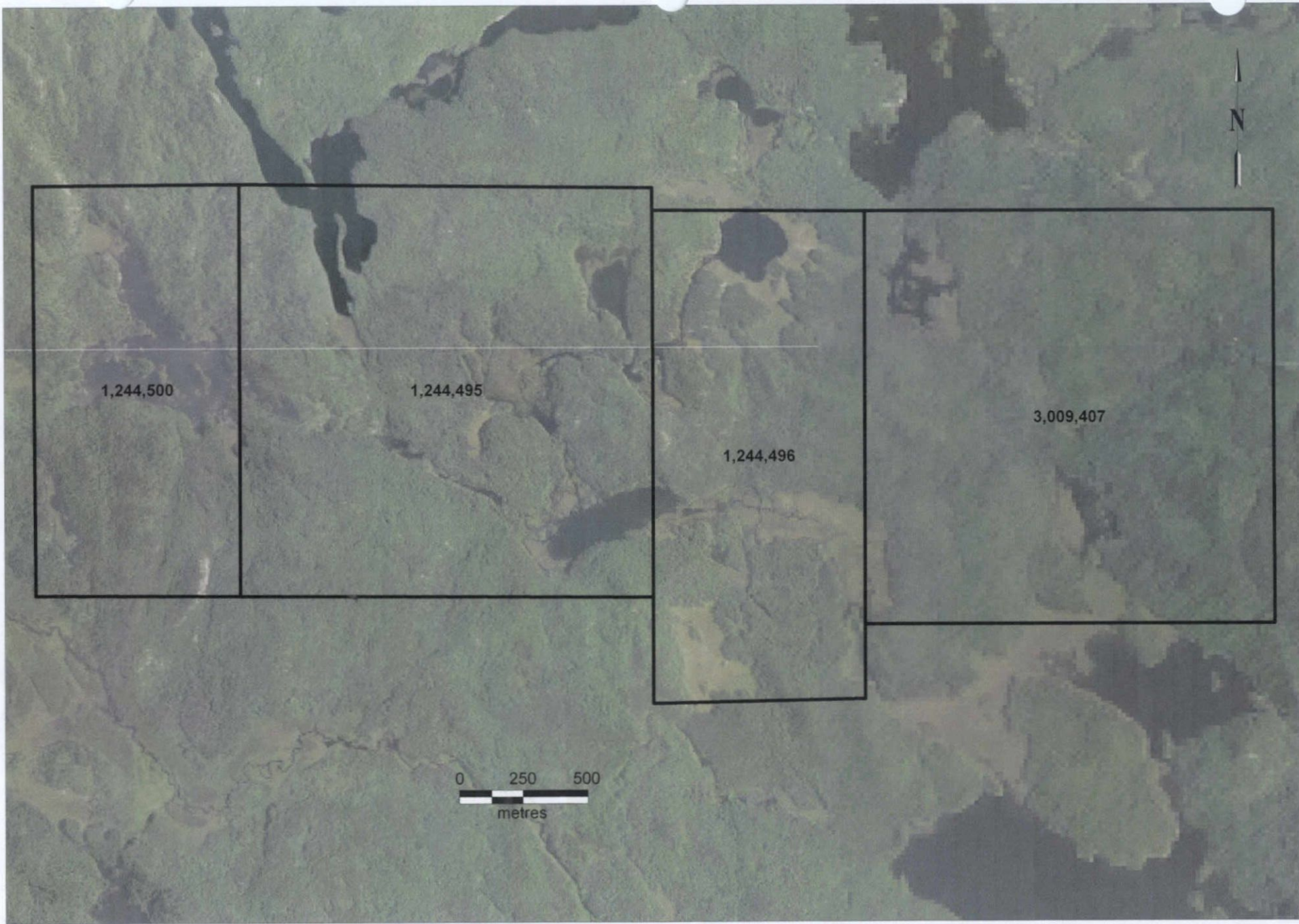
-The author of the Fugro report is:

Darcy Jamieson

He has a B.S.c.E. in geological engineering from Queens University in 2002.

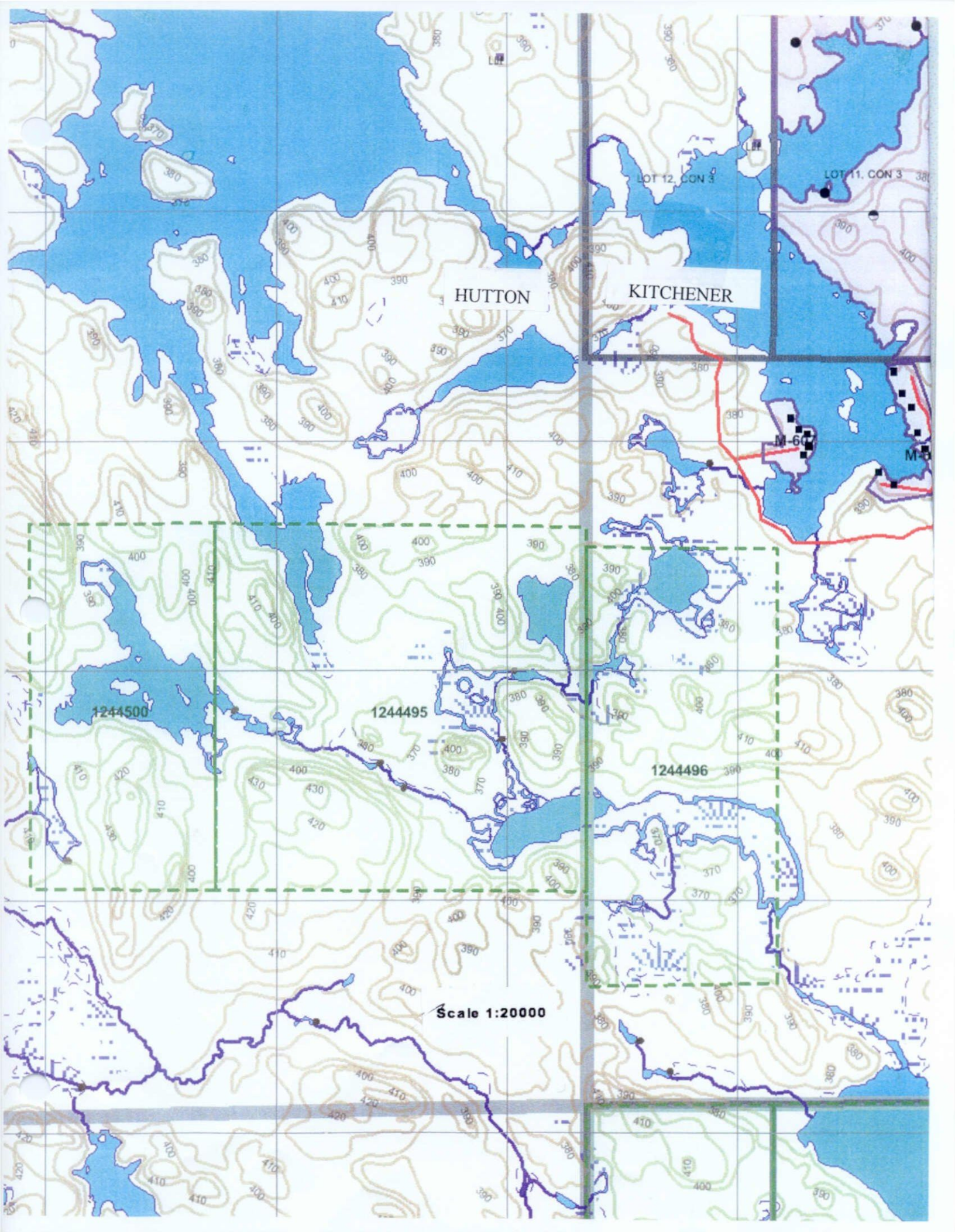
-A summary of previous work performed on the claims in question and on the claims on ground, held by Crowflight is included.

-There were no anomalous values on the property.



**COPENHAGEN BLOCK
TOPOGRAPHIC DETAILS**

Scale 1:20000



HUTTON

KITCHENER

LOT 12, CON 3

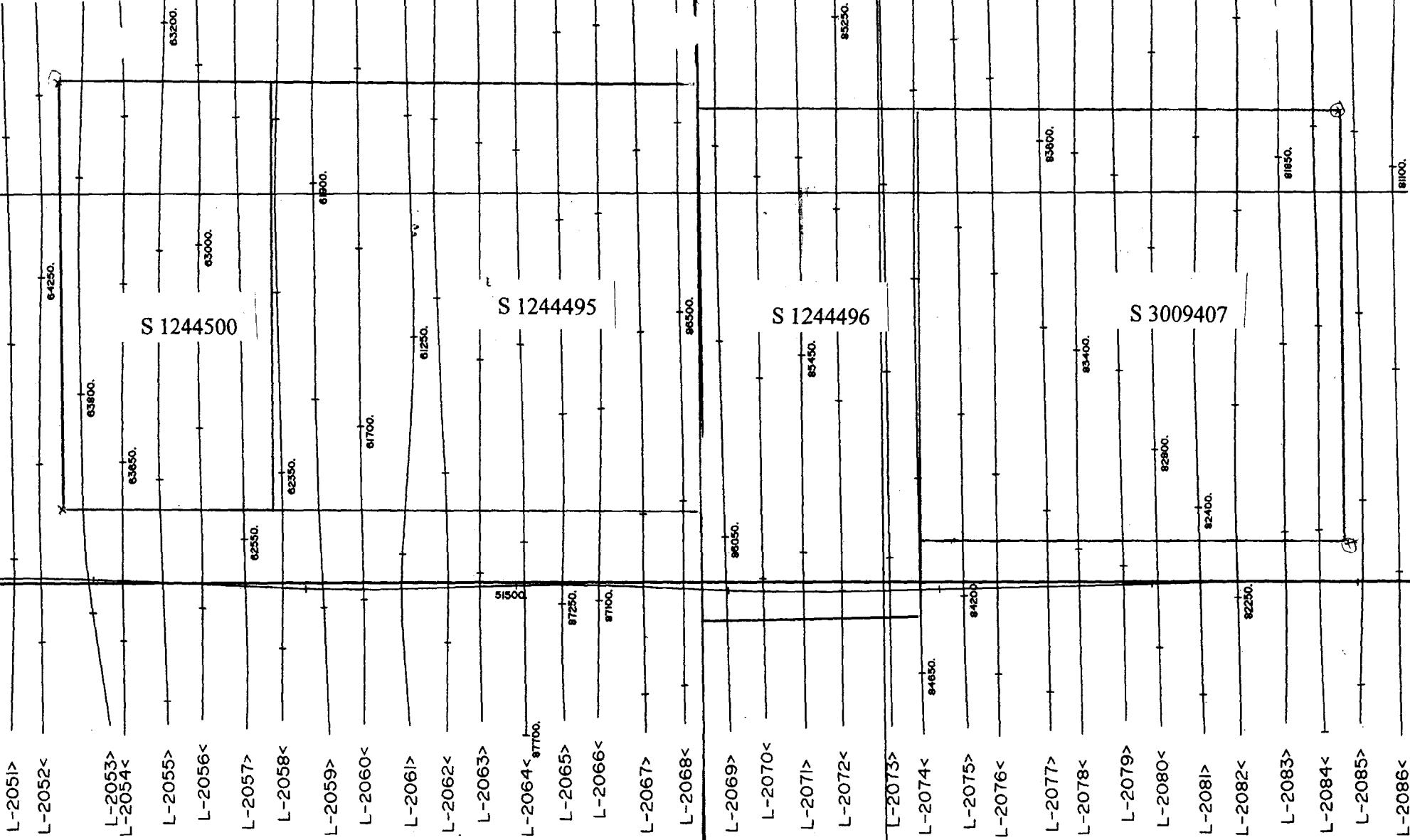
LOT 11, CON 3

1244500

1244495

1244496

Scale 1:20000



S 1244500

S 1244495

S 1244496

S 3009407

- L-2051>
- L-2052<
- L-2053>
- L-2054<
- L-2055>
- L-2056<
- L-2057>
- L-2058<
- L-2059>
- L-2060<
- L-2061>
- L-2062<
- L-2063>
- L-2064<
- L-2065>
- L-2066<
- L-2067>
- L-2068<
- L-2069>
- L-2070<
- L-2071>
- L-2072<
- L-2073>
- L-2074<
- L-2075>
- L-2076<
- L-2077>
- L-2078<
- L-2079>
- L-2080<
- L-2081>
- L-2082<
- L-2083>
- L-2084<
- L-2085>
- L-2086<

HUTTON

KITCHENER

495000E



Scale 1:20000

**COPENHAGEN BLOCK
FLIGHT LINES**

-81°5'



TABLE OF CONTENTS

INTRODUCTION	5
SURVEY OPERATIONS	6
Location of the Survey Area	6
Aircraft and Geophysical On-Board Equipment	7
Base Station Equipment	10
Field Office Equipment	10
Survey Specifications	10
Field Crew	11
Production Statistics	11
QUALITY CONTROL AND COMPILATION PROCEDURES	12
DATA PROCESSING	13
Flight Path Recovery	13
Altitude Data	13
Base Station Diurnal Magnetics	13
Airborne Magnetics	13
<i>Residual Magnetic Intensity</i>	14
<i>Magnetic First Vertical Derivative</i>	14
Electromagnetics	14
<i>dB/dt data</i>	14
<i>B-field data</i>	15
<i>Coil Oscillation Correction</i>	16
<i>Total Energy Envelope</i>	17
<i>Apparent Conductance from 1st Order Moment</i>	17
<i>EM Anomaly selection</i>	17
FINAL PRODUCTS	19
Digital Archives	19
Maps	19
Profile Plots	19
Report	19



APPENDICES

- A GEOTEM[®] ELECTROMAGNETIC SYSTEM**
- B GEOTEM[®] INTERPRETATION**
- C MULTICOMPONENT GEOTEM[®] MODELLING**
- D THE USEFULNESS OF MULTICOMPONENT, TIME-DOMAIN
AIRBORNE ELECTROMAGNETIC MEASUREMENTS**
- E DATA ARCHIVE DESCRIPTION**
- F TDEM ANOMALY SELECTION**
- G MAP PRODUCT GRIDS**

I

Introduction

Between April 15th and May 12th, 2004, Fugro Airborne Surveys conducted a MEGATEM[®] electromagnetic and magnetic survey of the North Range Blocks 1,2,3 and Airport Property on behalf of Crowflight Minerals Inc. Using North Bay, Ontario as the base of operations, a total of 4558.0 line kilometres of data was collected using a Dash 7 modified aircraft (Figure 1).

The survey data were processed and compiled in the Fugro Airborne Surveys Ottawa office. The collected and processed data are presented on colour or black and white maps, and multi-parameter profiles. The following maps were produced: Anomaly Selection with Flight Path, Residual Magnetic Intensity (RMI), First Vertical Derivative, Apparent Conductance and Total Energy Envelope. In addition, digital archives of the raw and processed survey data in line format, and gridded EM data were delivered.



Figure 1: Specially modified Dash-7 aircraft used by Fugro Airborne Surveys.

II

Survey Operations

Location of the Survey Area

The North Range Blocks 1,2,3 and Airport Property (Figure 2) were flown with North Bay, Ontario as the base of operations. A total of 433 traverse lines were flown ranging in length from 6.98 kms to 11.37 kms, with a spacing of 150 m between lines, and 18 tie lines were flown with a spacing of 2500 m to 3500 m between tie-lines totalling 4558 kms in the complete survey.

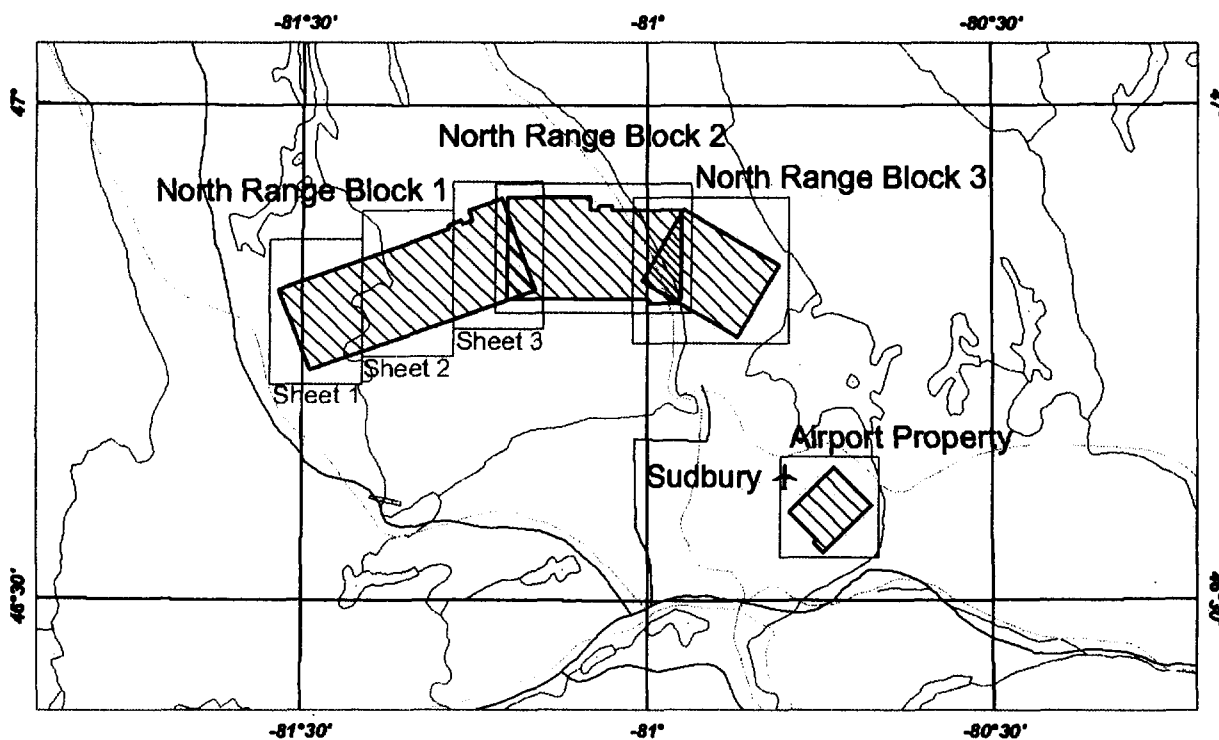


Figure 2: Survey location.

Aircraft and Geophysical On-Board Equipment

Aircraft	DeHavilland Dash-7
Operator	FUGRO AIRBORNE SURVEYS
Registration	C-GJPI
Survey Speed	125 knots / 145 mph / 65 m/s



Figure 3: EM receiver bird.

Magnetometer	Scintrex Cs-2 single cell cesium vapour, towed-bird installation, sensitivity = 0.01 nT^1 , sampling rate = 0.1 s, ambient range 20,000 to 100,000 nT. The general noise envelope was kept below 0.5 nT. The nominal sensor height was ~73 m above ground.
--------------	--

Electromagnetic system	MEGATEM [®] 20 channel Multicoil System
------------------------	--

Transmitter:	Vertical axis loop mounted on aircraft of 406 m^2
--------------	---

Number of turns: 6

Nominal height above ground of 120 m

Receiver :	Multicoil system (x, y and z) with a final recording rate of 4 samples/second, for the recording of 20 channels of x, y and z-coil data. The nominal height above ground is ~70 m, placed ~130 m behind the centre of the transmitter loop.
------------	---

Base frequency:	90 Hz
-----------------	-------

Pulse width:	2330 μs
--------------	--------------------

Pulse delay:	100 μs
--------------	-------------------

Off-time:	3126 μs
-----------	--------------------

Point value:	43.4 μs
--------------	--------------------

Transmitter Current:	605 A
----------------------	-------

Dipole moment:	$1.47 \times 10^6 \text{ Am}^2$
----------------	---------------------------------



Figure 4: Modified Dash-7 in flight.

¹ One nanotesla (nT) is the S.I. equivalent of one gamma.

Table 1: Electromagnetic Data Windows.

Channel	Start (p)	End (p)	Width (p)	Start (ms)	End (ms)	Width (ms)	Mid (ms)
1	4	11	8	0.13	0.477	0.347	0.304
2	12	25	14	0.477	1.085	0.608	0.781
3	26	39	14	1.085	1.693	0.608	1.389
4	40	53	14	1.693	2.3	0.608	1.997
5	54	59	6	2.3	2.561	0.26	2.431
6	60	61	2	2.561	2.648	0.087	2.604
7	62	64	3	2.648	2.778	0.13	2.713
8	65	67	3	2.778	2.908	0.13	2.843
9	68	71	4	2.908	3.082	0.174	2.995
10	72	75	4	3.082	3.255	0.174	3.168
11	76	79	4	3.255	3.429	0.174	3.342
12	80	83	4	3.429	3.602	0.174	3.516
13	84	87	4	3.602	3.776	0.174	3.689
14	88	92	5	3.776	3.993	0.217	3.885
15	93	97	5	3.993	4.21	0.217	4.102
16	98	102	5	4.21	4.427	0.217	4.319
17	103	108	6	4.427	4.688	0.26	4.557
18	109	114	6	4.688	4.948	0.26	4.818
19	115	121	7	4.948	5.252	0.304	5.1
20	122	128	7	5.252	5.556	0.304	5.404

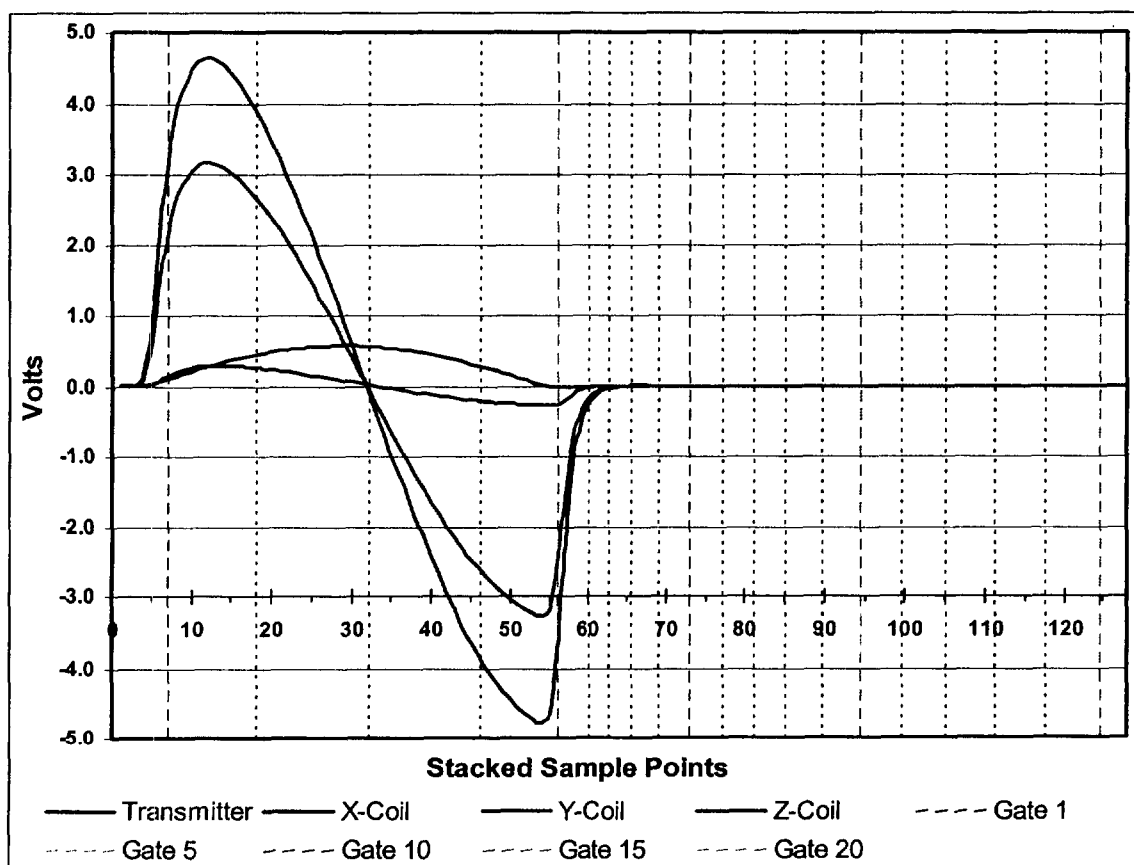


Figure 5: MEGATEM Waveform and response with gate centres showing positions in sample points.



Digital Acquisition FUGRO AIRBORNE SURVEYS GEODAS SYSTEM.

Analogue Recorder RMS GR-33, see below for analogue display and setup.

Barometric Altimeter Rosemount 1241M, sensitivity 1 ft, 1 sec recording interval.

Radar Altimeter King KRA405, accuracy 2%, sensitivity 1 ft, range 0 to 2500 ft, 1 sec recording interval.

Camera Panasonic colour video, super VHS, model WV-CL302.

Electronic Navigation NovAtel Propak 4E-3151-R, 1 sec recording interval, with a resolution of 0.00001 degree and an accuracy of ± 10 m.

Analogue Recorder Display Setup:

Name	Description	Scale	Unit
ZF10	dB/dt Z coil Time Filtered Channel 10	10000	pV/cm
ZF13	dB/dt Z coil Time Filtered Channel 13	10000	pV/cm
ZF18	dB/dt Z coil Time Filtered Channel 18	10000	pV/cm
BZ10	B-Field Z coil Time Filtered Channel 10	10000	pT/cm
BZ13	B-Field Z coil Time Filtered Channel 13	10000	pT/cm
BZ18	B-Field Z coil Time Filtered Channel 18	10000	pT/cm
XF10	dB/dt X coil Time Filtered Channel 10	10000	pV/cm
XF13	dB/dt X coil Time Filtered Channel 13	10000	pV/cm
XF18	dB/dt X coil Time Filtered Channel 18	10000	pV/cm
BX10	B-Field X coil Time Filtered Channel 10	10000	pT/cm
BX13	B-Field X coil Time Filtered Channel 13	10000	pT/cm
BX18	B-Field X coil Time Filtered Channel 18	10000	pT/cm
X20	dB/dt X coil Raw channel 20	20000	pV/cm
Y20	dB/dt Y coil Raw channel 20	20000	pV/cm
Z20	dB/dt X coil Raw channel 20	20000	pV/cm
BX20	B-Field X coil Raw Channel 20	20000	pT/cm
BZ20	B-Field Z coil Raw Channel 20	20000	pT/cm
X01	dB/dt X coil Raw channel 01	40000	pV/cm
XPL	Powerline Monitor	0.2	V/cm
XEFM	Earth Field Monitor	1	V/cm
YPRM	Y Primary Field	133.3	V/cm
TPRM	Transmitter Primary Field	0.02	V/cm
CMAG	Coarse Total Field Magnetic Intensity	1000	nT/cm
FMAG	Fine Total Field Magnetic Intensity	50	nT/cm
4DIF	Magnetic 4th Difference Filtered	1	nT/cm
RADR	Radar Altimeter	50	ft/cm
BARO	Barometric Altimeter	200	ft/cm



Base Station Equipment

Magnetometer:	Scintrex CS-2 single cell cesium vapour, mounted in a magnetically quiet area, measuring the total intensity of the earth's magnetic field in units of 0.01 nT at intervals of 0.5 sec, within a noise envelope of 0.20 nT.
GPS Receiver:	NovAtel, measuring all GPS channels, for up to 12 satellites.
Computer:	Laptop, model Pentium II, 220 MHz.
Converter:	Picodas, model MEP710 3/10901 GTS 780008

Field Office Equipment

Computers:	Dell Inspiron 8000 Pentium III laptop with 30 GB hard drive.
Printer:	Canon bubblejet printer BJC-85.
DVD writer Drive:	Ricoh 5.125 DVD+RW format.
Hard Drive:	8 GB Removable hard drive

Survey Specifications

Traverse Line Direction:	North Range Block 1: 160° - 340° North Range Block 2: 000° - 180° North Range Block 3: 030° - 210° Airport Property: 045° - 225°
Traverse Line Spacing:	150 m
Tie Line direction:	North Range Block 1: 070° - 250° North Range Block 2: 090° - 270° North Range Block 3: 120° - 300° Airport Property: 135° - 315°
Tie Line spacing:	2500 m – 3500 m
Navigation:	Differential GPS. Traverse and tie line spacing was not to deviate from theoretical by 50 m for more than 3 km.
Altitude:	The survey was flown at a mean terrain clearance of 120 m. Altitude was not to exceed 20 m over a distance greater than 3 km.
Magnetic Noise Levels:	The noise envelope on the magnetic data was not to exceed \pm 0.25 nT over a distance greater than 3 km.
EM Noise Levels:	The noise envelope on the raw electromagnetic dB/dt X- and Z-coil channel 20 was not to exceed \pm 3500 pT/s over a distance greater than 3 km as displayed on the raw analogue traces.



Field Crew

Data Processor: D.Jamieson, J.Kesik, D.Murray
Pilots: D.Wiens, A.Kirejew, C.Achtemichuck, M.Williston
Electronics Operator: D.Patzer, A.Proulx
Engineer: S.Dinel, C.Beattie, B.Fisher

Production Statistics

Flying dates: April 15th – May 12th, 2004
Total production: 4558 line kilometres
Number of production flights: 12
Days lost weather: 11

III

Quality Control and Compilation Procedures

In the field after each flight, all analogue records were examined as a preliminary assessment of the noise level of the recorded data. Altimeter deviations from the prescribed flying altitudes were also closely examined as well as the diurnal activity, as recorded on the base station.

All digital data were verified for validity and continuity. The data from the aircraft and base station was transferred to the PC's hard disk. Basic statistics were generated for each parameter recorded, these included: the minimum, maximum, and mean values; the standard deviation; and any null values located. All recorded parameters were edited for spikes or datum shifts, followed by final data verification via an interactive graphics screen with on-screen editing and interpolation routines.

The quality of the GPS navigation was controlled on a daily basis by recovering the flight path of the aircraft. The C3NavG2 correction procedure employs the raw ranges from the base station to create improved models of clock error, atmospheric error, satellite orbit, and selective availability. These models are used to improve the conversion of aircraft raw ranges to aircraft position.

Checking all data for adherence to specifications was carried out in the field by the FUGRO AIRBORNE SURVEYS field geophysicist.

IV

Data Processing

Flight Path Recovery

GPS Recovery:	GPS positions recalculated from the recorded raw range data, and differentially corrected.
Projection:	Universal Transverse Mercator (UTM Zone 17N)
Datum:	NAD 27
Central meridian:	81° West
False Easting:	500000 metres
False Northing:	0 metres
Scale factor:	0.9996

Altitude Data

Noise editing:	Alftrim median filter used to eliminate the highest and lowest values from the statistical distribution of a 5 point sample window for the radar altimeter, GPS elevation, and barometric altimeter.
----------------	--

Base Station Diurnal Magnetics

Noise editing:	Alftrim median filter used to eliminate the two highest and two lowest values from the statistical distribution of a 9 point sample window.
Culture editing:	Polynomial interpolation via a graphic screen editor.
Noise filtering:	Running average filter set to remove wavelengths less than 7 seconds.
Extraction of long wavelength component:	Running average filter to retain wavelengths greater than 57 seconds.

Airborne Magnetics

Lag correction:	3.4 s
Noise editing:	4th difference editing routine set to remove spikes greater than 0.5 nT.
Noise filtering:	Triangular filter set to remove noise events having a wavelength less than 0.9 seconds.
Diurnal subtraction:	The long wavelength component of the diurnal (greater than 57 seconds) was removed from the data with a base value of 56898 nT added back.
IGRF removal date:	2004.3

Residual Magnetic Intensity

The residual magnetic intensity (RMI) is calculated from the total magnetic intensity (TMI), the diurnal, and the regional magnetic field. The TMI is measured in the aircraft, the diurnal is measured from the ground station and the regional magnetic field is calculated from the International Geomagnetic Reference Field (IGRF). The low frequency component of the diurnal is extracted from the filtered ground station data and removed from the TMI. The average of the diurnal is then added back in to obtain the resultant TMI. The regional magnetic field, calculated for the specific survey location and the time of the survey, is removed from the resultant TMI to obtain the RMI. The final step is to Tie line level and microlevel the RMI data.

Magnetic First Vertical Derivative

The first vertical derivative was calculated in the frequency domain from the final grid values to enhance subtleties related to geological structures.

Electromagnetics

dB/dt data

Lag correction: 2.75 s

Data correction: The x, y and z-coil data were processed from the 20 raw channels recorded at 4 samples per second.

The following processing steps were applied to the dB/dt data from all coil sets:

- a) The data from channels 1 to 5 (on-time) and 6 to 20 (off-time) were corrected for drift in flight form (prior to cutting the recorded data back to the correct line limits) by passing a low order polynomial function through the baseline minima along each channel, via a graphic screen display;
- b) The data were edited for residual spheric spikes by examining the decay pattern of each individual EM transient. Bad decays (i.e. not fitting a normal exponential function) were deleted and replaced by interpolation;
- c) Corrections were made in the x- and z-coil data for low frequency, incoherent noise elements (that do not correlate from channel to channel) in the data, by analysing the decay patterns of channels 16 to 20 (OMEGA process).
- d) Noise filtering was done using an adaptive filter technique based on time domain triangular operators. Using a 2nd difference value to identify changes in gradient along each channel, minimal filtering (3 point convolution) is applied over the peaks of the anomalies, ranging in set increments up to a maximum amount of filtering in the resistive background areas (29 points for both the x-coil and the z-coil data).
- e) The filtered data from the x, y and z-coils were then re-sampled to a rate of 5 samples/s and combined into a common file for archiving.

B-field data

- Processing steps:* The processing of the B-Field data stream is very similar to the processing for the regular dB/dt data. The lag adjustment used was the same, followed by:
- 1) Drift adjustments;
 - 2) Spike editing for spheric events;
 - 3) Correction for coherent noise. By nature, the B-Field data will contain a higher degree of coherency of the noise that automatically gets eliminated (or considerably attenuated) in the regular dB/dt, since this is the time derivative of the signal.
 - 4) Final noise filtering with an adaptive filter.

Note: The introduction of the B-Field data stream, as part of the MEGATEM system, provides the explorationist with a more effective tool for exploration in a broader range of geological environments and for a larger class of target priorities.

The advantage of the B-Field data compared with the normal voltage data (dB/dt) are as follows:

1. A broader range of target conductance that the system is sensitive to. (The B-Field is sensitive to bodies with conductance as great as 100,000 Siemens);
2. Enhancement of the slowly decaying response of good conductors;
3. Suppression of rapidly decaying response of less conductive overburden;
4. Reduction in the effect of spherics on the data;
5. An enhanced ability to interpret anomalies due to conductors below thick conductive overburden;
6. Reduced dynamic range of the measured response (easier data processing
7. and display).

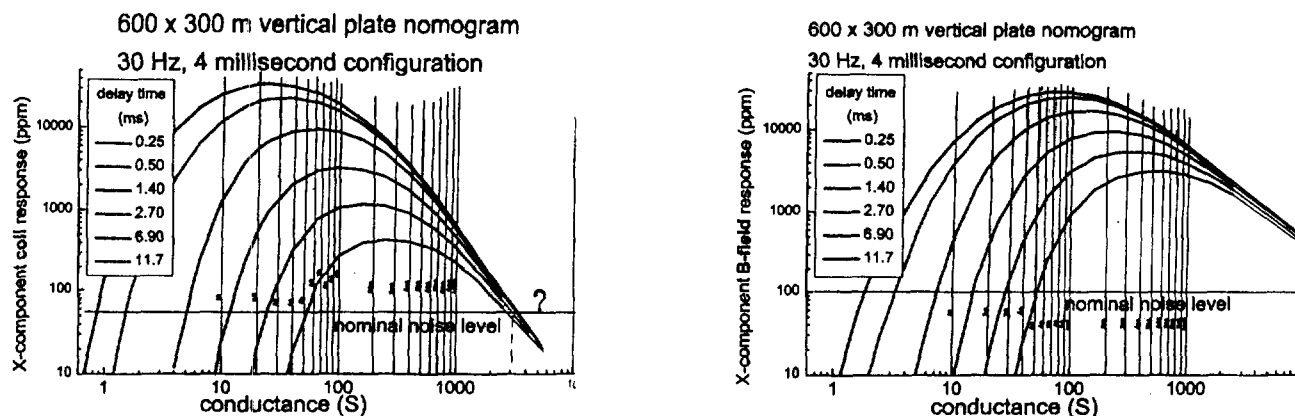


Figure 6: dB-dt vertical plate nomogram (left), B-field vertical plate nomogram (right).

Figure 6 displays the calculated vertical plate response for the MEGATEM[®] signal for the dB/dt and B-Field. For the dB/dt response, you will note that the amplitude of the early channel peaks at about 25 Siemens, and the late channels at about 250 Siemens. As the conductance exceeds 1000 Siemens the response curves quickly roll back into the noise level. For the B-Field response, the early channel amplitude peaks at about 80 Siemens and the late channel at about 550 Siemens. The projected extension of the graph in the direction of increasing conductance, where the response would roll back into the noise level, would be close to 100,000 Siemens. Thus, a strong conductor, having a conductance of several thousand Siemens, would be difficult to interpret on the dB/dt data, since the response would be mixed in with the background noise. However, this strong conductor would stand out clearly on the B-Field data, although it would have an unusual character, being a moderate to high amplitude response, exhibiting almost no decay.

In theory, the response from a super conductor (50,000 to 100,000 Siemens) would be seen on the B-Field data as a low amplitude, non-decaying anomaly, not visible in the off-time channels of the dB/dt stream. Caution must be exercised here, as this signature can also reflect a residual noise event in the B-Field data. In this situation, careful examination of the dB/dt on-time (in-pulse) data is required to resolve the ambiguity. If the feature were strictly a noise event, it would not be present in the dB/dt off-time data stream. This would locate the response at the resistive limit, and the mid in-pulse channel (normally identified as channel 3) would reflect little but background noise, or at best a weak negative peak. If, on the other hand, the feature does indeed reflect a superconductor, then this would locate the response at the inductive limit. In this situation, channel 3 of the dB/dt stream will be a mirror image of the transmitted pulse, i.e. a large negative.

Coil Oscillation Correction

The electromagnetic receiver sensor is housed in a bird, which is towed behind the aircraft using a cable. Any changes in airspeed of the aircraft, variable crosswinds, or other turbulence will result in the bird swinging from side to side. This can result in the induction sensors inside the bird rotating about their mean orientation. The rotation is most marked when the air is particularly turbulent. The changes in orientation result in variable coupling of the induction coils to the primary and secondary fields. For example, if the sensor that is normally aligned to measure the x-axis response pitches upward, it will be measuring a response that will include a mixture of the X and Z component responses. The effect of coil oscillation on the data increases as the signal from the ground

(conductivity) increases and may not be noticeable when flying over areas which are generally resistive. This becomes more of a concern when flying over highly conductive ground.

Using the changes in the coupling of the primary field, it is possible to estimate the pitch, roll and yaw of the receiver sensors. In the estimation process, it is assumed that a smoothed version of the primary field represents the primary field that would be measured when the sensors are in the mean orientation. The orientations are estimated using a non-linear inversion procedure, so erroneous orientations are sometimes obtained. These are reviewed and edited to insure smoothly varying values of orientations. These orientations can then be used to unmix the measured data to generate a response that would be measured if the sensors were in the correct orientation. (For more information on this procedure, see:

http://www.fugroairborne.com/TechnicalPapers/r_atem.shtml).

For the present dataset, the data from all 20 channels of dB/dt and B-Field parameters have been corrected for coil oscillation.

Total Energy Envelope

To combine the benefits of the measurement from both the X and Z coil data and reduce the asymmetry in the signature of the anomalies, the channel data from both the X and Z coils can be used to compute the Total Energy Envelope of the response. This is done through an Hilbert Transform and essentially reflects the square root of the sum of the squares of each component.

For the present dataset, channel 10 of the B-Field component (mid-time position of 738 μ sec after turn-off) was selected as the optimum window along the transient to map the response over features of interest. This channel is sufficiently late in time to avoid minor variations in the signal due to overburden conductivity and altitude effects and yet, not so late in time that the possible weak response over features of interest would get lost in the background.

Apparent Conductance from 1st Order Moment

The n^{th} moment of the impulse response is defined as

$$M^n = \int_0^{\infty} t^n I(t) dt ,$$

where $I(t)$ is the impulse response. These moments can be converted to an estimate of the conductance. The first moment estimate is indicative of the material in the top 50 to 100 m, while higher-order moments are indicative of deeper material. For the present dataset, the 1st Order Moment channel was calculated from the B-Field X Coil data with the corresponding conductance values based on the thin sheet model. The Apparent Conductance values are stored in milliSiemens.

For more details on calculating the conductivity or conductance from moments, see:

<http://www.fugroairborne.com/TechnicalPapers/RealizableMoments.shtml> .

EM Anomaly selection

EM anomalies were selected by fitting the data from the standard dB/dt X-coil channels 9 to 20 to a vertical plate model, in order to extract conductance and depth information. Comparisons of the response from the X and Z coil data were made during the anomaly review for the final selection of the anomalies.



Refer to b1_anom.lst, b2_anom.lst, b3_anom.lst and airport_property_anom.lst for a full listing of the anomaly selections, which provides the particulars of each selected anomaly, including the conductivity-thickness-product (CTP) and the depth of the conductor below surface. It is important to note that the derived values of CTP and depth associated with the anomaly selections are only valid if the geometry of the conductive source can be well approximated by a vertical plate of 300 by 600 m. A note is also included to guide the correct evaluation of the anomaly information.

V

Final Products

Digital Archives

Line and grid data in the form of Geosoft database and grids have been written to CD-ROM as well the Reference Waveform files (PTA's), Geosoft Map files of the final products and a digital copy of the anomaly listings. The formats and layouts of these archives are further described in Appendix E (Data Archive Description). Hardcopies of all maps have been created as outlined below.

Maps

Black & White

Scale: 1:20,000
Parameter: Anomaly Selection and Flight Path Map
Media/Copies: 3 paper prints

Colour

Scale: 1:20,000
Parameters: Residual Magnetic Intensity
First Vertical Derivative of the Residual Magnetic Intensity
Apparent Conductance derived from the 1st Order Moment of B Field X Component
Total Energy Envelope of B Field Channel 10
Media/Copies: 3 paper prints

Profile Plots

Scale: 1:20,000
Parameters: Multi-channel presentation with channels 8-20 of both dB/dt and B-field X- and Z-coil, Residual Magnetic Intensity, First Vertical Derivative of RMI, Radar Altimeter, EM Primary Field, and Hz Monitor.
Media/Copies: 1 Paper of Each Line

Report

Media/Copies: 2 Paper & 1 digital (PDF format)



Appendix A

GEOTEM[®] ELECTROMAGNETIC SYSTEM



GEOTEM® ELECTROMAGNETIC SYSTEM

General

The operation of a towed-bird time-domain electromagnetic system (EM) involves the measurement of decaying secondary electromagnetic fields induced in the ground by a series of short current pulses generated from an aircraft-mounted transmitter. Variations in the decay characteristics of the secondary field (sampled and displayed as windows) are analyzed and interpreted to provide information about the subsurface geology. The response of such a system utilizing a vertical-axis transmitter dipole and a multicomponent receiver coil has been documented by various authors including Smith and Keating (1991, *Geophysics* v.61, p. 74-81).

The principle of sampling the induced secondary field in the absence of the primary field (during the "off-time") and the large separation of the receiver coils from the transmitter combine with the large dipole moment and power available from the fixed wing platform to provide excellent signal-to-noise ratio and depth of penetration. Such a system is also relatively free of noise due to air turbulence. However, also sampling in the "on-time" (Annan et al., 1991, *Geophysics* v.61, p. 93-99) can result in excellent sensitivity for mapping very resistive features and very conductive features, and thus mapping geology.

Through free-air model studies using the University of Toronto's Plate and Layered Earth programs it may be shown that the "depth of investigation" depends upon the geometry of the target. Typical depth limits would be 400 m below surface for a homogeneous half-space, 550 m for a flat-lying inductively thin sheet or 350 m for a large vertical plate conductor. These depth estimates are based on the assumptions that the overlying or surrounding material is resistive.

The method also offers very good discrimination of conductor geometry. This ability to distinguish between flat-lying and vertical conductors combined with excellent depth penetration results in good differentiation of bedrock conductors from surficial conductors.

Methodology

GEOTEM® (GEOterrex Transient ElectroMagnetic system) is a time-domain towed-bird electromagnetic system incorporating a high-speed digital EM receiver. The primary electromagnetic pulses are created by a series of discontinuous sinusoidal current pulses fed into a three- or six-turn transmitting loop surrounding the aircraft and fixed to the nose, tail and wing tips. The base frequency rate is selectable: 25, 30, 75, 90, 125, 150, 225 and 270 Hz. The length of the pulse can be tailored to suit the targets. Standard pulse widths available are 0.6, 1.0, 2.0 and 4.0 ms. The available off-time can be selected to be as great as 16 ms. The current depends on the pulse width but the dipole moment can be as great as $6.7 \times 10^5 \text{ Am}^2$.

The receiver is a three-axis (x,y,z) induction coil which is towed by the aircraft on a 135-metre or 125-metre cable. The tow cable is non-magnetic, to reduce noise levels. The usual mean terrain clearance for the aircraft is 120 m with the EM bird being situated nominally 50 m below and 125 m behind the aircraft (see figure 1).

For each primary pulse a secondary magnetic field is produced by decaying eddy currents in the ground. These in turn induce a voltage in the receiver coils, which is the electromagnetic response.

The measured signals pass through anti-aliasing filters and are then digitized with an A/D converter at sampling rates of up to 80 kHz. The digital data flows from the A/D converter into an industrial-grade computer where the data are processed to reduce the noise.

Operations, which are carried out in the receiver, are:

1. *Primary-field removal:*

In addition to measuring the secondary response from the ground, the receiver sensor coils also measure the primary response from the transmitter. During flight, the bird position and orientation changes slightly, and this has a very strong effect on the magnitude of the total response (primary plus secondary) measured at the receiver coils. The variable primary field response is distracting because it is unrelated to the ground response. The primary field can be measured by flying at an altitude such that no ground response is measurable. These calibration signals are used to define the shape of the primary waveform. By definition this primary field includes the response of the current in the transmitter loop plus the response of any slowly decaying eddy currents induced in the aircraft. We assume that the shape of the primary will be unchanged as the bird position changes, but that the amplitude will vary. The primary field removal procedure involves solving for the amplitude of the primary field in the measured response and removing this from the total response to leave a secondary response. Note that this procedure removes any ("in-phase") response from the ground which has the same shape as the primary field. For more details on the primary-field removal procedure, see <http://www.fugroairborne.com/TechnicalPapers/inphasequad.shtml>

1. *Transient Analysis:* Transient analysis permits the separation of specific types of noise from the signal in real time.
2. *Digital Stacking:* Stacking is carried out to reduce the effect of broadband noise on the data.
3. *Windowing of data:* The GEOTEM[®] digital receiver samples the secondary and primary electromagnetic field at 64, 128 or 384 points per EM pulse and windows the signal in up to 20 time gates whose centres and widths are software selectable and which may be placed anywhere within or outside the transmitter pulse. This flexibility offers the advantage of arranging the gates to suit the goals of a particular survey, ensuring that the signal is appropriately sampled through its entire dynamic range.
4. *Power Line Filtering:* Digital comb filters are applied to the data during real-time processing to remove power line interference while leaving the EM signal undisturbed. The RMS power line voltage (at all harmonics in the receiver passband) are computed, displayed and recorded for each data stack.
5. *Primary Field:* The primary field at the towed sensor is measured for each stack and recorded as a separate data channel to assess the variation in coupling between the aircraft and the towed sensor induced by changes in system geometry.
6. *Earth Field Monitor:* A monitor of sensor coil motion noise induced by coil motion in the Earth's magnetic field is also extracted in the course of the real-time digital processing. This information is also displayed on the real-time chart as well as being recorded for post-survey diagnostic processes.

7. *Noise/Performance:* A monitor computes the RMS signal level on an early off-time channel over a running 10-second window. This monitor provides a measure of noise levels in areas of low ground response. This information is printed at regular intervals on the side of the flight record and is recorded for every data stack.

One of the major roles of the GEOTEM[®] digital receiver is to provide diagnostic information on system functions and to allow for identification of noise events, such as spherics, which may be selectively removed from the EM signal.

GEOTEM[®]'s high digital sampling rate yields maximum resolution of the secondary field. The absence of an analog system time-constant filter results in minimal signal distortion and, therefore, superior representation of the anomaly amplitudes and shapes.

System Hardware

The GEOTEM[®] system is an integrated whole, consisting of the CASA 212 aircraft, the on-board hardware, and the software packages controlling the hardware.

The software packages in the GEODAS data acquisition system and in the GEOTEM[®] receiver were developed in-house. Likewise, certain elements of the hardware (GEOTEM[®] transmitter, system timing clock, towed-bird receiver system) were developed in-house.

Transmitter System

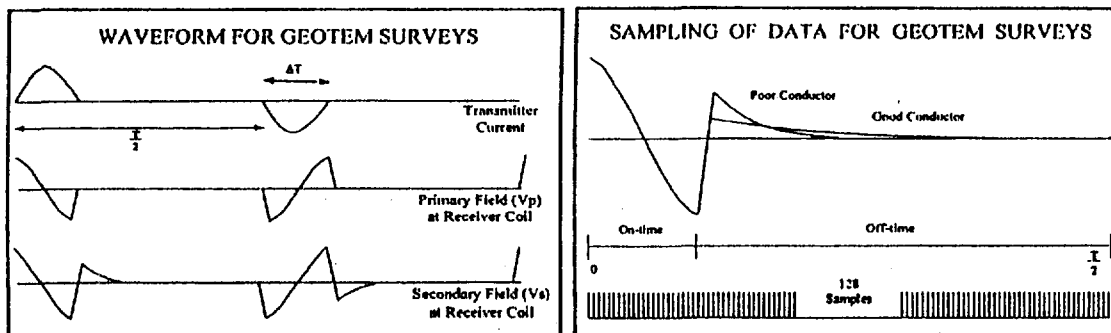
The transmitter system drives high-current pulses of an appropriate shape and duration through the coils mounted on the CASA aircraft.

System Timing Clock

This subsystem provides appropriate timing signals to the transmitter, and also to the analog-to-digital converter, in order to produce output pulses and capture the ground response.

Towed-Bird Receiver System

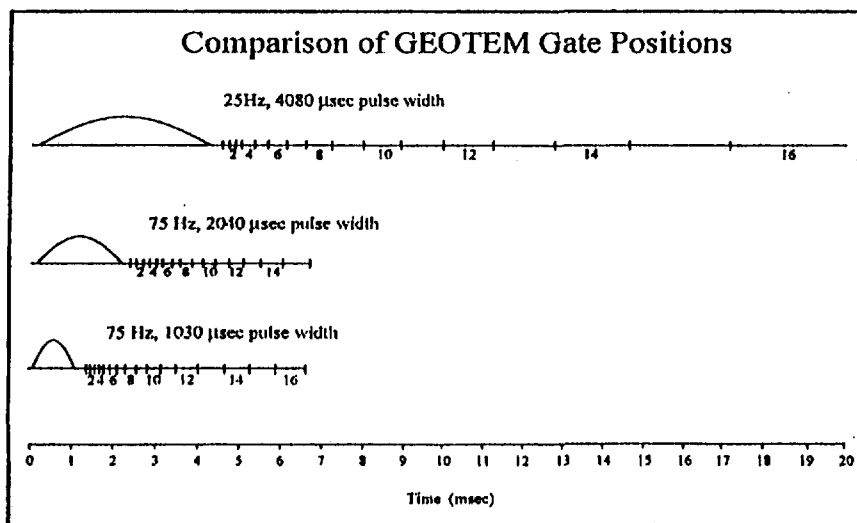
A three-axis induction coil is mounted inside a towed bird, which is typically 50 metres below and 125 metres behind the aircraft. (A second bird, housing the magnetometer sensor, is typically 45 metres below and 80 metres behind the aircraft.)



The GEOTEM system waveform (left frame) and sampling (right frame)

Timing of GEOTEM™ data acquisition for typical configurations

Base Frequency [Hz]	150	90	30	125	75	25
Pulse Width [ms]	1.02	2.04	4.14	1.02	2.04	4.14
Total Halfcycle [ms]	3.33	5.56	16.67	4.00	6.67	20.00
Off-Time [ms]	2.31	3.52	12.53	2.98	4.63	15.86
TX pulses / second	240	144	48	200	120	40
Eff. Digitising Rate [samples/sec]	38,400	23,040	7,680	32,000	19,200	6,400
Pulses per Reading	60	36	12	50	30	10
Stored readings / second	4	4	4	4	4	4
Samples per transient	128	128	128	128	128	128
Number of Channels	20	20	20	20	20	20
- off-time	16	15	15	16	15	16
- in-pulse	4	5	5	4	5	4



Standard GEOTEM gate positions



Appendix B

GEOTEM[®] Interpretation

GEOTEM[®] Interpretation

Introduction

The basis of the transient electromagnetic (EM) geophysical surveying technique relies on the premise that changes in the primary EM field produced in the transmitting loop will result in eddy currents being generated in any conductors in the ground. The eddy currents then decay to produce a secondary EM field which may be sensed as a voltage in the receiver coil.

GEOTEM1 (GEOterrex Transient ElectroMagnetic system) is an airborne transient (or time-domain) towed-bird EM system incorporating a high-speed digital receiver which records the secondary field response with a high degree of accuracy. Most often the total magnetic field is recorded concurrently.

Although the approach to GEOTEM interpretation varies from one survey to another depending on the type of data presentation, objectives and local conditions, the following generalizations may provide the reader with some helpful background information.

The main purpose of the interpretation is to determine the probable origin of the conductors detected during the survey and to suggest recommendations for further exploration. This is possible through an objective analysis of all characteristics of the different types of conductors and associated magnetic anomalies, if any. If possible the airborne results are compared to other available data. A certitude is seldom reached, but a high probability is achieved in identifying the conductive causes in most cases. One of the most difficult problems is usually the differentiation between surface conductors and bedrock conductors.

Types Of Conductors

Bedrock Conductors

The different types of bedrock conductors normally encountered are the following:

1. Graphites. Graphitic horizons (including a large variety of carbonaceous rocks) occur in sedimentary formations of the Precambrian as well as in volcanic tuffs, often concentrated in shear zones. They correspond generally to long, multiple conductors lying in parallel bands. They have no magnetic expression unless associated with pyrrhotite or magnetite. Their conductivity is variable but generally high.
2. Massive sulphides. Massive sulphide deposits usually manifest themselves as short conductors of high conductivity, often with a coincident magnetic anomaly. Some massive sulphides, however, are not magnetic, others are not very conductive (discontinuous mineralization), and some may be located among formational conductors so that one must not be too rigid in applying the selection criteria.

In addition, there are syngenetic sulphides whose conductive pattern may be similar to that of graphitic horizons but these are generally not as prevalent as graphites.

1 GEOTEM[®]: Registered Trade Mark of Fugro Airborne Surveys Corporation.

3. Magnetite and some serpentinized ultrabasics. These rocks are conductive and very magnetic.
4. Manganese oxides. This mineralization may give rise to a weak EM response.

Surficial Conductors

1. Beds of clay and alluvium, some swamps, and brackish ground water are usually poorly conductive to moderately conductive.
2. Lateritic formations, residual soils and the weathered layer of the bedrock may cause surface anomalous zones, the conductivity of which is generally low to medium but can occasionally be high. Their presence is often related to the underlying bedrock.

Cultural Conductors (Man-Made)

3. Power lines. These frequently, but not always, produce a conductive type of response on the GEOTEM record. In the case of direct radiation of its field, a power line is easily recognized by a GEOTEM anomaly which exhibits phase changes between different channels. In the case of a grounded wire, or steel pylon, the anomaly may look very much like a bedrock conductor.
4. Grounded fences or pipelines. These will invariably produce responses much like a bedrock conductor. Whenever they cannot be identified positively, a ground check is recommended.
5. General culture. Other localized sources such as certain buildings, bridges, irrigation systems, tailings ponds etc., may produce GEOTEM anomalies. Their instances, however, are rare and often they can be identified on the visual path recovery system.

Analysis Of The Conductors

The apparent conductivity alone is not generally a decisive criterion in the analysis of a conductor. In particular, one should note:

its shape and size,
all local variations of characteristics within a conductive zone,
any associated geophysical parameter (e.g. magnetics),
the geological environment,
the structural context, and
the pattern of surrounding conductors.

The first objective of the interpretation is to classify each conductive zone according to one of the three categories which best defines its probable origin. The categories are cultural, surficial and bedrock. A second objective is to assign to each zone a priority rating as to its potential as an economic prospect.

Bedrock Conductors

This category comprises those anomalies which cannot be classified according to the criteria established for cultural and surficial responses. It is difficult to assign a universal set of values which typify bedrock conductivity because any individual zone or anomaly might exhibit some, but not all, of these values and still be a bedrock conductor. The following criteria are considered indicative of a bedrock conductor:

An intermediate to high conductivity identified by a response with slow decay, with deflections most often present in the later channels.

The anomaly should be narrow, relatively symmetrical, with a well-defined peak.

There should be no serious displacement of anomaly position or change in anomaly shape (other than mirror image) with respect to flight direction, except in the case of non-vertical dipping bodies. The alternating character of the response as a result of line direction can be diagnostic of conductor geometry. Figures 2 to 6 illustrate anomalies associated with different target models.

A small to intermediate amplitude. Large amplitudes are normally associated with surficial conductors. The amplitude varies according to the depth of the source.

A degree of continuity of the EM characteristics across several lines.

An associated magnetic response of similar dimensions. One should note, however, that those rocks which weather to produce a conductive upper layer will possess this magnetic association. In the absence of one or more of the characteristics defined in 1, 2, 3 and 4, the related magnetic response cannot be considered significant.

Most obvious bedrock conductors occur in long, relatively monotonous, sometimes multiple zones following formational strike. Graphitic material is usually the most probable source. Massive syngenetic sulphides extending for many kilometres are known in nature but, in general, they are not

common. Long formational structures associated with a strong magnetic expression may be indicative of banded iron formations.

A bedrock conductor reflecting the presence of a massive sulphide would normally exhibit the following characteristics:

- a high conductivity,
- a good anomaly shape (narrow and well-defined peak),
- a small to intermediate amplitude,
- an isolated setting,
- a short strike length (in general, not exceeding one kilometre), and
- preferably, with a localized magnetic anomaly of matching dimensions.

Surficial Conductors

This term is used for geological conductors in the overburden, either glacial or residual in origin, and in the weathered layer of the bedrock. Most surficial conductors are probably caused by clay minerals. In some environments the presence of salts will contribute to the conductivity. Other possible electrolytic conductors are residual soils, swamps, brackish ground water and alluvium such as lake or river-bottom deposits, flood plains and estuaries.

Normally, most surficial materials have low to intermediate conductivity so they are not easily mistaken for highly conductive bedrock features. Also, many of them are wide and their anomaly shapes are typical of broad horizontal sheets.

When surficial conductivity is high it is usually still possible to distinguish between a horizontal plate (more likely to be surficial material) and a vertical body (more likely to be a bedrock source) thanks to the asymmetry of the GEOTEM responses observed at the edges of a broad conductor when flying adjacent lines in opposite directions. The configuration of the system is such that the response recorded at the leading edge is more pronounced than that registered at the trailing edge. Figure 1 illustrates the "edge effect" and the resulting conductive pattern in plan view. In practice there are many variations on this very diagnostic phenomenon.

One of the more ambiguous situations as to the true source of the response is when surface conductivity is related to bedrock lithology as for example, surface alteration of an underlying bedrock unit. At times, it is also difficult to distinguish between a weak conductor within the bedrock (e.g. near-massive sulphides) and a surficial source.

In the search for massive sulphides or other bedrock targets, surficial conductivity is generally considered as interference but there are situations where the interpretation of surficial-type conductors is the primary goal. When soils, weathered or altered products are conductive, and in-situ, the GEOTEM responses are a very useful aid to geologic mapping. Shears and faults are often identified by weak, usually narrow, anomalies.

Analysis of surficial conductivity can be used in the exploration for such features as lignite deposits, kimberlites, paleochannels and ground water. In coastal or arid areas, surficial responses may serve to define the limits of fresh, brackish and salty water.

Cultural Conductors

The majority of cultural anomalies occur along roads and are accompanied by a response on the

power line monitor. (This monitor is set to 50 or 60 Hz, depending on the local power grid.) Power lines are the most common source of the anomalies and many are recognized immediately by virtue of phase reversals or an abnormal rate of decay. A certain number yield normal GEOTEM anomalies which could be mistaken for bedrock responses. There are also some power lines which have no GEOTEM response whatsoever.

The power line monitor, of course, is of great assistance in identifying cultural anomalies of this type. It is important to note, however, that geological conductors in the vicinity of power lines may exhibit a weak response on the monitor because of current induction via the earth.

Fences, pipelines, communication lines, railways and other man-made conductors can give rise to GEOTEM responses, the strength of which will depend on the grounding of these objects.

Another facet of this analysis is the line-to-line comparison of anomaly character along suspected man-made conductors. In general, the amplitude, the rate of decay, and the anomaly width should not vary a great deal along any one conductor, except for the change in amplitude related to terrain clearance variation. A marked departure from the average response character along any given feature gives rise to the possibility of a second conductor.

In most cases a visual examination of the site will suffice to verify the presence of a man-made conductor. If a second conductor is suspected the ground check is more difficult to accomplish. The object would be to determine if there is (i) a change in the man-made construction, (ii) a difference in the grounding conditions, (iii) a second cultural source, or (iv) if there is, indeed, a geological conductor in addition to the known man-made source.

The selection of targets from within extensive (formational) belts is much more difficult than in the case of isolated conductors. Local variations in the EM characteristics, such as in the amplitude, decay, shape etc., can be used as evidence for a relatively localized occurrence. Changes in the character of the EM responses, however, may be simply reflecting differences in the conductive formations themselves rather than indicating the presence of massive sulphides and, for this reason, the degree of confidence is reduced.

Another useful guide for identifying localized variations within formational conductors is to examine the magnetic data compiled as isomagnetic contours. Further study of the magnetic data can reveal the presence of faults, contacts, and other features which, in turn, help define areas of potential economic interest.

Finally, once ground investigations begin, it must be remembered that the continual comparison of ground knowledge to the airborne information is an essential step in maximizing the usefulness of the GEOTEM data.

EDGE EFFECT

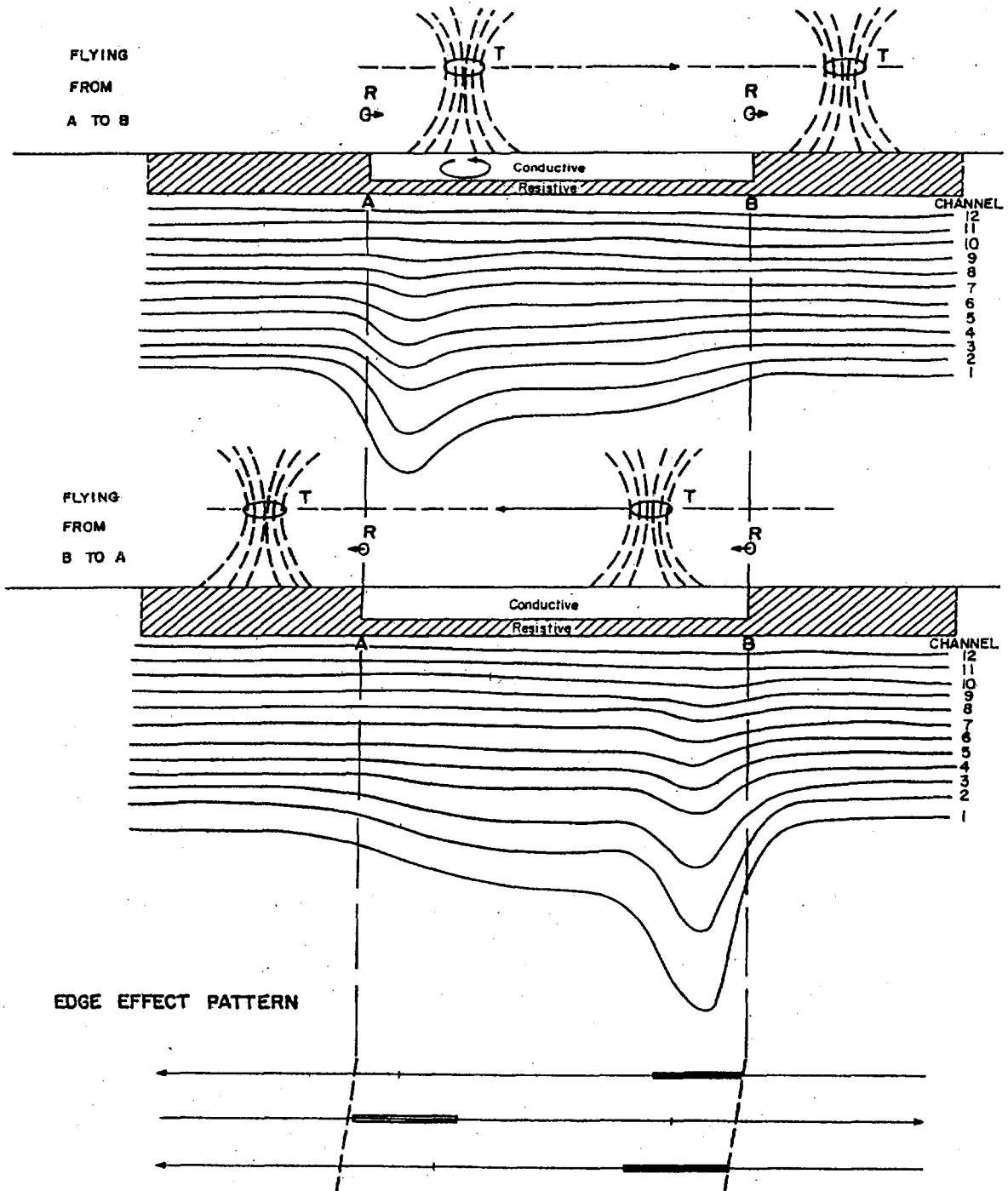


FIGURE 1

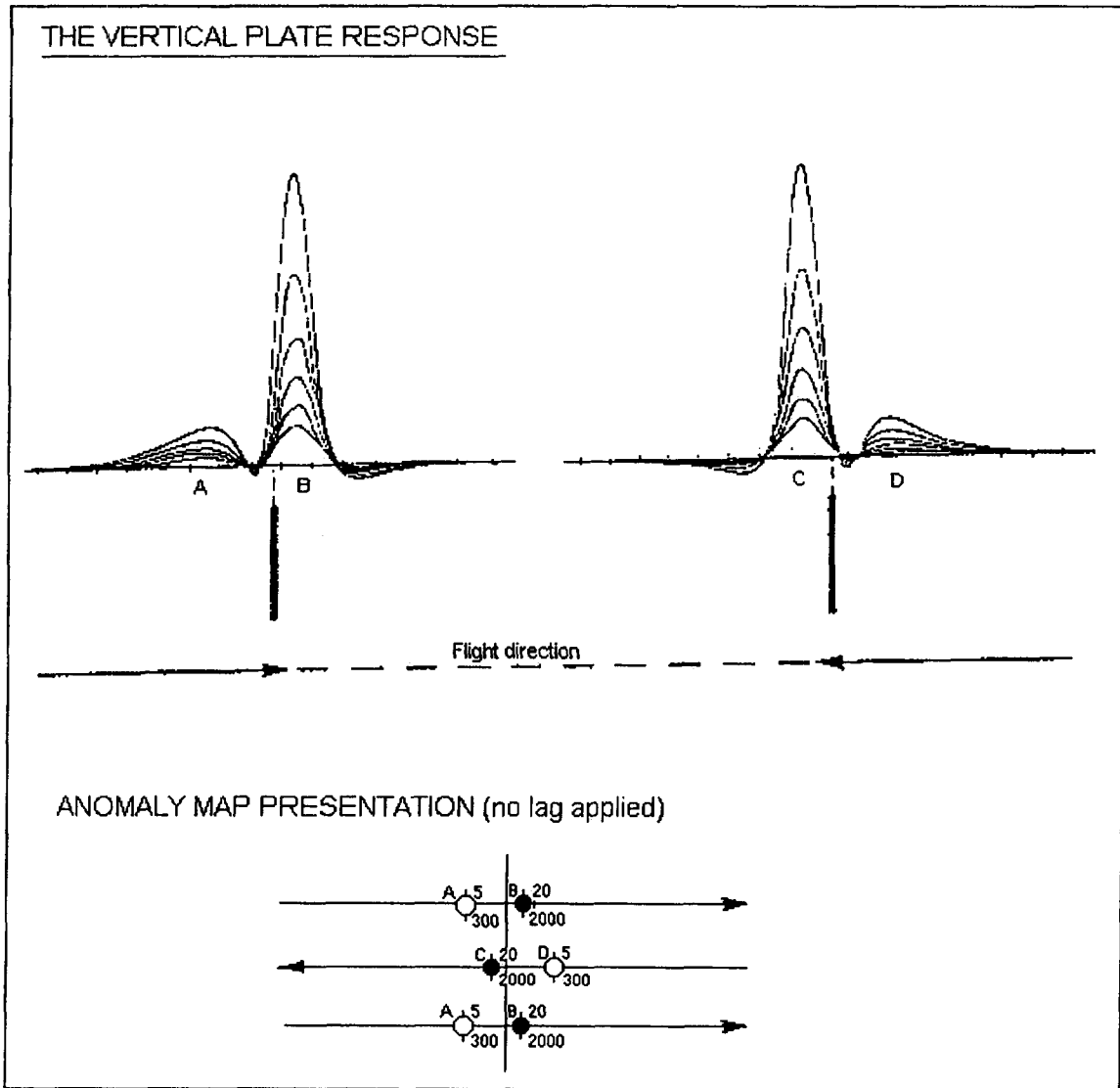


Figure 2

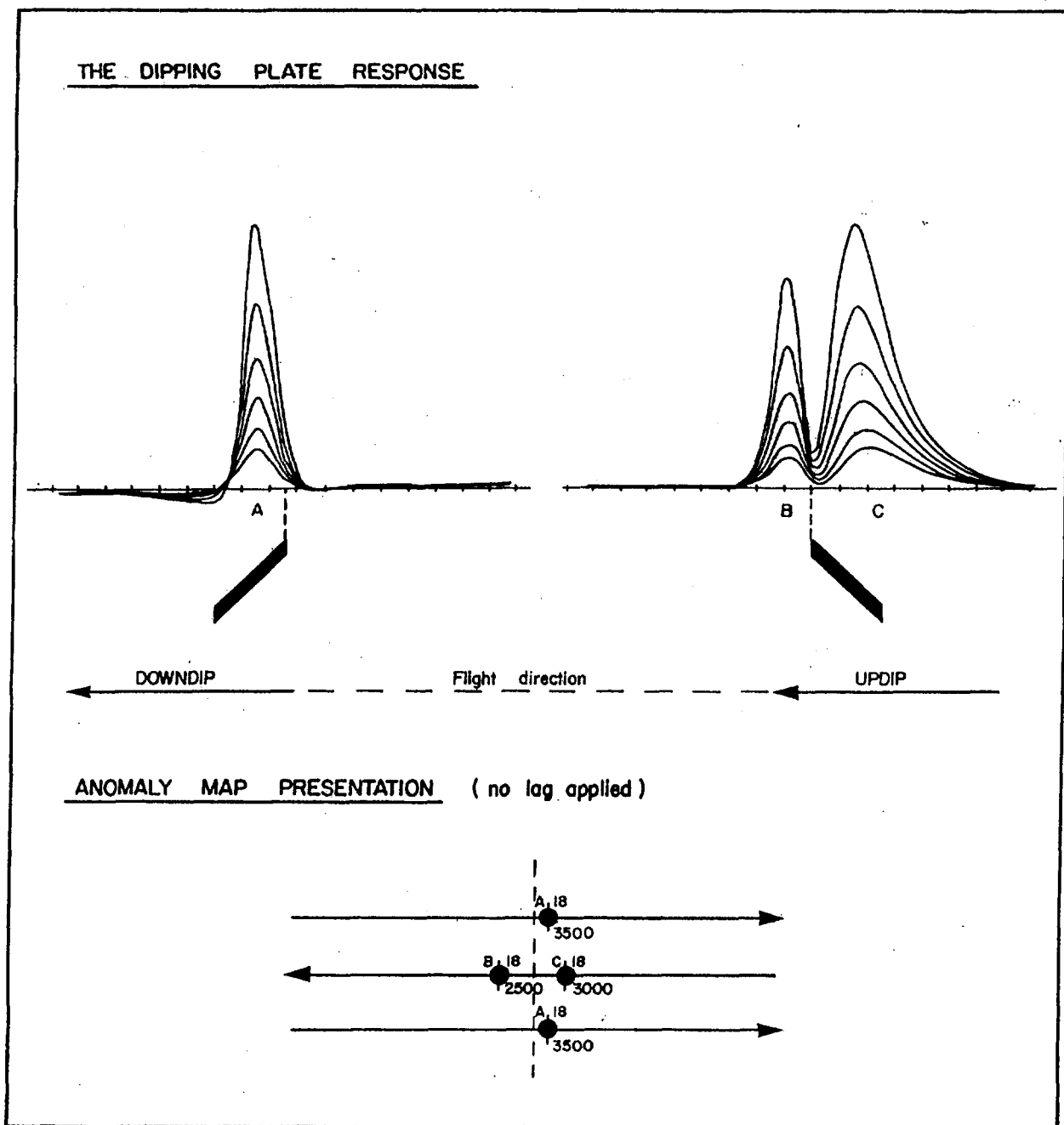


Figure 3

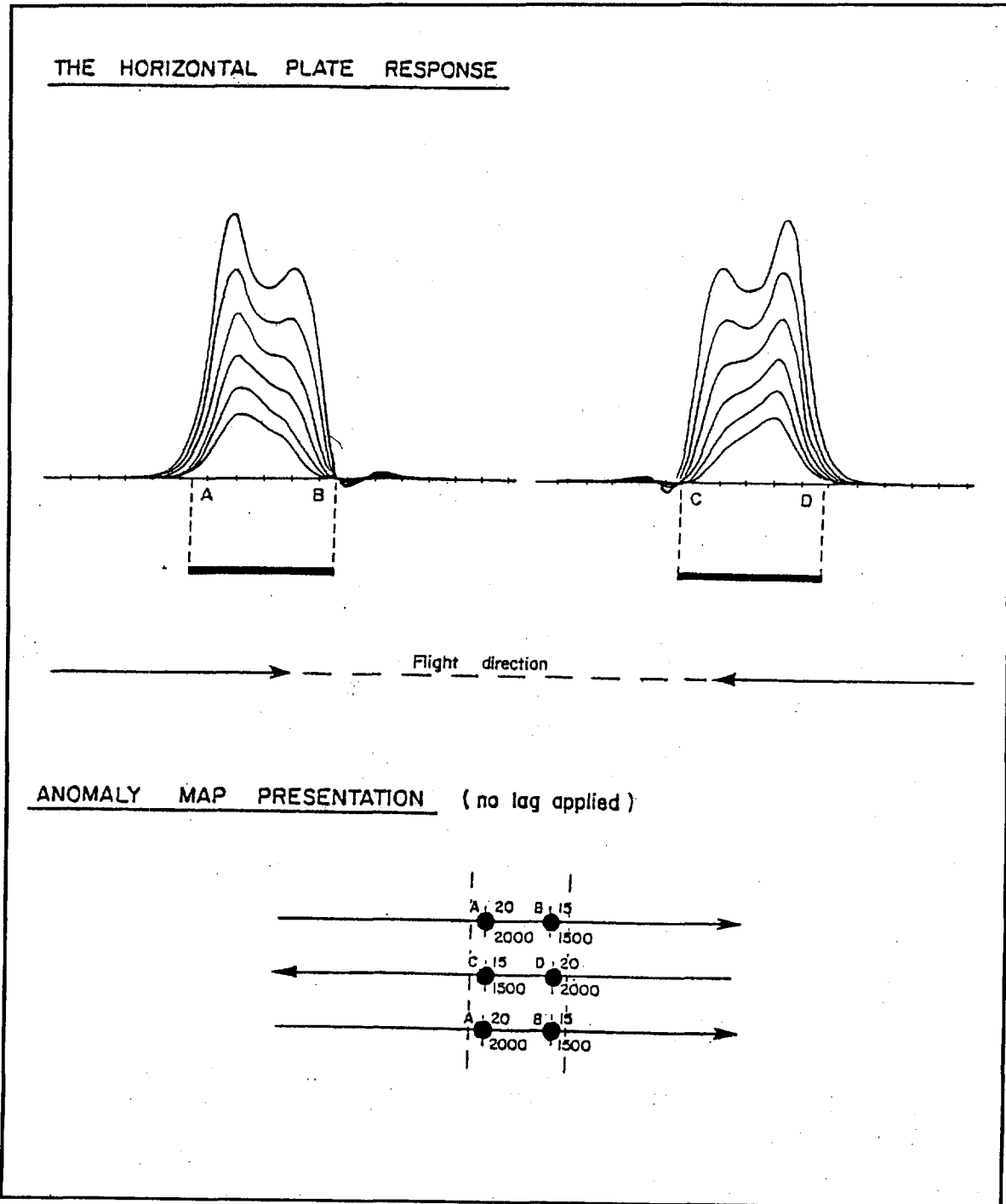
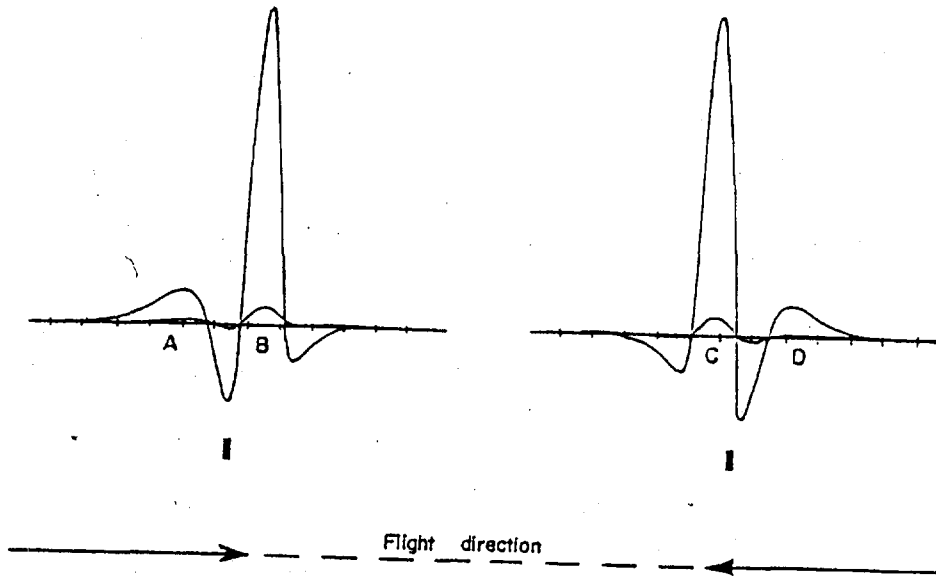


Figure 4

THE VERTICAL RIBBON RESPONSE



ANOMALY MAP PRESENTATION (no lag applied)

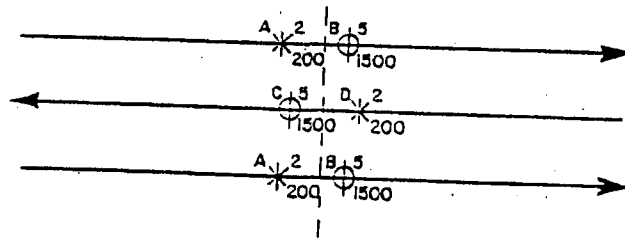


Figure 5

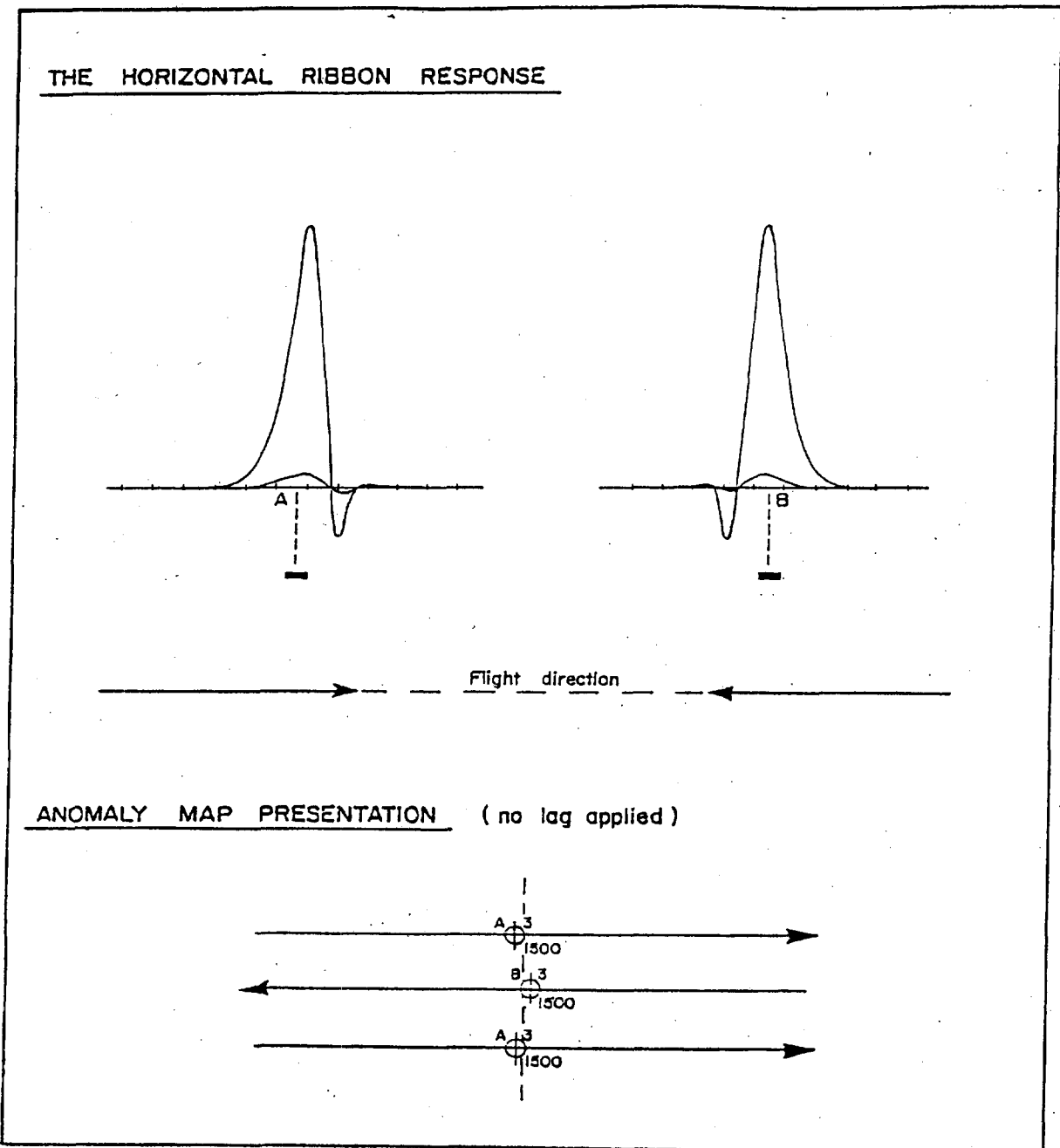


Figure 6



Appendix C

Multicomponent GEOTEM[®] modelling

Multicomponent GEOTEM[®] modelling

Introduction

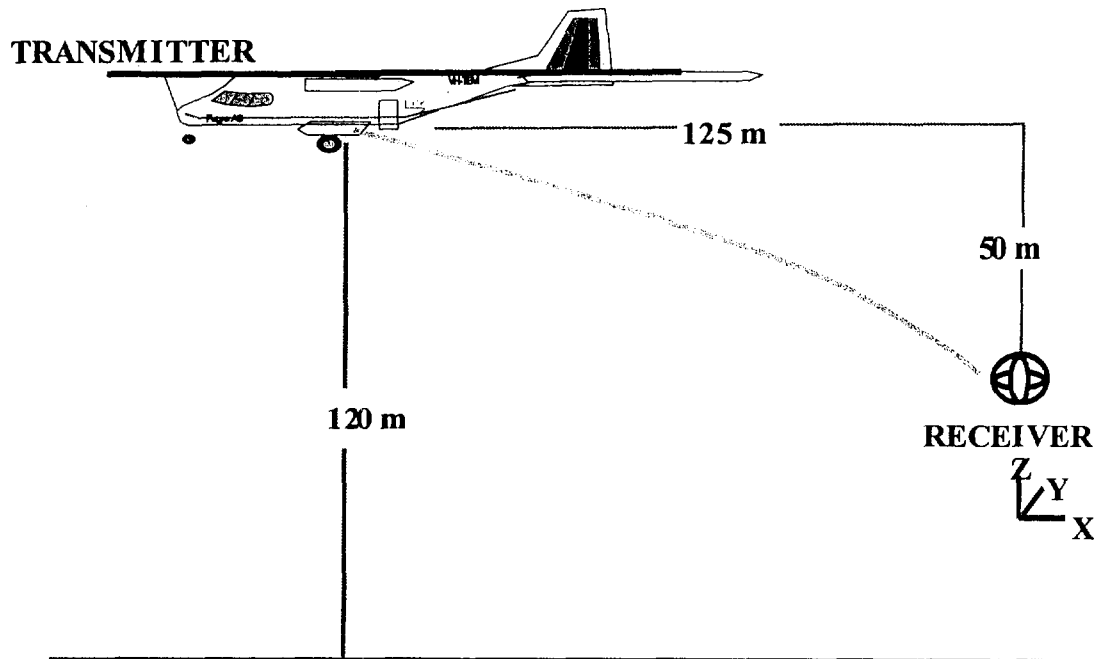
The PLATE program has been used to generate synthetic responses over a number of plate models with varying depth of burial (0, 150 and 300m) and dips (0, 45, 90 and 135 degrees). The geometry assumed for the GEOTEM system is shown on the following page, and the transmitter waveform on the subsequent page. For simplicity, only six receiver gates have been calculated and plotted.

In all cases the plate has a strike length of 600 m with a strike direction into the page. The width of the plate is 300 m. As the flight path traverses the centre of the plate, the y component is zero and has not been plotted.

The conductance of the plate is 20 S. In cases when the conductance is different, an indication of how the amplitudes may vary can be obtained from the nomogram included.

In the following plots all components are normalized to the total primary field.

Nominal GEOTEM geometry



Transmitter waveform and receiver sampling (90 Hz)

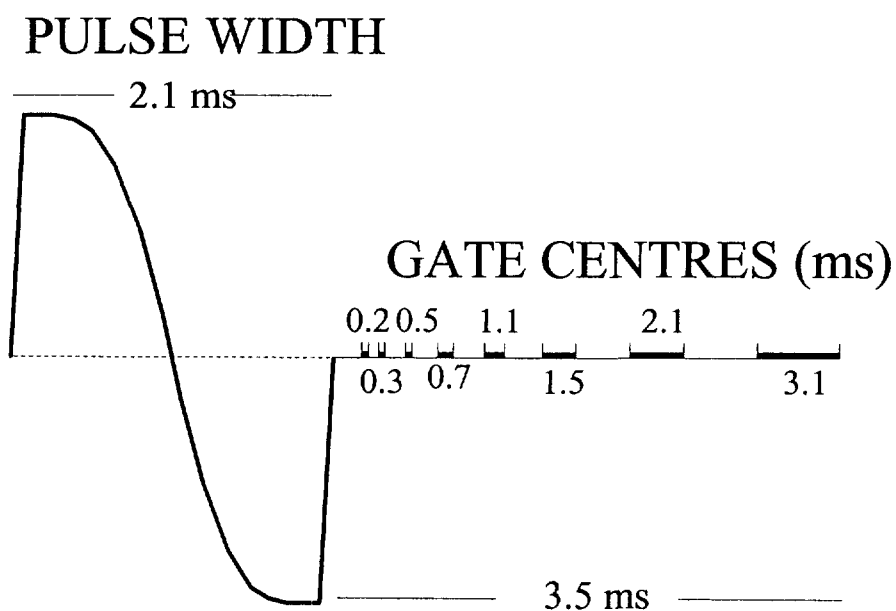


Plate: depth = 0; dip = 0

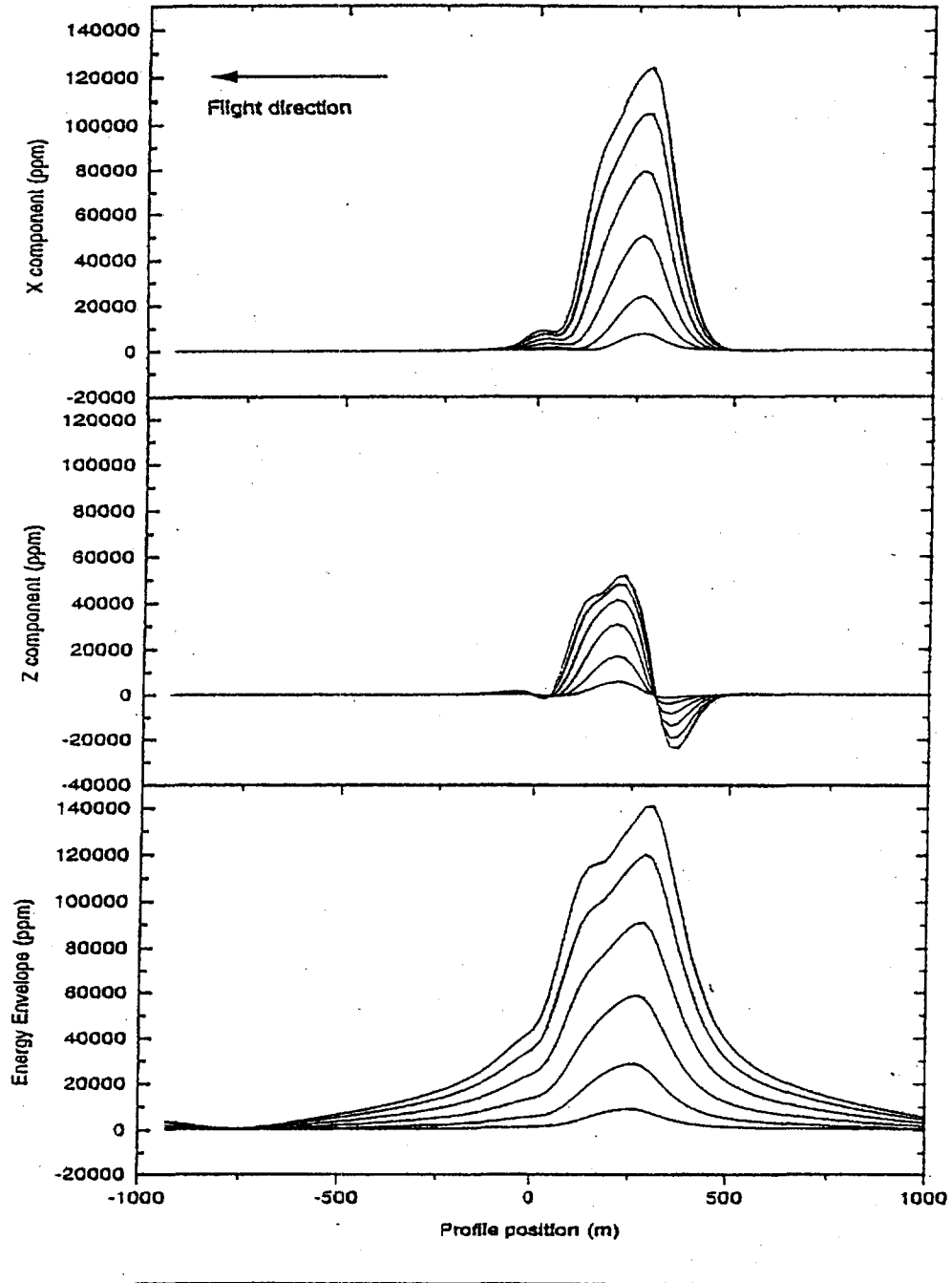


Plate: depth =0; dip =45

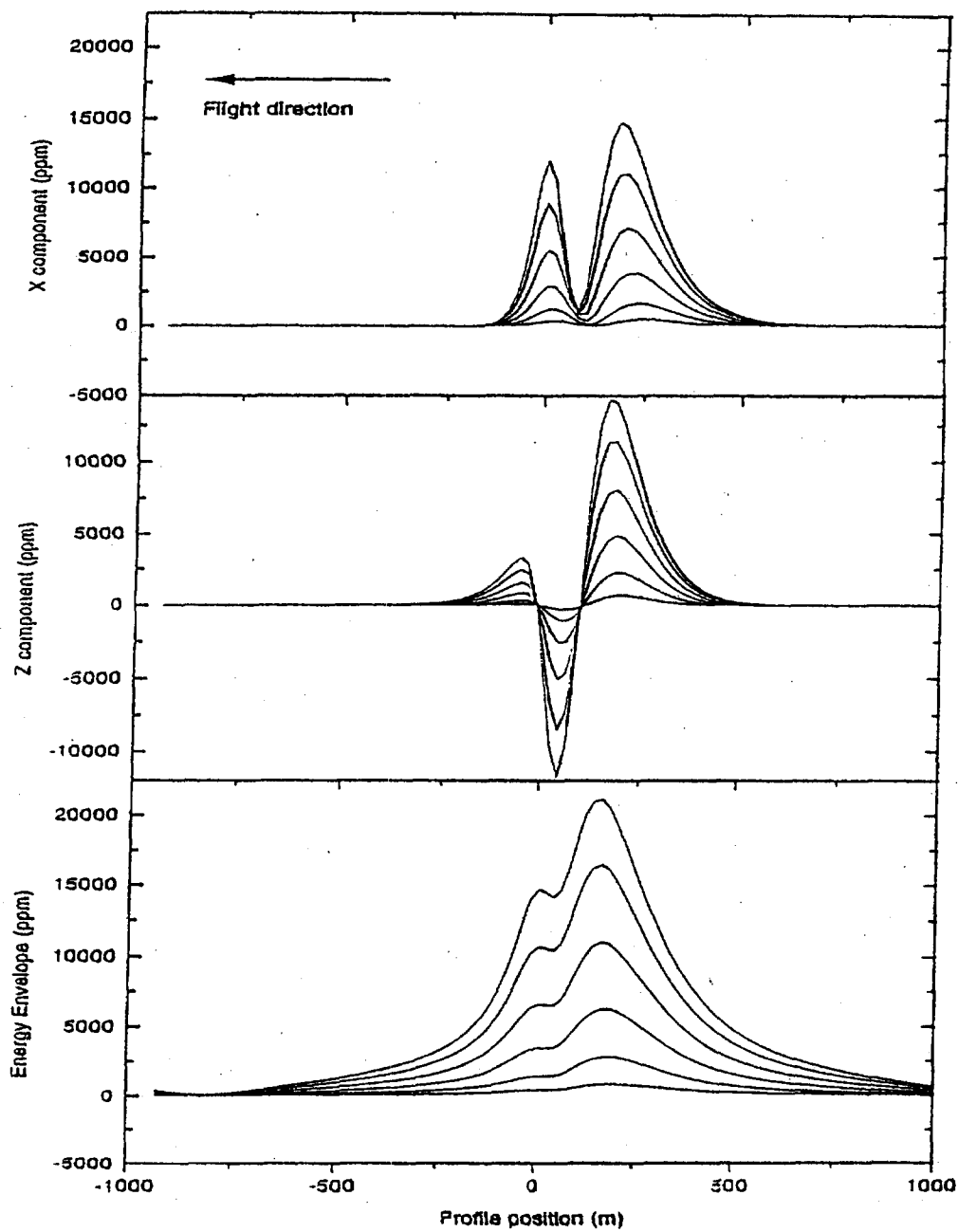


Plate: depth = 0; dip = 90

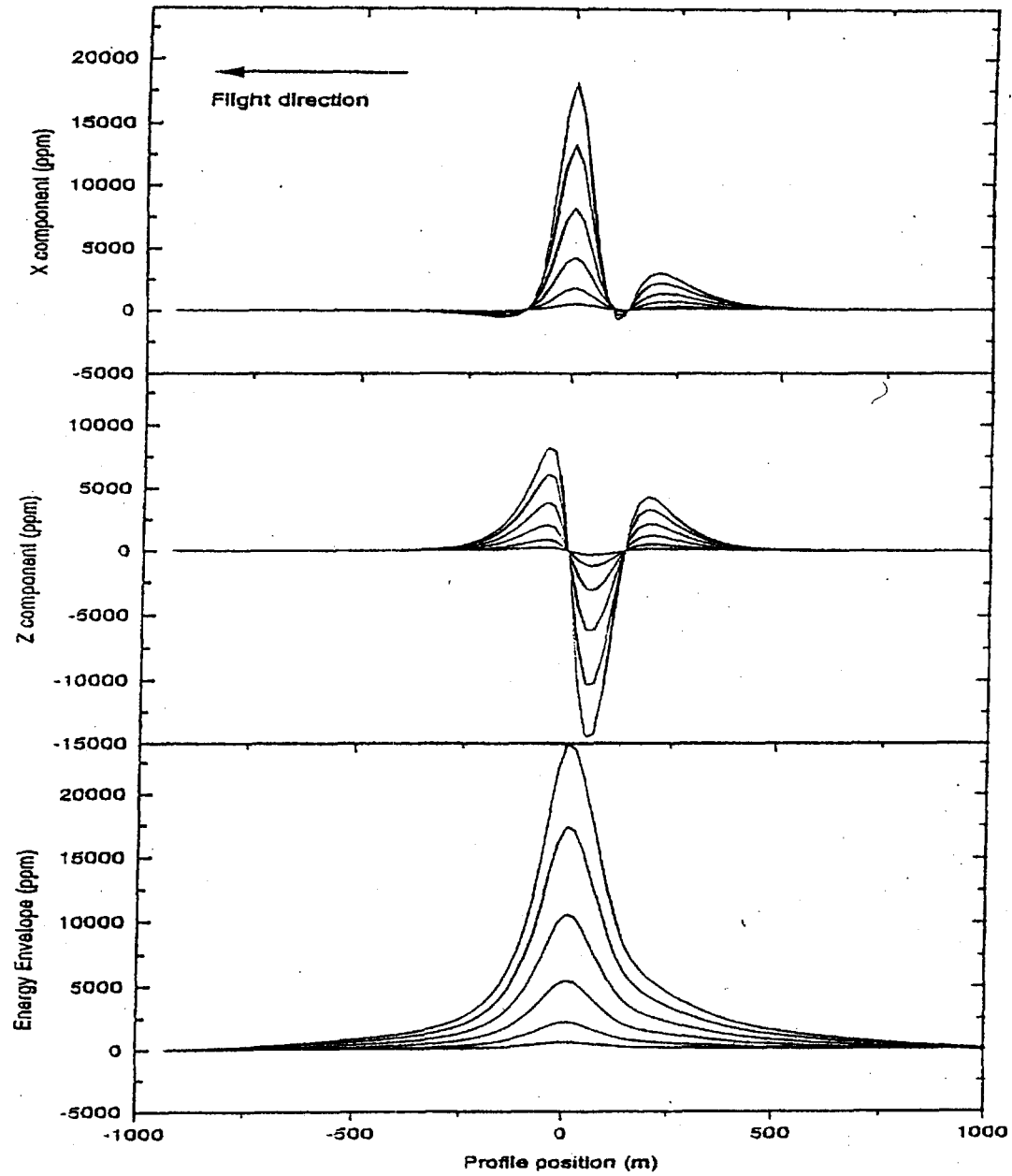


Plate: depth = 0; dip = 135

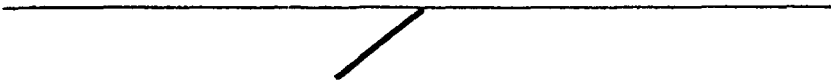
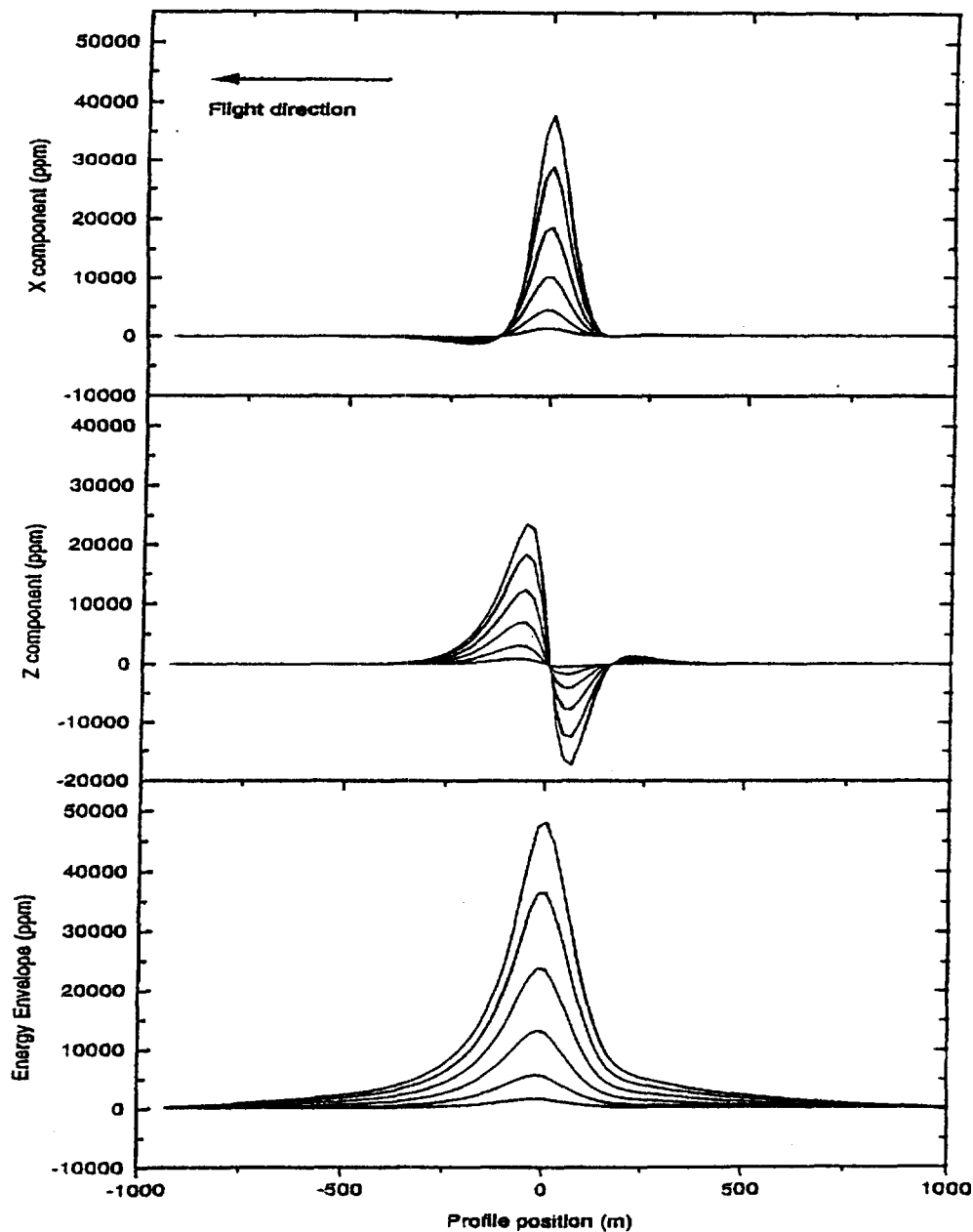


Plate: depth = 150; dip = 0

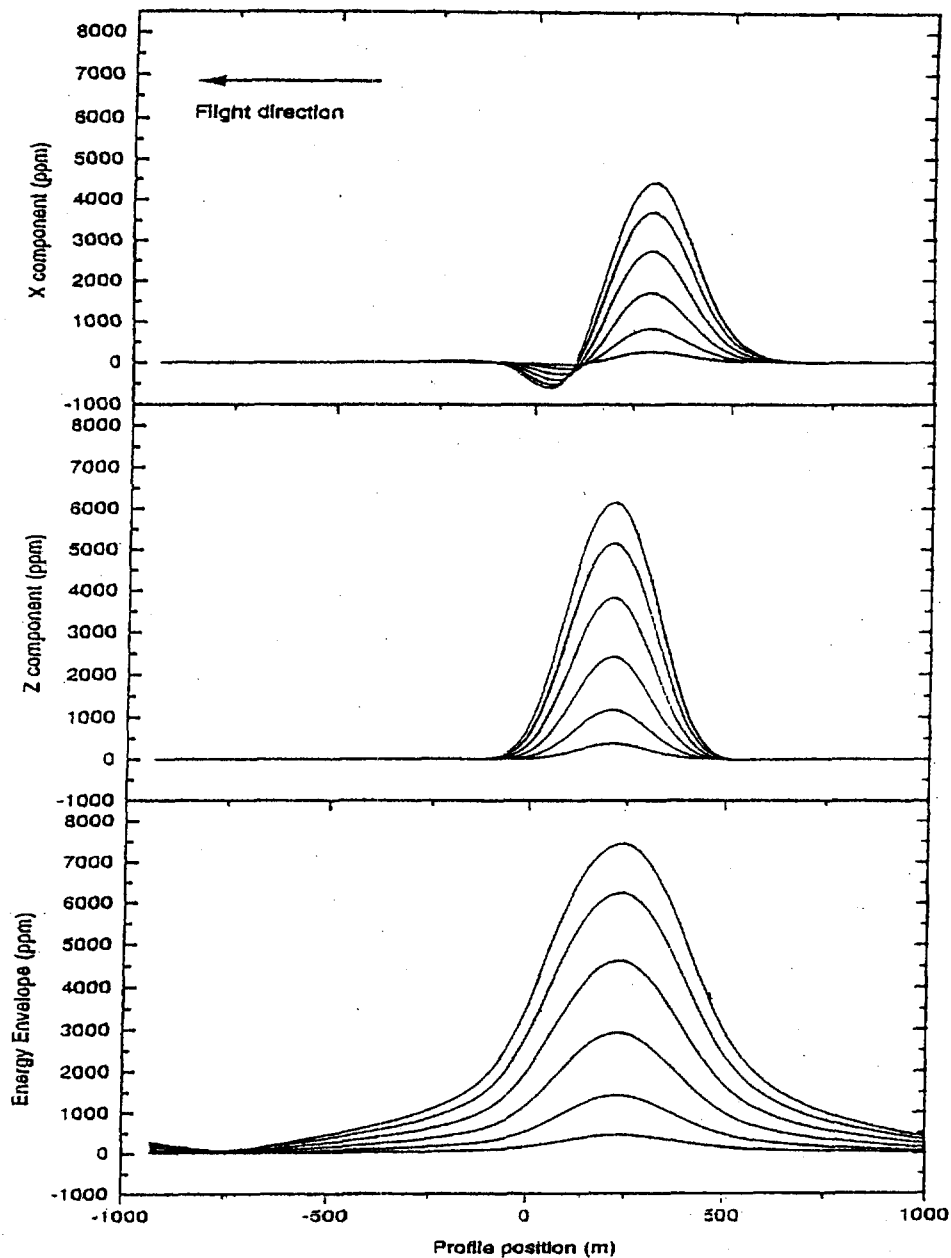


Plate: depth = 150; dip = 45

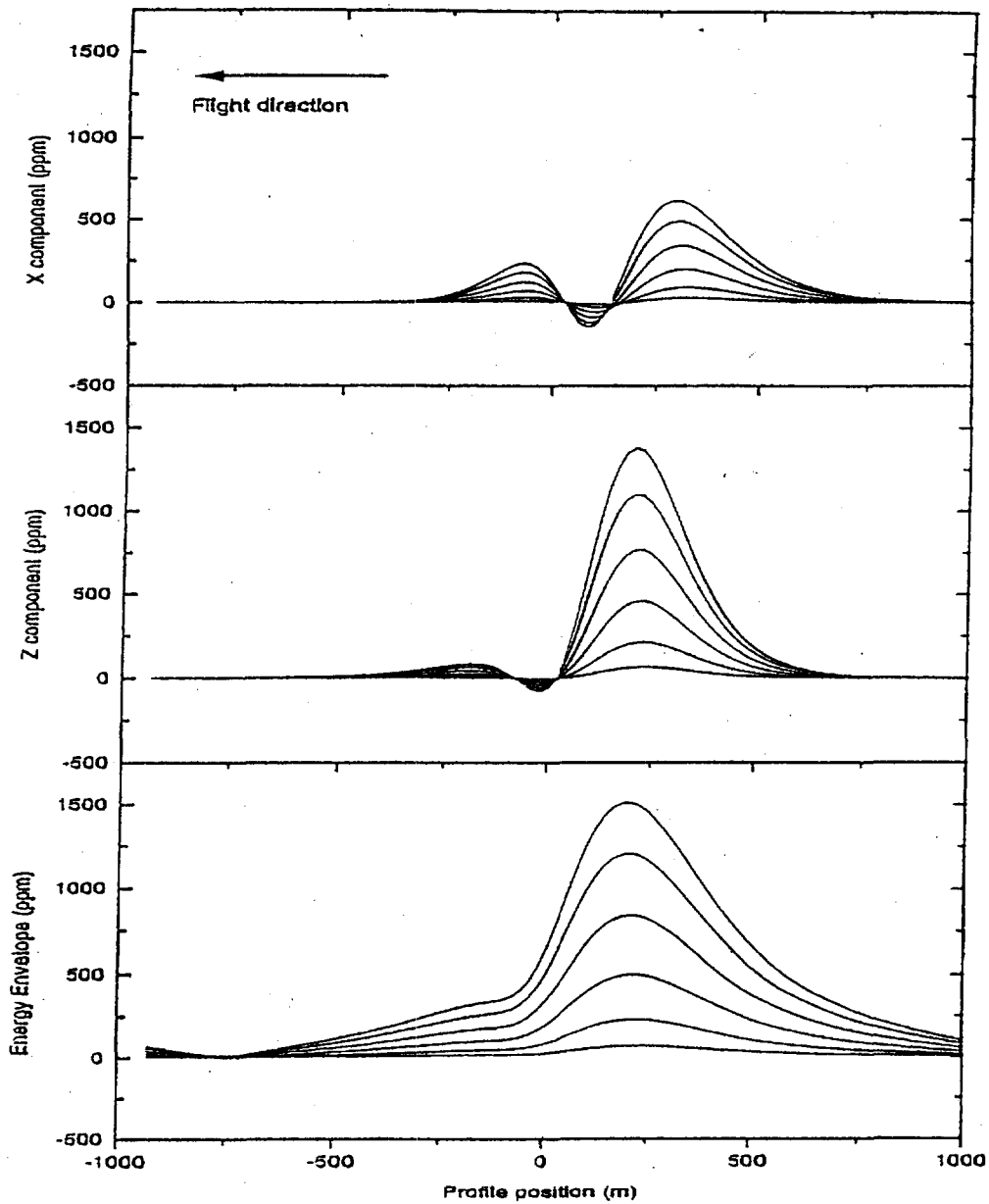


Plate: depth = 150; dip = 90

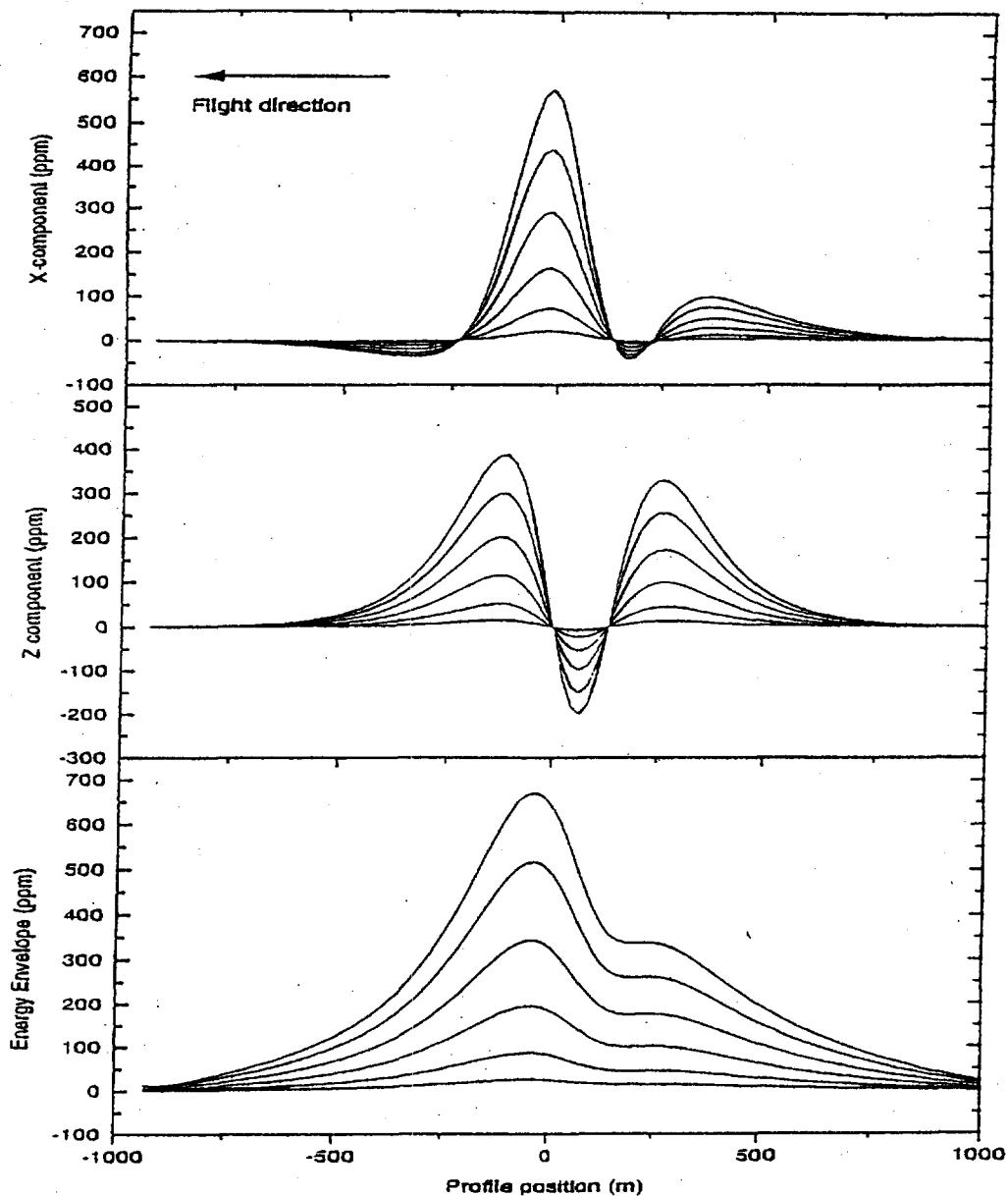


Plate: depth =150; dip =135

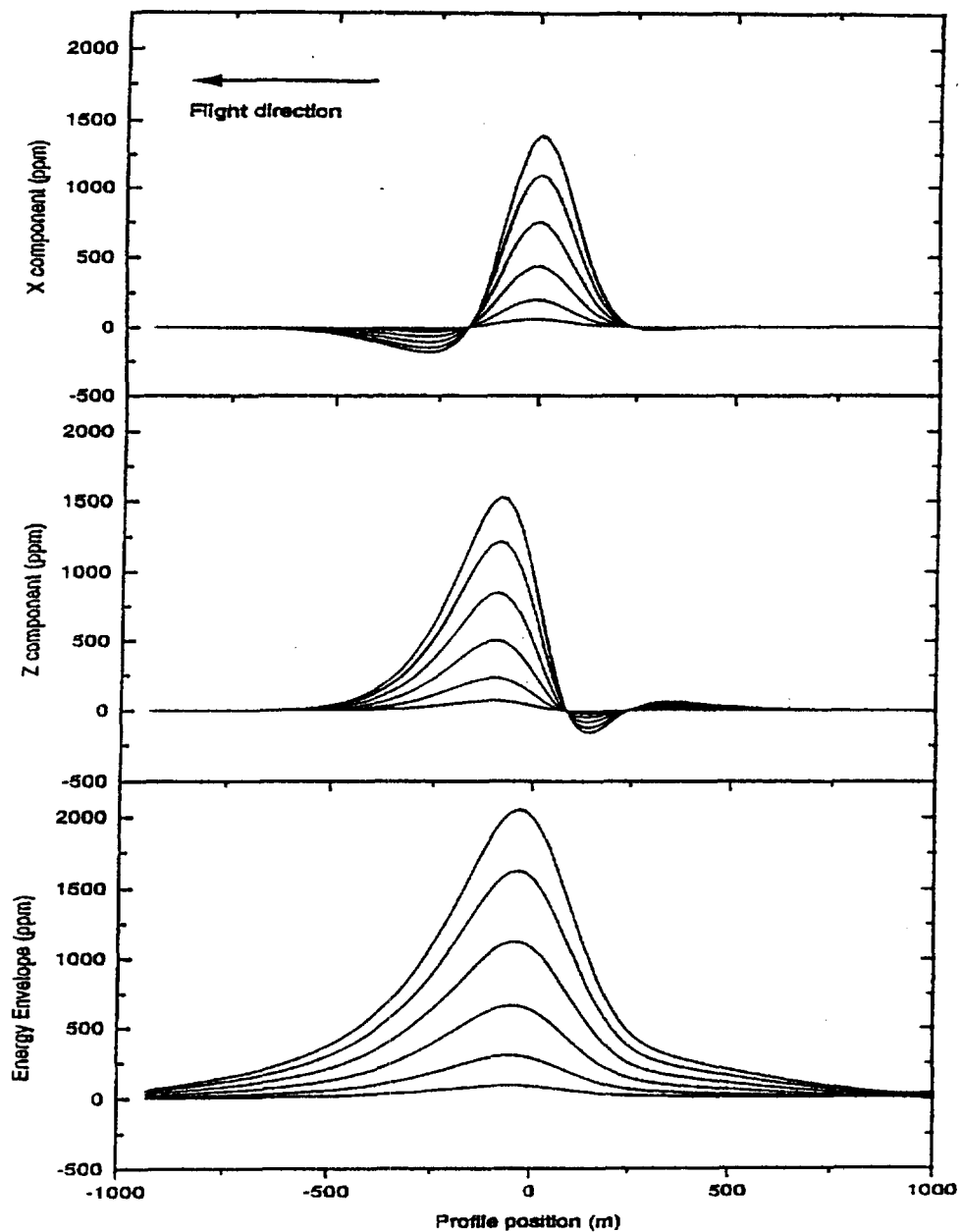


Plate: depth = 300; dip = 0

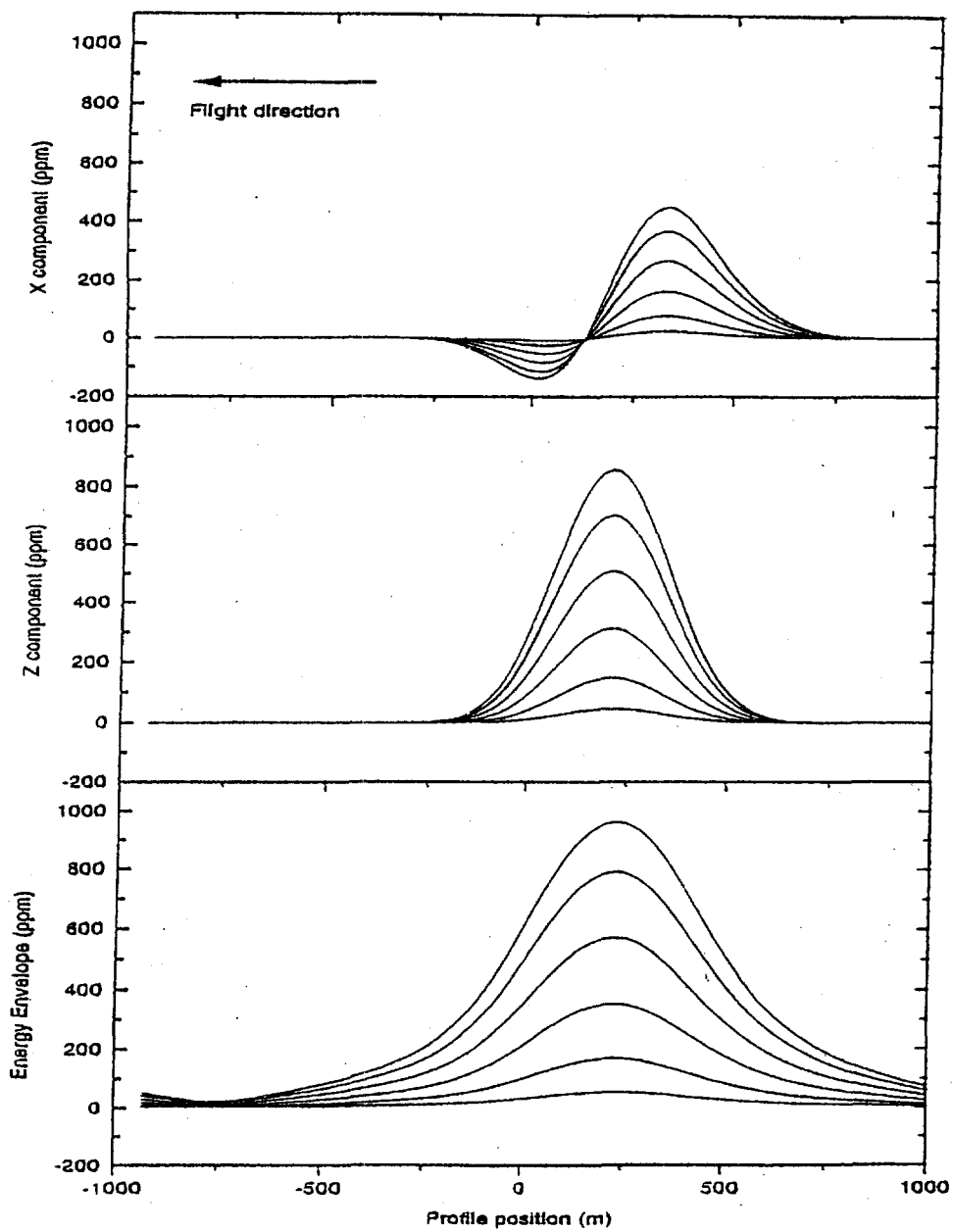


Plate: depth = 300; dip = 45

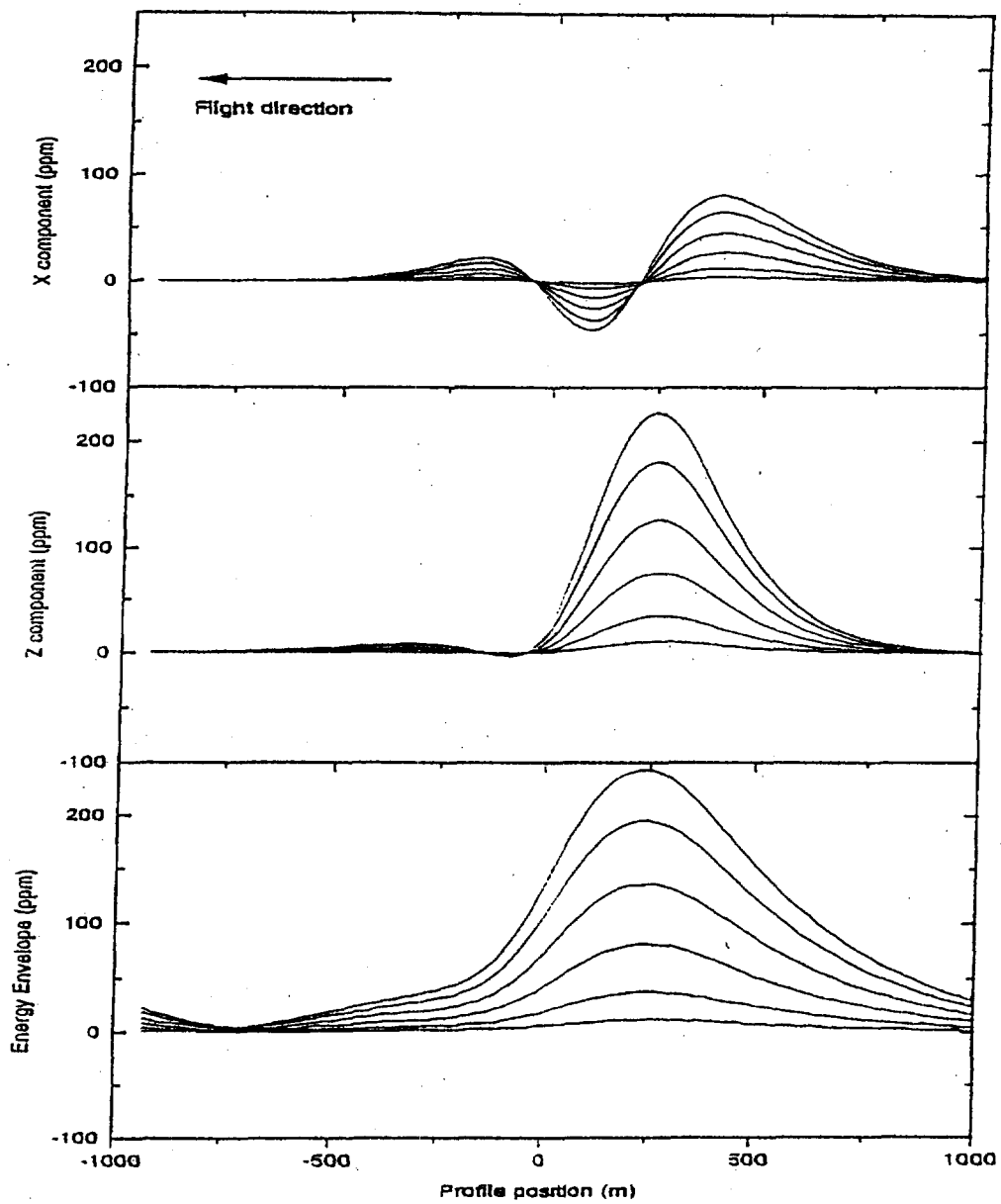


Plate: depth =300; dip =90

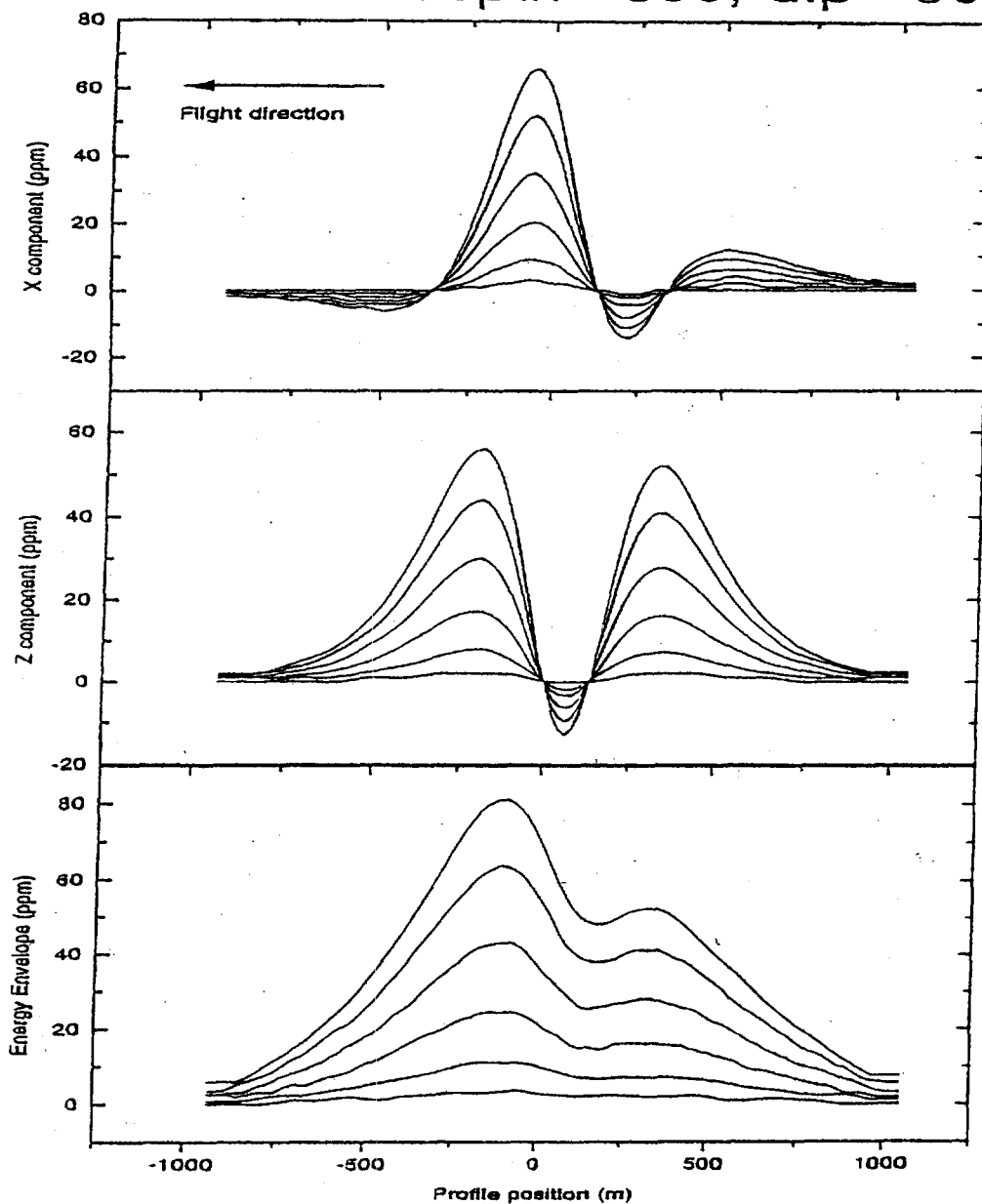
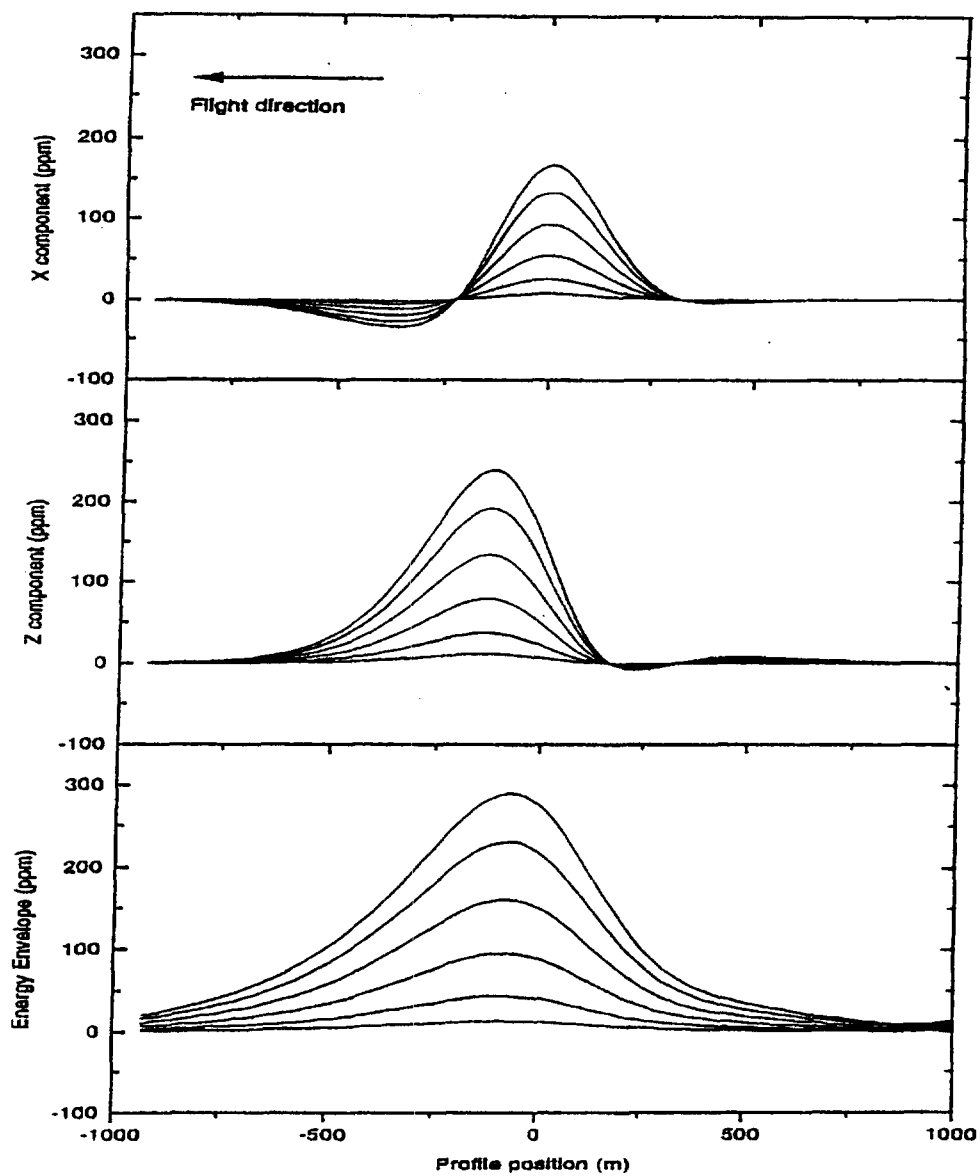


Plate: depth = 300; dip = 135



Appendix D

The Usefulness Of Multicomponent, Time-Domain Airborne Electromagnetic Measurements

GEOPHYSICS, VOL 61, NO. 1 (JANUARY-FEBRUARY 1996); P. 74-81, 17 FIGS.

The Usefulness Of Multicomponent, Time-Domain Airborne Electromagnetic Measurements

Richard S. Smith* and Pierre B. Keating ‡

ABSTRACT

Time-domain airborne electromagnetic (AEM) systems historically measure the inline horizontal (x) component. New versions of the electromagnetic systems are designed to collect two additional components [the vertical (z) and the lateral horizontal (y) component] to provide greater diagnostic information.

In areas where the geology is near horizontal, the z -component response provides greater signal to noise, particularly at late delay times. This allows the conductivity to be determined to greater depth. In a layered environment, the symmetry implies that the y component will be zero; hence a non-zero y component will indicate a lateral inhomogeneity.

Three components can be combined to give the "energy envelope" of the response. Over a vertical plate, the response profile of this envelope has a single positive peak and no side lobes. The shape of the energy envelope is dependent on the flight direction, but less so than the x component.

In the interpretation of discrete conductors, the z component data can be used to ascertain the dip and depth to the conductor using simple rules of thumb. When the profile line is perpendicular to the strike direction and over the center of the conductor, the y component will be zero; otherwise it appears to be a combination of the x and z components. The extent of contamination by the x and z components can be used to ascertain the strike direction and the lateral offset of the target respectively.

Having the z and y component data increases the total response when the profile line has not traversed the target. This increases the possibility of detecting a target located between adjacent flight lines or beyond a survey boundary.

Presented at the Airborne Electromagnetics Workshop, Tucson, AZ, September 13-16, 1993. Manuscript received by the Editor February 28, 1994; revised manuscript received September 16, 1994.

*Geotrex, 2060 Walkley Rd., Ottawa, Ontario, K1G 3P5, Canada.

‡Geological Survey of Canada, 1 Observatory Crescent, Ottawa, Ontario K1A 0Y3, Canada.

© 1996 Society of Exploration Geophysicists. All rights reserved.

INTRODUCTION

The acquisition of multiple-component electromagnetic (EM) data is becoming more commonplace. In some techniques, such as those which use the plane-wave assumption (MT, CSAMT and VLF) more than one component has been acquired as a matter of routine for some time (see reviews by Vozoff, 1990, 1991; Zonge and Hughes, 1991; McNeill and Labson, 1991). Historically, commercially available controlled-waveform finite-source systems generally measure only one component. The only systems designed to acquire multiple component data are generally experimental [e.g., those described in the appendixes of Spies and Frischknecht (1991) or proprietary (the EMP system of Newmont Exploration)].

Slingram EM systems, comprising a moving dipolar transmitter and a moving receiver, generally only measure one component of the response. Although the MaxMin system was designed with a capability to measure a second (minimum coupled) component, this capability is not used extensively in practice. The only systems that use two receiver coils in practice are those that measure the wavetilt or polarization ellipse (Frischknecht et al., 1991).

Historically, time-domain EM systems have been capable of collecting multicomponent data in a sequential manner by reorienting the sensor for each component direction. The usefulness of additional components is discussed by Macnae (1984) for the case of the UTEM system. Macnae concluded that, as extra time was required to acquire the additional components, this time was better spent collecting more densely spaced vertical-component data. The vertical-component, which is less subject to spheric noise, could subsequently be converted to the horizontal components using the Hilbert transform operators.

Recent instrument developments have been towards multicomponent systems. For example, commercially available ground-EM systems such as the Geonics PROTEM, the Zonge GDP-32 and the SIROTEM have been expanded to include multiple input channels that allow three (or more) components to be acquired simultaneously. There is also a version of the UTEM system currently being developed at Lamontagne Geophysics Ltd. These multichannel receivers require complimentary multicomponent sensors -- for ground-based systems these have been developed by Geonics Ltd and Zonge Engineering and Research Organization. The interpretation of fixed-source, multi-component ground-EM data is described in Barnett (1984) and Macnae (1984).

In the past, multi-component borehole measurements have been hindered by the lack of availability of multi-component sensor probes. Following the development of two prototype probes (Lee, 1986; Hodges et al., 1991), multi-component sensors are now available from Crone Geophysics and Exploration Ltd and Geonics. Three component UTEM and SIROTEM borehole sensors are also in development at Lamontagne and Monash University (Cull, 1993), respectively. Hodges et al. (1991) present an excellent discussion of techniques that can be used to interpret three-component borehole data.

Airborne systems such as frequency-domain helicopter electromagnetic methods acquire data using multiple sensors. However, each receiver has a corresponding transmitter that either operates at a different frequency or has a different coil orientation (Palacky and West, 1991). Hence, these systems are essentially multiple single-component systems. The exception to this rule is the now superseded Dighem III system (Fraser, 1972) which used one transmitter and three receivers.

The only multicomponent airborne EM (AEM) system currently in operation is the SPECTREM system (Macnae, et al., 1991). This is a proprietary (owned and operated by Anglo-

American Corporation of South Africa Ltd.), based on the PROSPECT system (Annan, 1986). The Prospect system was originally designed to acquire the x, y and z components, but SPECTREM is apparently only collecting two components (x and z) at the time of writing. Other multi-component systems currently in development are:

- i) the SALTMAP system,
- ii) a helicopter time-domain system (Hogg, 1986), and a new version of the GEOTEM[®] system (GEOTEM is a registered trademark of Geoterrex).

Apart from a few type curves in Hogg (1986), there is little literature available which describes how to interpret data from these systems.

This paper is intended to give an insight into the types of responses expected with the new multi-component AEM systems, and the information that can be extracted from the data. The insight could be of some assistance in interpreting data from multicomponent moving-source ground EM systems (should this type of data be acquired).

The use of multi-component data will be discussed for a number of different applications. For illustration purposes, this paper will use the transmitter-receiver geometry of the GEOTEM system (Figure 1), which is comparable to the other fixed-wing geometries (SPECTREM and SALTMAP). The GEOTEM system is a digital transient EM system utilizing a bipolar half-sinusoidal current waveform [more details are in Annan and Lockwood (1991)]. The sign convention used in this paper is shown in Figure 1, with the y component being into the page. In a practical EM system, the receiver coils will rotate in flight. We will assume that the three components of the measured primary field and an assumed bird position have been used to correct for any rotation of the coil.

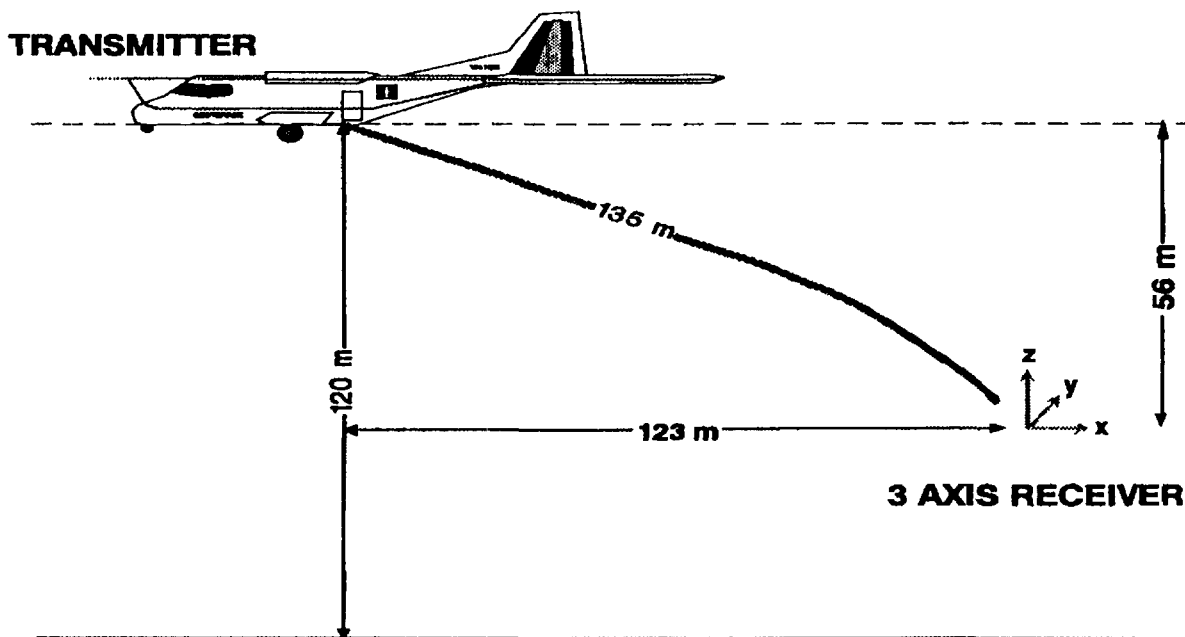


Figure 0: The geometric configuration of the GEOTEM system. The system comprises a transmitter on the aircraft and a receiver sensor in a "bird" towed behind the aircraft. The z direction is positive up, x is positive behind the aircraft, and y is into the page (forming a right-hand coordinate system).

SOUNDING IN LAYERED ENVIRONMENTS

In a layered environment, the induced current flow is horizontal (Morrison et al., 1969) so the z component of the secondary response (V_z) is much larger than the x component (V_x), particularly in resistive ground and/or at late delay times. At the same time, the sferic noise in the z direction is 5 to 10 times less than in the horizontal directions (Macnae, 1984; McCracken et al., 1986), so V_z has a greater signal-to-noise ratio. Figure 2 shows theoretical curves over two different, but similar, layered earth models. One model is a half-space of $500 \Omega\cdot\text{m}$ and the other is a 350 m thick layer of $500 \Omega\cdot\text{m}$ overlying a highly resistive basement. In this plot the data have been normalized by the total primary field. The z component (V_z) is 6 to 10 times larger than V_x , and both curves are above the noise level, at least for part of the measured transient. On this plot, a noise level of 30 ppm has been assumed, which would be a typical noise level for both components when the sferic activity is low. To distinguish between the response of the half-space and thick layer, the difference between the response of one model and the response of the other model must be greater than the noise level. Figure 3 shows this difference for both components. Only the V_z difference is above the noise level. Hence for the case shown, V_z is more useful than V_x for determining whether there is a resistive layer at 350 m depth. Because V_z is generally larger in a layered environment, the vertical component will generally be better at resolving the conductivity at depth.

In the above discussion, we have assumed that corrections have been made for the coil rotation. An alternative approach is to calculate and model the magnitude of the total field, as this quantity is independent of the receiver orientation. Macnae et al. (1991) used this strategy when calculating the conductivity depth sections for SPECTREM data.

The symmetry of the secondary field of a layered environment is such that the y component response (V_y) will always be zero. In fact, the V_y component will be zero whenever the conductivity structure on both sides of the aircraft is the same. A non-zero V_y is therefore useful in identifying off-line lateral inhomogeneities in the ground.

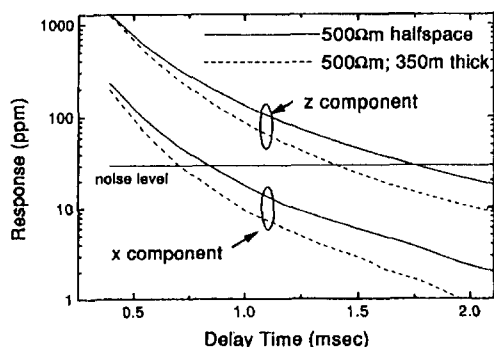


Figure 2: The response for a $500 \Omega\cdot\text{m}$ half-space (solid line) and a $500 \Omega\cdot\text{m}$ layer of thickness 350 m overlying a resistive half-space (dashed line). The z -component responses are the two curves with the larger amplitudes and the two x -component response curves are 6 to 10 times smaller than the corresponding z component. A noise level of 30 ppm is considered to be typical of both components in the absence of strong sferics.

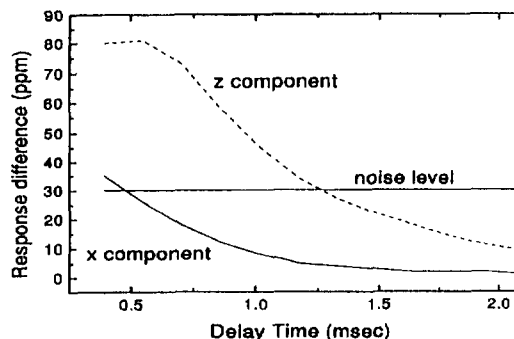


Figure 3: The difference in the response of each component for the half-space and thick layer models of Figure 2. Only the z component difference is above the noise level for a significant portion of the transient. Therefore, this is the only component capable of distinguishing between the responses of the two models.

DISCRETE CONDUCTORS

In our discrete conductor study, models have been calculated using a simple plate in free-space model (Dyck and West, 1984) to provide some insight into the geometry of the induced field. The extension to more complex models, such as those incorporating current gathering, will not be considered in this paper.

Historically, airborne transient electromagnetic (TEM) data have been used for conductor detection. The old INPUT system was designed to measure V_x because this component gave a large response when the receiver passed over the top of a vertical conductor. The bottom part of Figure 4 shows the response over a vertical conductor, which has been plotted at the receiver position. The V_x profile (smaller of the two solid lines) has a large peak corresponding with the conductor position. Note that there is also a peak at 200 m, just before the transmitter passes over the conductor, and a trailing edge negative to the left of the conductor. The z component (dashed line) has two peaks and a large negative trough just before the conductor. Because of the symmetry, the V_y response (dotted line) is zero.

All the peaks, troughs and negatives make the response of a single conductor complicated to display and hence interpret. The display can be simplified by plotting the "energy envelope" (EE) of the response. This quantity is defined as follows:

$$EE = \sqrt{V_x^2 + \bar{V}_x^2 + V_y^2 + \bar{V}_y^2 + V_z^2 + \bar{V}_z^2},$$

where $\bar{\quad}$ denotes the Hilbert transform of the quantity. The energy envelope plotted on Figure 4 (the larger of the two solid curves) is almost symmetric, and would be a good quantity to present in plan form (as contours or as an image). For flat-lying conductors, the energy envelope has a maximum at the leading edge (just after the aircraft flies onto the conductor).

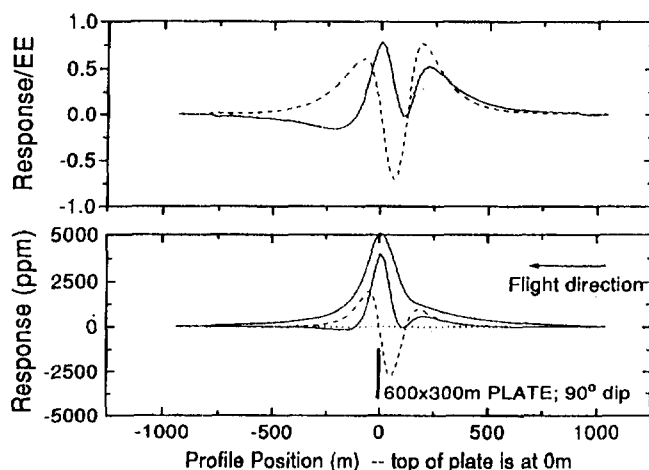


Figure 4: (Bottom) The response of a 600 by 300 m plate 120 m below an aircraft flying from right to left. The plotting point for the response is below the receiver. The x-component response is the smaller amplitude solid line, the z-component is the dashed line, and the y-component response is the dotted line. The larger amplitude solid line is the "energy envelope" of all three components. (Top) The z- and x-components normalized by the energy envelope. These and all subsequent curves are for a delay time of 0.4 ms after the transmitter current is turned off.

What little asymmetry remains in the energy envelope is a good indication of the coupling of the AEM system to the conductor. If the response profile for each component is normalized by the energy envelope, then the effect of system coupling will be removed (at least partially) and the profiles will appear more symmetric. For example, the top part of Figure 4 shows the V_x and V_z normalized by the energy envelope at each point. The size of the two x peaks and the two z peaks are now roughly comparable.

Dip determination

The response of a plate with a dip of 120° is shown on Figure 5. For the V_x/EE and V_z/EE profiles, the peak on the down dip side is larger. For shallow dips, it becomes difficult to identify both V_x/EE peaks, but the two positive V_z/EE peaks remain discernable. Plotting the ratio of the magnitudes of these two V_z/EE peaks, as has been done with solid squares on Figure 6, shows that the ratio is very close to the tangent of the dip divided by 2. Hence, calculating the ratio of the peak amplitudes (R) will yield the dip angle θ using the following formula:

$$\theta = 2 \tan^{-1}(R).$$

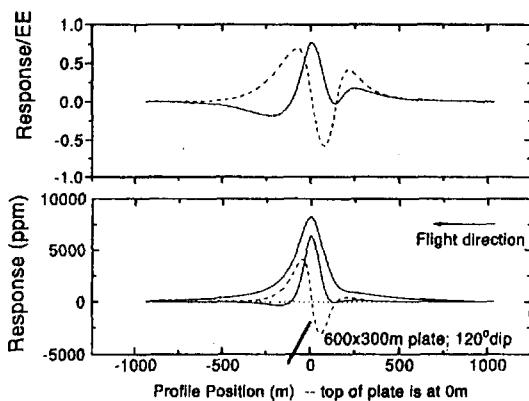


FIG. 5. (Bottom) same as Figure 4, except the plate is now dipping at 120° . On the top graph note that the down-dip (left) peak on the normalized z -component response is larger than the right peak (cf. Figure 4).

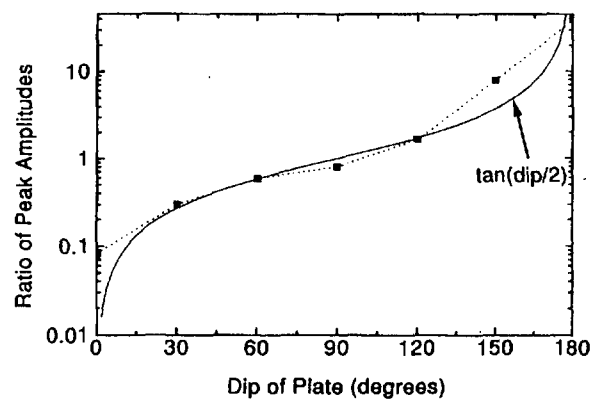


FIG. 6. The ratio of the peak amplitudes of the normalized z -component response (left/right) plotted with solid squares. The ratio plots very close to the tangent of half the dip angle θ of the plate.

Depth Determination

As the depth of the body increases, there is a corresponding increase in the distance between the two positive peaks in the V_z/EE profile. As an example of this, Figure 7 shows the case of a plate 150 m deeper than the plate of Figure 4. The peaks are now 450 m apart, as compared with 275 m on Figure 4. A plot of the peak-to-peak distances for a range of depths is shown on Figure 8 for plates with 60° , 90° and 120° dips. Because the points follow a straight line, it can be concluded that for near vertical bodies (60° to 120° dips), the depth to the top of the body d can be determined from the measured peak-to-peak distances using the linear relationship depicted in Figure 8. The expected error would be about 25 m. Such an error is tolerable in airborne EM interpretation. More traditional methods for determining d analyze the rate of decay of the measured response (Palacky and West, 1973). Our method requires only the V_z/EE response profile at a single delay time. Analyzing this response profile for each delay time allows d to be determined as a function of delay time, and hence any migration of the current system in the conductor could be tracked.

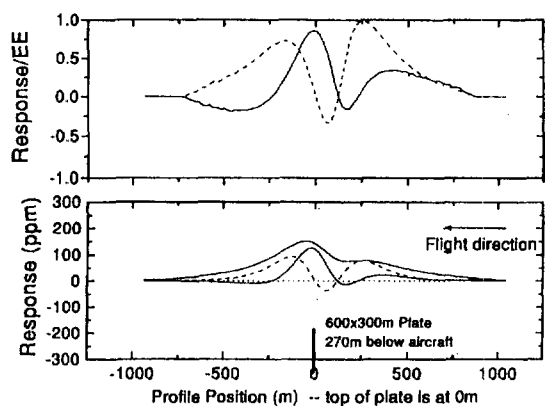


FIG. 7. The same as Figure 4, except the plate is now 270 m below the aircraft. Note that the distance between the z-component peaks is now much greater.

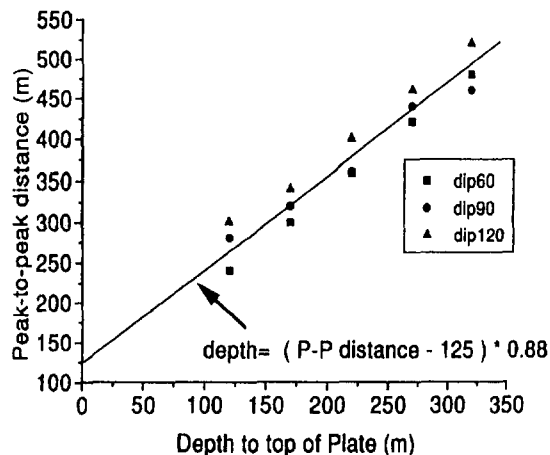


FIG. 8. The peak-to-peak distance as a function of plate depth for three different dip angles θ . A variation in dip of $\pm 30^\circ$ does not result in a large change in the peak-to-peak distance.

Strike and offset determination

The response shown in Figure 4 varies in cases when the plate has a strike different from 90° or the flight path is offset from the center of the plate.

Figure 9 shows the response for a plate with zero offset and Figure 10 shows the plate when it is offset by 150 m from the profile line. The calculated voltages V_z and V_x are little changed from the no offset case, but the V_y response, is no longer zero. In fact, the shape of the V_y curve appears to be the mirror image of the V_z curve.

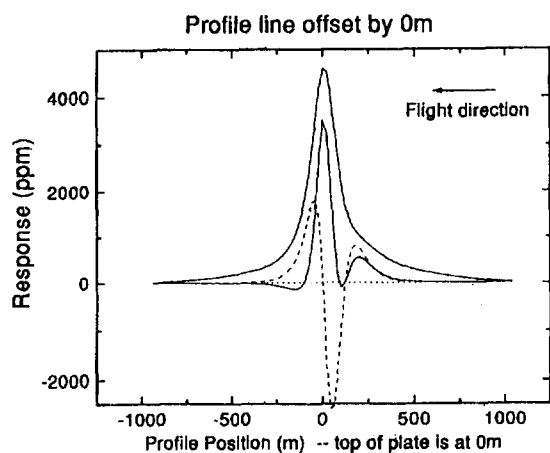


FIG. 9. The response of a 300 by 300 m plate traversed by a profile line crossing the center of the plate in a direction perpendicular to the strike of the plate (the strike angle ζ of the plate with respect to the profile line is 90°).

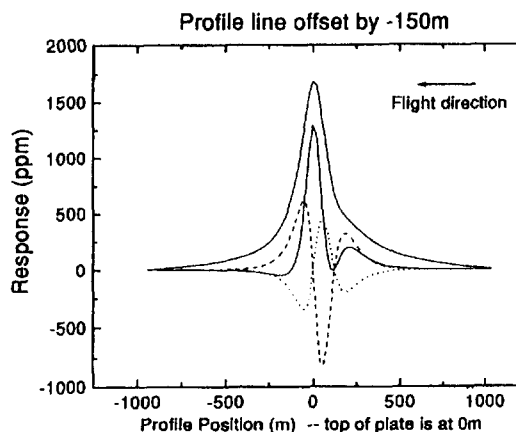


FIG. 10. Same as Figure 9, except the profile line has been offset from the center of the plate by -150 m in the y direction (equivalent to a +150 m displacement of the plate).

In the case when the plate strikes at 45° , the y component is similar in shape but opposite in sign to the x -component response (Figure 11).

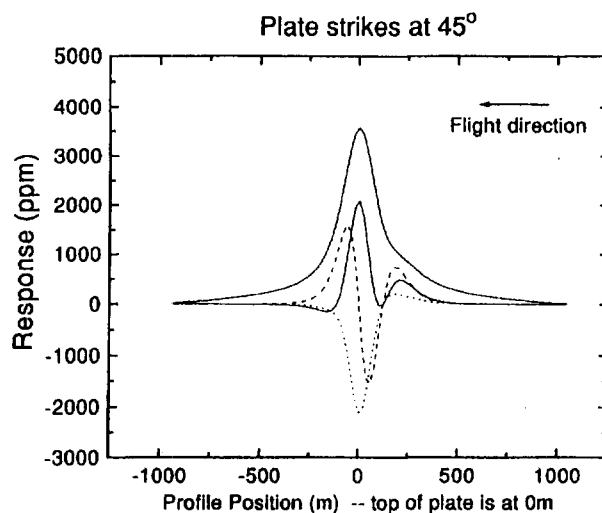


FIG. 11. Same as Figure 9, except the profile line traverses the plate such that the strike angle ζ of the plate, with respect to the profile line, is 45° .

These similarities can be better understood by looking at schematic diagrams of the secondary field from the plate. Figure 12 shows a plate and the field in section. For zero offset, the field is vertical (z only). As the offset increases, the aircraft and receiver moves to the right and the measured field rotates into the y -component.

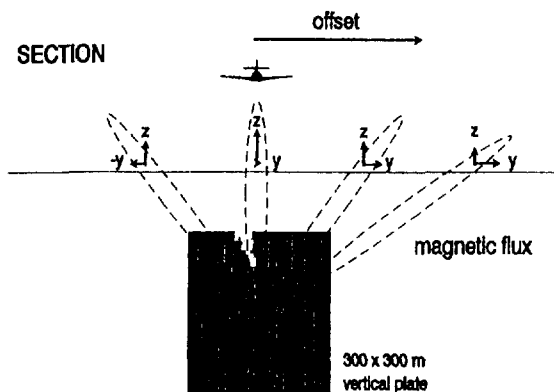


FIG. 12. A schematic diagram of the plate and the magnetic flux of the secondary field (section view). For increasing offset of the aircraft and receiver from the center of the plate, the magnetic field at the receiver rotates from the z to the y component.

The secondary field is depicted in plan view in Figure 13. Variable strike is simulated by leaving the plate stationary and changing the flight direction. When the strike of the plate is different from 90° , the effective rotation of the EM system means that the secondary field, which was previously measured purely in the x direction, is now also measured in the y direction.

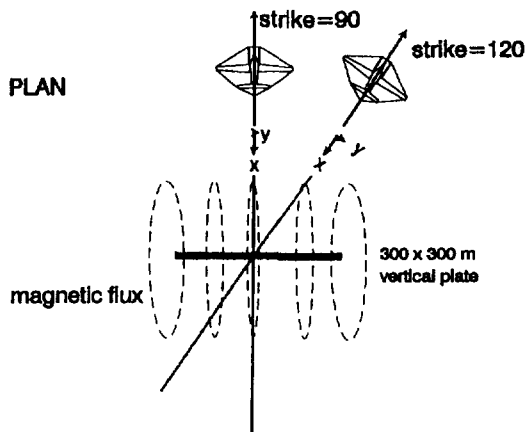


FIG. 13. A schematic diagram of the plate and the magnetic flux of the secondary field (plan view). Here varying strike is depicted by an equivalent variation of the flight direction. As the flight direction rotates from a strike angle of 90°, the receiver rotates so as to measure a greater response in the y direction.

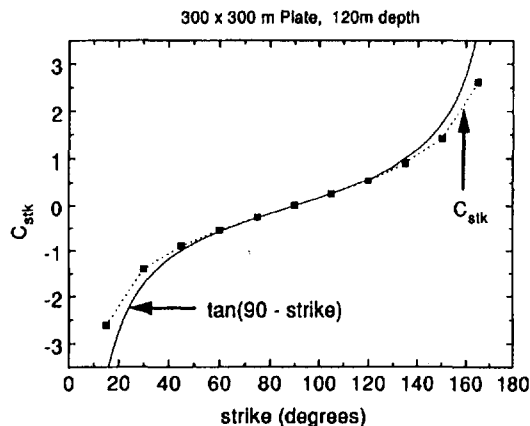


FIG. 14. The ratio $C_{stk} = V_y/V_x$ plotted as a function of varying strike angle (solid squares). The data agree very closely with the cotangent of the ξ .

The y component (V_y) can thus be considered to be a mixture of V_x and V_z components,

$$V_y = C_{stk} V_x + C_{off} V_z,$$

an equation that is only approximate. The response for a variety of strike angles and offset distances has been calculated and in each case the y-component response has been decomposed into the x and z components by solving for the constants of proportionality C_{stk} and C_{off} .

A plot of C_{stk} for the case of zero offset and varying strike direction ξ is seen on Figure 14. The values of C_{stk} determined from the data are plotted with solid squares and compared with the $\tan(90^\circ - \xi)$. Because the agreement is so good, the formula

$$\xi = 90 - \tan^{-1}(C_{stk})$$

can be used to determine the strike. This relation was first obtained by Fraser (1972).

When the strike is fixed at 90°, and the offset varies, the corresponding values obtained for C_{off} have been plotted with solid squares on Figure 15. Again, there is good agreement with the arctangent of C_{off} and the angle ϕ between a vertical line and the line that joins the center of the top edge of the plate with the position where the aircraft traverse crosses the plate containing the plate. If an estimate of the distance to the top of the conductor D is already obtained using the method described above, or by the method described in Palacky and West (1973), then

$$D = \sqrt{O^2 + d^2},$$

(where d is the depth below surface). Hence, the offset distance O can be written as follows

$$\begin{aligned} O &= d \tan(\phi) \\ &= d C_{off} \\ &= C_{off} \sqrt{D^2 - O^2} \end{aligned}$$

which can be rearranged to give

$$O = C_{off} D / \sqrt{1 + C_{off}^2}.$$

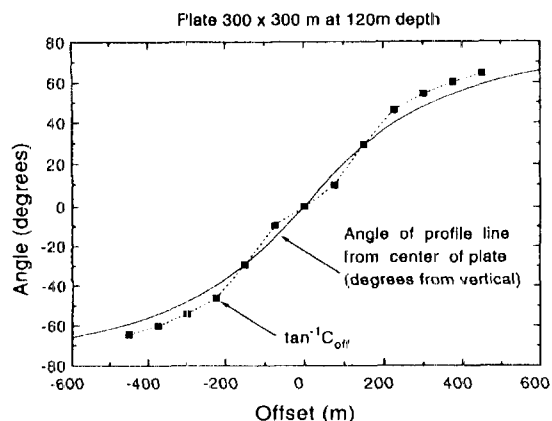


FIG. 15. The arctangent of $C_{off} = V_y/V_z$, plotted as a function of varying offset (solid squares). There is good agreement between this quantity and the angle ϕ between a vertical line and the line from the center of the top edge of the plate to the profile line.

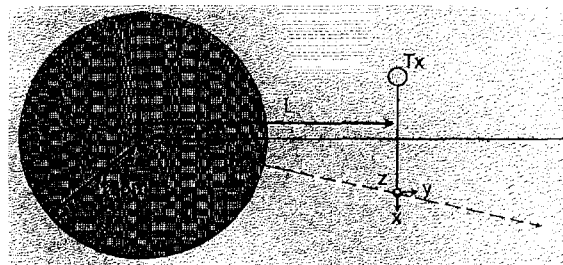


FIG. 16. Plan view of a flat-lying conductor (a circular loop with a radius of 125 m). The AEM system is offset a distance L from the center of the conductor in a direction perpendicular to the traverse direction. The traverse direction of the system is from the bottom to the top of the figure.

Lateral detectability

Figure 12 illustrates that V_y becomes relatively strong as the lateral displacement from the conductor is increased. Thus, if V_y is measured, then the total signal will remain above the noise level at larger lateral displacements of the traverse line from the conductor. This has been illustrated by assuming a flat-lying conductor, here approximated by a wire-loop circuit of radius 125 m (Figure 16). The x , y and z components of the response have been computed using the formula for the large-loop magnetic fields in Wait (1982). The results are plotted on Figure 17 as a function of increasing lateral displacement L of the transmitter/receiver from the center of the conductor. The transmitter and receiver are separated in a direction perpendicular L to simulate the case when the system is maximal coupled to the conductor, but the flight line misses the target by an increasing amount. The effect of varying the conductance or measurement time has been removed by normalizing the response to the total response measured when the system is at zero displacement. At displacements greater than 80 m, the y component is clearly larger than any other component. Assuming the same sensitivity and noise level for each component (which is a realistic assumption if the data are corrected for coil rotation and the spheric activity is low), it is clearly an advantage to measure V_y , as this will increase the chances of detecting the target when the flight line has not passed directly over the conductor.

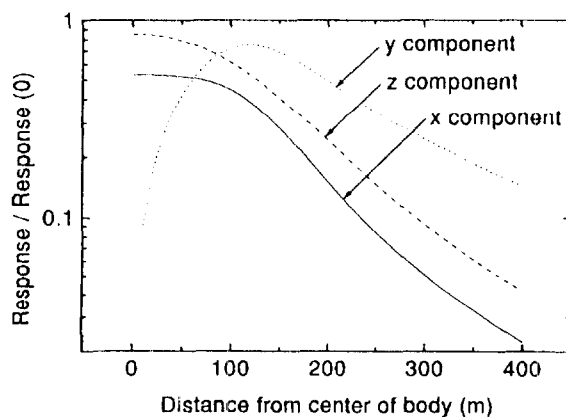


FIG. 17. The normalized response of the EM system plotted as a function of increasing offset distance L . The x component falls off most rapidly and the y component most slowly with increasing offset distance.

CONCLUSIONS

AEM systems measuring three components of the response can be used to infer more and/or better information than those systems that measure with only one component, i.e., V_x .

The z-component data enhances the ability of the AEM system to resolve layered structures as the z-component has a larger signal and a smaller proportion of spheric noise than any other component. If all the components are employed to correct for coil rotation, then the data quality and resolving power is increased further, as individual components are not contaminated by another component. Having better signal-to-noise and greater fidelity in the data will allow deeper layers to be interpreted with confidence.

A non-zero y component is helpful in identifying when the conductivity structure has a lateral inhomogeneity that is not symmetric about the flight line.

All components can be used to calculate the energy envelope, which is a valuable quantity to image. The energy envelope has a single peak over a vertical conductor and two peaks over a dipping conductor (one at either end). The asymmetry in the response profile of each individual component can be reduced by normalizing each profile by the energy envelope.

All three components are of great use in determining the characteristics of discrete conductors. For example, the distance between the two positive peaks in the V_z/EE profile can be employed to determine the depth. Also, the ratio of the magnitude of the two V_z/EE peaks helps to ascertain the dip of the conductor. The x component has been used in the past for these purposes, but is not as versatile, as it requires the data at all delay times, or an ability to identify a very small peak.

The y component can be utilized to extract information about the conductor that cannot be obtained from single component AEM data. The degree of mixing between the y and z components can give the lateral offset of the conductor (provided the depth is known), while the mixing between the y and x component gives the strike of a vertical conductor.

Finally, because the y component decreases most slowly with increasing lateral offset, this component gives an enhanced ability to detect a conductor positioned at relatively large lateral distances from the profile line, either between lines or beyond the edge of a survey boundary.

ACKNOWLEDGMENTS

The authors wish to thank Geoterrex for the permission to publish the results of this model study. This paper has been allocated Geological Survey of Canada Contribution No. 36894.

REFERENCES

- Annan, A. P., 1986, Development of the PROSPECT I airborne electromagnetic system, in Palacky, G. J., Ed., Airborne resistivity mapping : Geol. Surv. Can. Paper 86-22, 63-70.
- Annan, A. P., and Lockwood, R., 1991, An application of airborne GEOTEM in Australian conditions: Expl., Geophys., 22, 5-12.
- Barnett, C. T., 1984, Simple inversion of time-domain electromagnetic data: Geophysics, 49, 925-933.
- Cull, J. P., 1993, Downhole three component TEM probes: Expl. Geophys., 24, 437-442.

- Dyck, A. V., and West G. F., 1984, The role of simple computer models in interpretations of wide-band, drill-hole electromagnetic surveys in mineral exploration: *Geophysics*, 49, 957-980.
- Fraser, D. C., 1972, A new multicoil aerial electromagnetic prospecting system: *Geophysics*, 37, 518-537.
- Frischknecht, F. C., Labson, V. F., Spies, B. R., and Anderson, W. L., 1991, Profiling methods using small sources, in Nabighian M. N., Ed., *Electromagnetic methods in applied geophysics*, Vol. 2, Applications: Soc. Expl. Geophys. Investigations in geophysics, no. 3, 105-270.
- Hodges, D. G., Crone, J. D., and Pemberton, R., 1991, A new multiple component downhole pulse EM probe for directional interpretation: Proc. 4th Int. MGLS/KEGS Sym. on Borehole Geophys. For Min. Geotech. And Groundwater Appl.
- Hogg, R. L. S., 1986, The Aerodat multigeometry, broadband transient helicopter electromagnetic system, in Palacky. G. J., Ed., *Airborne resistivity mapping: Geol. Surv. Can. Paper 86-22*, 79-89.
- Lee, J., 1986, A three component drill-hole EM receiver probe: M.Sc. thesis, Univ. of Toronto.
- Macnae, J. C., 1984, Survey design for multicomponent electromagnetic systems: *Geophysics*, 49, 265-273.
- Macnae, J. C., Smith, R. S., Polzer, B. D., Lamontagne, Y., and Klinkert, P. S., 1991, Conductivity-depth imaging of airborne electromagnetic step-response data: *Geophysics*, 56, 102-114.
- McCracken, K. G., Oristaglio, M. L., and Hohmann, G. W., 1986, Minimization of noise in electromagnetic exploration systems: *Geophysics*, 51, 819-132.
- McNeill, J.D., and Labson, V., 1991, Geological mapping using VLF radio fields, in Nabighian M. N., Ed., *Electromagnetic methods in applied geophysics*, Vol. 2, Applications: Soc. Expl. Geophys. Investigations in geophysics, no. 3, 521-640.
- Morrison, H.F., Phillips, R.J., and O'Brien, D.P., 1969, Quantitative interpretation of transient electromagnetic fields over a layered earth: *Geophys. Prosp.* 17, 82-101.
- Palacky, G. J., and West, G. F., 1973, Quantitative measurements of Input AEM measurements: *Geophysics*, 38, 1145-1158.
- Palacky, G. J., and West, G. F., 1991, Airborne electromagnetic methods, in Nabighian M. N., Ed., *Electromagnetic methods in applied geophysics*, Vol. 2, Applications: Soc. Expl. Geophys. Investigations in geophysics, no. 3, 811-879.
- Spies, B. R., and Frischknecht, F. C., 1991, Electromagnetic sounding, in Nabighian M. N., Ed., *Electromagnetic methods in applied geophysics*, Vol. 2, Applications: Soc. Expl. Geophys. Investigations in geophysics, no. 3, 285-425.
- Vozoff, K., 1990, Magnetotellurics: Principles and practices: *Proc. Indian Acad. Sci.*, 99, 441-471.
- Vozoff, K., 1991, The magnetotelluric method, in Nabighian M. N., Ed., *Electromagnetic methods in applied geophysics*, Vol. 2, Applications: Soc. Expl. Geophys. Investigations in geophysics, no. 3, 641-711.
- Wait, J. R., 1982, *Geo-electromagnetism*: Academic Press Inc.
- Zonge K. L., and Hughes, L. J., 1991, Controlled-source audio-magnetotellurics, in Nabighian M. N., Ed., *Electromagnetic methods in applied geophysics*, Vol. 2, Application: Soc. Expl. Geophys. Investigations in geophysics, no. 3, 713-809

Appendix E

Data Archive Description

Data Archive Description:

Survey Details

Survey Area Name	North Range Blocks 1,2,3 and Airport Property
Job number	04408
Client	Crowflight Minerals Inc.
Survey Company Name	Fugro Airborne Surveys
Flown and compiled dates	April 15 – May 12, 2004
Archive Creation Date	June 28, 2004

Survey Specifications

Traverse Line Azimuth	North Range Block 1: 160° - 340° North Range Block 2: 000° - 180° North Range Block 3: 030° - 210° Airport Property: 045° - 225°
Traverse Line Spacing	150m
Tie Line Azimuth	North Range Block 1: 070° - 250° North Range Block 2: 090° - 270° North Range Block 3: 120° - 300° Airport Property: 135° - 315°
Tie Line Spacing	2500m – 3500 m
Flying Elevation	120 m Mean Terrain Clearance
Average Aircraft Speed	65 m/s

Geodetic Information for map products

Projection:	Universal Transverse Mercator
Datum:	NAD 27
Central meridian:	81° West
False Easting:	500000 metres
False Northing:	0 metres
Scale factor:	0.9996
UTM Zone	17 North
I.G.R.F. Model	2003
I.G.R.F. Correction Date	2004.3

Equipment Specifications:

Navigation

Differential GPS Receiver	NovAtel Propak 4E-3151-R 12 Channel
Aircraft	DeHavilland Dash-7
Video Camera	Panasonic WV-CL302

Magnetics

Type	Scintrex CS-2 Cesium Vapour
Installation	Towed bird

Sensitivity 0.01 nT
 Sampling 0.10s

Electromagnetics

Type MEGATEM®, 20 channel multicoil system
 Installation Vertical axis loop (406m² area with 6 turns) mounted on the aircraft.
 Receiver coils in a towed bird.
 Coil Orientation X, Y and Z
 Frequency 90 Hz
 Pulse Width 2 ms
 Geometry Tx-Rx horizontal separation of ~130 m
 Tx-Rx vertical separation of ~50 m
 Sampling 0.25 s

System Configuration:

Pulse repetition rate 90Hz
 Pulse width 2330µs
 Offtime 3126µs
 Receiver-transmitter horizontal separation 130m
 Receiver-transmitter vertical separation 50m

Data Windows:

Channel	Start (p)	End (p)	Width (p)	Start (ms)	End (ms)	Width (ms)	Mid (ms)
1	4	11	8	0.13	0.477	0.347	0.304
2	12	25	14	0.477	1.085	0.608	0.781
3	26	39	14	1.085	1.693	0.608	1.389
4	40	53	14	1.693	2.3	0.608	1.997
5	54	59	6	2.3	2.561	0.26	2.431
6	60	61	2	2.561	2.648	0.087	2.604
7	62	64	3	2.648	2.778	0.13	2.713
8	65	67	3	2.778	2.908	0.13	2.843
9	68	71	4	2.908	3.082	0.174	2.995
10	72	75	4	3.082	3.255	0.174	3.168
11	76	79	4	3.255	3.429	0.174	3.342
12	80	83	4	3.429	3.602	0.174	3.516
13	84	87	4	3.602	3.776	0.174	3.689
14	88	92	5	3.776	3.993	0.217	3.885
15	93	97	5	3.993	4.21	0.217	4.102
16	98	102	5	4.21	4.427	0.217	4.319
17	103	108	6	4.427	4.688	0.26	4.557
18	109	114	6	4.688	4.948	0.26	4.818
19	115	121	7	4.948	5.252	0.304	5.1
20	122	128	7	5.252	5.556	0.304	5.404



Geosoft Database Line Archive File Layout (AREA_archive.gdb):

Variable	Description	Units
Line	Line Number	
Fiducial	Seconds after midnight	sec.
Flight	Flight number	-
Date	Date of the survey flight	ddmmyy
Lat_nad27	Latitude in Nad27	degrees
Long_nad27	Longitude in Nad27	degrees
X_nad27z17n	Easting (X) in Nad27 Zone 17 North	m
Y_nad27z17n	Northing (Y) in Nad27 Zone 17 North	m
GPS_Z	Gps elevation (above WGS84 datum)	m
Radar	Radar altimeter	m
DTM	Terrain (above WGS84 datum)	m
Diurnal	Ground Magnetic Intensity	nT
TMI_raw	Raw Airborne Total Magnetic Intensity	nT
IGRF	International Geomagnetic Reference Field	nT
RMI	Final Airborne Residual Magnetic Intensity	nT
Primary_field	Electromagnetic Primary Field	μV
Hz_monitor	Powerline Monitor (60 Hz)	μV
1vd	First Vertical Derivative of the RMI	nT/m
cond_1o	Apparent Conductance from the 1 st Order Moment of B Field X Coil	mS
teeb10	Total Energy Envelope of B Field Channel 10	fT
x01-x20	Final dB/dt X-Coil Channels 1-20	pT/s
y01-y20	Final dB/dt Y-Coil Channels 1-20	pT/s
z01-z20	Final dB/dt Z-Coil Channels 1-20	pT/s
Bx01-Bx20	Final B-Field X-coil Channels 1-20	fT
By01-By20	Final B-Field Y-coil Channels 1-20	fT
Bz01-Bz20	Final B-Field Z-coil Channels 1-20	fT

Grid Archive File Description:

The grids are in Geosoft format. A grid cell size of 30 m was used for all area grids.

FILE	DESCRIPTION	UNITS
area_rmi.grd	Residual Magnetic Intensity	nT
area_1vd.grd	First Vertical Derivative	nT/m
area_teeb10.grd	Total Energy Envelope from B field Ch 10	fT
area_cond_1o.grd	Apparent Conductance from 1 st Order moment of B Field X Coil	mS



Line List for North Range Block 1:

FLIGHT	LINE	PART	START FIDUCIAL	END FIDUCIAL
10	1001	1	54473	54618
10	1002	1	54757	54902
10	1003	1	55058	55203
10	1004	1	55342	55487
10	1005	1	55636	55780
12	1006	1	64683	64820
12	1007	1	68189	68345
12	1008	1	65220	65356
12	1009	1	68725	68883
12	1010	1	65747	65886
12	1011	1	69248	69404
12	1012	1	66277	66417
12	1013	1	69753	69910
12	1014	1	66810	66948
12	1015	1	70271	70427
12	1016	1	67356	67493
12	1017	1	70771	70924
12	1018	1	67911	68048
12	1019	1	64929	65086
12	1020	1	68461	68598
12	1021	1	65475	65631
12	1022	1	69000	69139
12	1023	1	66003	66155
12	1024	1	69504	69644
12	1025	1	66532	66689
12	1026	1	70018	70159
12	1027	1	67067	67226
12	1028	1	70527	70665
12	1029	1	67624	67780
12	1030	1	71040	71176
12	1031	1	71322	71480
12	1032	1	71607	71746
12	1033	1	71923	72075
12	1034	1	72232	72369
12	1035	1	72524	72679
13	1036	1	42511	42667
13	1037	1	46049	46191
13	1038	1	43045	43198
13	1039	1	46593	46737
13	1040	1	43587	43739

13	1041	1	47124	47269
13	1042	1	44137	44289
13	1043	1	47663	47806
13	1044	1	44671	44824
13	1045	1	48191	48334
13	1046	1	45206	45357
13	1047	1	48702	48842
13	1048	1	45762	45914
13	1049	1	42772	42912
13	1050	1	46317	46469
13	1051	1	43317	43458
13	1052	1	46860	47014
13	1053	1	43869	44012
13	1054	1	47380	47533
13	1055	1	44396	44537
13	1056	1	47923	48073
13	1057	1	44940	45081
13	1058	1	48447	48599
13	1059	1	45494	45634
13	1060	1	48956	49109
13	1061	1	53342	53487
13	1062	1	49516	49670
13	1063	1	53908	54053
13	1064	1	50065	50217
13	1065	1	54428	54571
13	1066	1	50590	50740
13	1067	1	54939	55084
13	1068	1	51122	51273
13	1069	1	55458	55603
13	1070	1	51661	51811
13	1071	1	55960	56104
13	1072	1	52203	52354
13	1073	1	49246	49390
13	1074	1	53606	53755
13	1075	1	49790	49935
13	1076	1	54163	54310
13	1077	1	50330	50475
13	1078	1	54684	54835
13	1079	1	50851	50998
13	1080	1	55190	55339
13	1081	1	51386	51533
13	1082	1	55704	55851
13	1083	1	51943	52090
13	1084	1	56208	56360

13	1085	1	52493	52642
13	1086	1	52835	52983
11	1087	1	58469	58619
11	1088	1	58160	58306
11	1089	1	57879	58028
11	1090	1	57582	57726
11	1091	1	57287	57438
11	1092	1	57010	57155
11	1093	1	56721	56872
11	1094	1	56439	56582
11	1095	1	56148	56299
11	1096	1	55865	56009
11	1097	1	55577	55729
11	1098	1	55290	55436
11	1099	1	55007	55158
11	1100	1	54726	54873
11	1101	1	54446	54599
11	1102	1	54166	54312
11	1103	1	53880	54032
11	1104	1	53595	53741
11	1105	1	53279	53430
11	1106	1	52987	53133
11	1107	1	49013	49164
11	1108	1	52464	52611
11	1109	1	48478	48628
11	1110	1	51935	52081
11	1111	1	47923	48074
11	1112	1	51383	51530
11	1113	1	47366	47517
11	1114	1	50639	50788
11	1115	1	46799	46950
12	1116	1	72887	73024
11	1117	1	46201	46351
11	1118	1	49283	49434
11	1119	1	52729	52881
11	1120	1	48755	48908
11	1121	1	52204	52353
11	1122	1	48219	48367
11	1123	1	51672	51821
11	1124	1	47651	47802
11	1125	1	50938	51088
11	1126	1	47093	47239
11	1127	1	50372	50520
11	1128	1	46511	46659

11	1129	1	49605	49754
11	1130	1	45893	46040
6	1131	1	75364	75520
6	1132	1	75076	75219
6	1133	1	74797	74959
6	1134	1	74518	74668
6	1135	1	74216	74382
6	1136	1	73939	74089
6	1137	1	73650	73814
6	1138	1	73375	73524
6	1139	1	73077	73243
6	1140	1	72819	72965
6	1141	1	72501	72664
6	1142	1	72218	72368
6	1143	1	71939	72103
6	1144	1	71655	71798
6	1145	1	71373	71531
6	1146	1	71081	71224
6	1147	1	70792	70951
6	1148	1	70493	70636
6	1149	1	70214	70369
6	1150	1	69891	70032
6	1151	1	69584	69762
6	1152	1	69271	69427
6	1153	1	68973	69146
6	1154	1	68672	68830
6	1155	1	68367	68542
6	1156	1	68048	68206
6	1157	1	67727	67904
6	1158	1	67422	67580
6	1159	1	67110	67285
6	1160	1	66820	66976
6	1161	1	66502	66677
6	1162	1	66196	66357
6	1163	1	65892	66067
6	1164	1	65586	65747
6	1165	1	65232	65407
6	1166	1	64922	65082
6	1167	1	64611	64788
6	1168	1	64283	64444
6	1169	1	63959	64132
4	1170	1	68669	68828
4	1171	1	68325	68502
4	1172	1	68023	68182



4	1173	1	67689	67862
4	1174	1	67397	67556
4	1175	1	67077	67251
4	1176	1	66774	66933
4	1177	1	66474	66649
10	1801	1	51994	52410
10	1802	1	52507	52854
10	1803	1	52966	53373
10	1804	1	53469	53812
10	1805	1	53925	54327

Line List for North Range Block 2:

FLIGHT	LINE	PART	START FIDUCIAL	END FIDUCIAL
10	2001	1	49569	49731
10	2002	1	49243	49424
10	2003	1	48930	49090
10	2004	1	48617	48795
10	2005	1	48317	48479
10	2006	1	47996	48179
10	2007	1	47699	47859
10	2008	1	47385	47569
10	2009	1	47070	47229
10	2010	1	46757	46941
10	2011	1	46448	46609
10	2012	1	46138	46322
10	2013	1	45821	45982
10	2014	1	45502	45688
10	2015	1	44721	44818
10	2015	1	44923	45077
10	2015	1	45191	45349
10	2016	1	44427	44613
10	2017	1	44106	44267
10	2018	1	43798	43984
10	2019	1	43499	43658
10	2020	1	43199	43387
10	2021	1	42889	43048
10	2022	1	42574	42765
9	2023	1	73502	73656
9	2024	1	73171	73359
9	2025	1	72858	73012
9	2026	1	72512	72703
9	2027	1	72203	72353

9	2028	1	71866	72056
9	2029	1	71553	71705
9	2030	1	71226	71420
9	2031	1	70915	71072
9	2032	1	70602	70795
9	2033	1	70300	70455
9	2034	1	69993	70184
9	2035	1	69690	69844
9	2036	1	69390	69577
9	2037	1	69076	69233
9	2038	1	68759	68946
9	2039	1	68458	68616
9	2040	1	68143	68332
9	2041	1	67822	67977
9	2042	1	67482	67669
9	2043	1	67151	67306
9	2044	1	66800	66986
9	2045	1	66486	66641
9	2046	1	66148	66334
9	2047	1	65819	65976
9	2048	1	65483	65669
9	2049	1	65159	65317
9	2050	1	64819	65004
9	2051	1	64462	64621
9	2052	1	64094	64275
9	2053	1	63785	63942
9	2054	1	63475	63665
9	2055	1	63169	63324
9	2056	1	62845	63026
9	2057	1	62541	62699
9	2058	1	62177	62364
9	2059	1	61874	62031
9	2060	1	61527	61717
9	2061	1	61232	61389
9	2062	1	60907	61095
9	2063	1	60603	60759
8	2064	1	87546	87700
8	2065	1	87244	87399
8	2066	1	86951	87106
8	2067	1	86658	86815
8	2068	1	86365	86522
8	2069	1	86040	86203
8	2070	1	85740	85897
8	2071	1	85431	85592

8	2072	1	85128	85287
8	2073	1	84801	84966
8	2074	1	84494	84653
8	2075	1	84193	84357
8	2076	1	83886	84043
8	2077	1	83568	83735
8	2078	1	83261	83419
8	2079	1	82952	83115
8	2080	1	82662	82814
8	2081	1	82388	82548
8	2082	1	82103	82257
8	2083	1	81820	81974
8	2084	1	81537	81690
8	2085	1	81258	81417
8	2086	1	80977	81128
8	2087	1	80692	80850
8	2088	1	80408	80559
8	2089	1	80105	80266
8	2090	1	79816	79967
8	2091	1	79528	79690
8	2092	1	79243	79394
8	2093	1	78946	79106
8	2094	1	78631	78784
8	2095	1	78324	78482
8	2096	1	78030	78182
8	2097	1	77728	77888
8	2098	1	77425	77576
8	2099	1	77122	77280
8	2100	1	76820	76973
8	2101	1	76503	76663
8	2102	1	76189	76339
8	2103	1	75880	76038
8	2104	1	75571	75723
8	2105	1	75264	75422
7	2106	1	63054	63209
7	2107	1	62733	62902
7	2108	1	62446	62598
7	2109	1	62124	62293
7	2110	1	61837	61993
7	2111	1	61510	61681
7	2112	1	61216	61369
7	2113	1	60897	61063
7	2114	1	60602	60754
6	2115	1	63419	63572



6	2116	1	63100	63268
6	2117	1	62791	62941
6	2118	1	62456	62627
6	2119	1	62152	62302
6	2120	1	61817	61986
6	2121	1	61501	61653
6	2122	1	61170	61339
6	2123	1	60843	60996
5	2124	1	82111	82264
5	2125	1	81788	81958
5	2126	1	81485	81641
5	2127	1	81156	81326
5	2128	1	80855	81010
5	2129	1	80530	80696
5	2130	1	80229	80383
5	2131	1	79896	80064
5	2132	1	79614	79770
10	2801	1	51378	51636
10	2802	1	50989	51288
10	2803	1	50627	50886
10	2804	1	50225	50533
10	2805	1	49855	50113

Line List for North Range Block 3:

FLIGHT	LINE	PART	START FIDUCIAL	END FIDUCIAL
5	3001	1	77696	77848
5	3002	1	77423	77562
5	3003	1	77106	77258
5	3004	1	76826	76964
5	3005	1	76517	76671
5	3006	1	76236	76375
5	3007	1	75920	76073
5	3008	1	75633	75771
5	3009	1	75337	75490
5	3010	1	75054	75194
5	3011	1	74748	74903
5	3012	1	74474	74614
5	3013	1	74140	74295
5	3014	1	73849	73986
5	3015	1	73538	73695
5	3016	1	73252	73390
5	3017	1	72797	72950
5	3018	1	72490	72627

5	3019	1	72164	72317
5	3020	1	71876	72014
5	3021	1	71573	71727
5	3022	1	71272	71412
5	3023	1	70963	71118
5	3024	1	70686	70824
5	3025	1	70371	70525
5	3026	1	70063	70201
5	3027	1	69768	69922
5	3028	1	69485	69624
5	3029	1	69196	69348
5	3030	1	68916	69056
4	3031	1	65798	65940
4	3032	1	65515	65661
3	3033	1	83317	83466
3	3034	1	83054	83186
3	3035	1	82788	82935
3	3036	1	82514	82648
3	3037	1	82242	82386
3	3038	1	81977	82111
3	3039	1	81704	81850
3	3040	1	81433	81569
3	3041	1	81145	81289
3	3042	1	80876	81015
3	3043	1	80559	80708
3	3044	1	80288	80428
3	3045	1	79994	80142
3	3046	1	79716	79854
3	3047	1	79435	79580
3	3048	1	79157	79291
3	3049	1	78854	78998
3	3050	1	78581	78718
3	3051	1	78302	78447
3	3052	1	78039	78173
3	3053	1	77728	77872
3	3054	1	77467	77605
3	3055	1	77153	77299
3	3056	1	76877	77015
3	3057	1	76564	76711
3	3058	1	76282	76421
3	3059	1	75989	76133
3	3060	1	75727	75867
3	3061	1	75436	75583
3	3062	1	75162	75303



3	3063	1	74863	75008
3	3064	1	74583	74726
3	3065	1	74299	74444
3	3066	1	74027	74170
3	3067	1	73739	73883
3	3068	1	73465	73607
3	3069	1	73191	73335
3	3070	1	72916	73061
3	3071	1	72642	72786
3	3072	1	72369	72510
3	3073	1	72108	72249
3	3074	1	71826	71966
3	3075	1	71561	71704
3	3076	1	71275	71414
3	3077	1	71010	71152
3	3078	1	70723	70863
3	3079	1	70448	70591
3	3080	1	70171	70310
3	3081	1	69897	70041
3	3082	1	69617	69756
3	3083	1	69343	69488
3	3084	1	69070	69208
5	3801	1	82489	82676
5	3802	1	79023	79214
5	3803	1	78698	78885
5	3804	1	78367	78559
5	3805	1	78022	78213

Line List for Airport Property:

FLIGHT	LINE	PART	START FIDUCIAL	END FIDUCIAL
1	4001	1	45421	45538
1	4002	1	46001	46104
1	4003	1	46259	46380
1	4004	1	46538	46642
1	4005	1	46785	46905
1	4006	1	47065	47167
1	4007	1	47316	47436
1	4008	1	47586	47691
1	4009	1	47820	47938
1	4010	1	48101	48206
1	4011	1	48344	48461
1	4012	1	48607	48713
1	4013	1	48866	48982

1	4014	1	49111	49217
1	4015	1	49979	50096
1	4016	1	50213	50319
1	4017	1	50479	50596
1	4018	1	50714	50819
1	4019	1	50965	51082
1	4020	1	51197	51301
1	4021	1	51501	51618
1	4022	1	51737	51841
1	4023	1	51987	52107
1	4024	1	52226	52330
1	4025	1	52476	52594
1	4026	1	52701	52800
1	4027	1	52930	53047
1	4028	1	53163	53266
1	4029	1	53417	53535
1	4030	1	53649	53759
1	4031	1	53903	54031
1	4032	1	54144	54252
1	4033	1	54387	54516
1	4034	1	54638	54747
1	4035	1	54897	55028
1	4036	1	55137	55246
1	4037	1	55375	55505
1	4038	1	55613	55722
1	4039	1	55910	56042
1	4040	1	56160	56268
1	4801	1	56979	57067
1	4802	1	56774	56879
1	4803	1	56420	56507



Appendix F

TDEM ANOMALY SELECTION

Current approach to TDEM anomaly selection

The current routine for the selection and fitting of EM anomalies is still based on the University of Toronto plate program which fits the response (at the anomaly peak) from the X-coil channels to a vertical plate nomogram. Given that the current GEOTEM and MEGATEM system have evolved to offer the response from coils of 3 different orientations (X, Y and Z) and from dB/dt and B-Field, this approach to the classification of the anomalies is limited and no longer fully reflects all the information being measured by the system. The resulting shortcomings are:

- All anomaly peaks, from the x-coil response, are fitted to a vertical plate model of fixed dimensions, regardless of the nature of the conductive source. The derived CTP and depth-to-source values are then only valid if the conductor can be properly represented by a vertical plate. CTP and depth values derived from “non vertical plate” type conductors will be erroneous. In some conductive terrains, marked by prominent conductive overburden or surface alteration of other sorts, “non-vertical” type conductors may represent 90 % or more of the conductive response.
- The response from the conductor must deflect a minimum of 6 channels above the background to be fitted to the nomogram. CTP or depth-to-source values will not be calculated for a valid but weaker response (a weak or deep source).
- Only the response from the X-coil channels are used in the selection and fitting. A response appearing only on the Z-coil will not be identified. This is sometimes the case for a very deep source. As the depth to the conductor increases, although it may have considerable depth extent, the system becomes less sensitive to the vertical extent of the body and conductors will appear to be more flat-lying than vertical. As a result, as depth of burial increases, the coupling of the response may disappear on the X-coil response but will persist on the Z-coil response (see figure 1, anomalies A and B).
- The fitting of the response is only done from the amplitudes at the peak position of the anomaly and does not take-in the full shape of the anomaly or relate the difference in response between the X-coil and Z-coil. This does not allow for the distinction between vertical, flat-lying or dipping plates.

Fugro is presently working on the development of a new anomaly selection and classification routine which will use a window of data centered about the anomaly peak (to properly define the entire anomaly shape), using both the response from the X and Z coils and fitting to a suite of models from flat-lying to dipping to vertical plates and spheres. This will hopefully address all the above shortcomings of the present method.

Unfortunately the current anomaly fitting program must continue to be in use until this new routine is made available. Until such time, our approach is to present the full information being measured by the system within the confines of the present program's limitations. Some responses may not be visible on the regular channels of the dB/dt X-coil data but will be identified on either the B-Field response or the Z-coil response. The initial selection of the anomalies is still being derived from the X-coil channels of the dB/dt data but at the “review” stage (via a graphic screen editor), the response from all components (X and Z, dB/dt and B-Field) are examined. All significant responses from any of the components are inserted in the anomaly field. Since all anomaly edits are still being updated by the same routine, again only fitting the X-coil response from the dB/dt data, many of these “other” responses which have no measurable signature on the dB/dt X-coil data will only be flagged as an anomaly location with no measurable response suitable for fitting to the reference nomogram.

Although improperly represented, these “other” anomalies, at the very least, are identified by their location in the EM anomaly database (listing) and on the anomaly map.

Figures 1 and 2 provide examples of a typical display of the channel data used when reviewing the EM anomaly selection. Given the limited space available on a computer screen, a good display can include every even numbered channel, 8 to 20 (in more resistive areas, often all off-time channels can be displayed) for X and Z for both dB/dt and B-Field, along with the Hz monitor and the radar altimeter (the EM primary field can also be very useful).

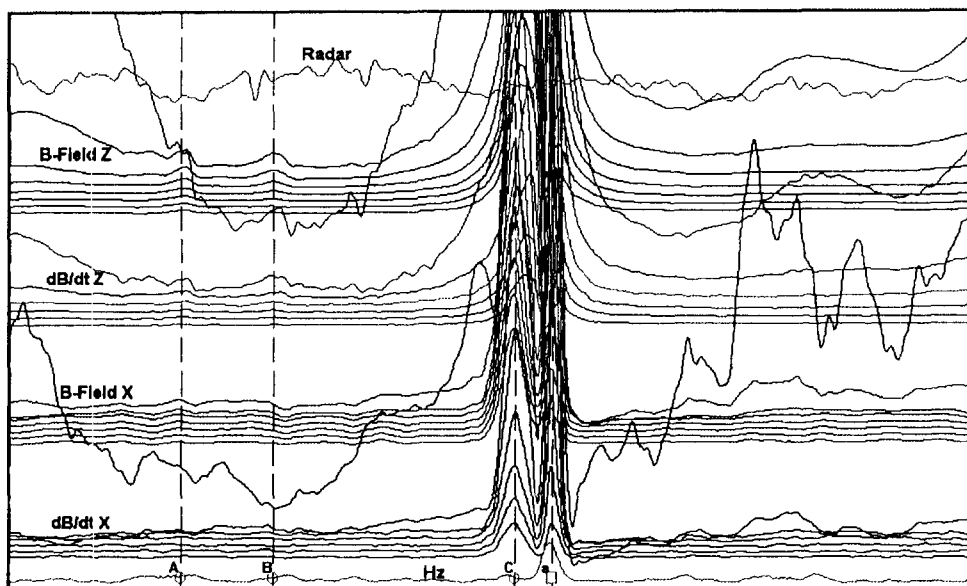


Figure 1

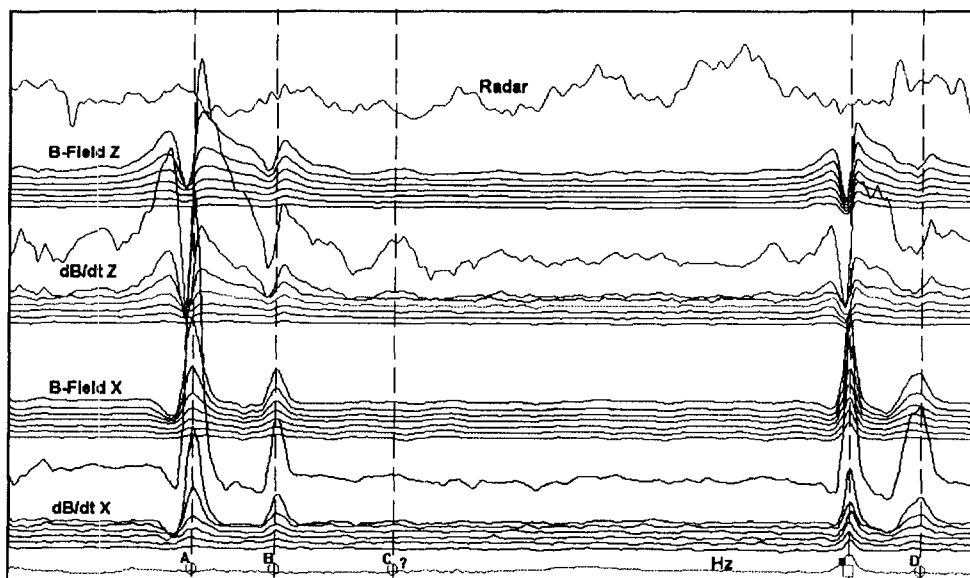


Figure 2

In **Figure 1**, anomalies identified as A and B could be indicative of a very deep source, where the coupling of the response is lost on the X-coil but persists on the Z-coil. The dB/dt X-coil response is devoid of any response while a weak response is visible of the Z-coil of the dB/dt response. Greater support for this selection is provided by the response on the B-Field. Although weak and very questionable on the X-coil (close to the noise level) the response is clearly marked on the Z-coil, as a low amplitude response of slow decay. This is a good indication of a high conductance body having a long time constant and therefore enhanced by the B-Field. These two anomalies may be prime targets for mineralization but will be indistinguishable from weak surface responses, as represented on the anomaly map or in the anomaly listing. Hence, the importance of always reviewing the EM anomaly selection against the data profiles.

In **Figure 2**, anomaly C? is similar to the responses discussed in Figure 1 above, in that it presents no measurable signature on the X-coil response (for both dB/dt and B-Field) but a weak response on the Z-coil response. The difference here however, is that the B-Field response does not show an enhancement of the response on the Z-coil but an attenuation. This is indicative of a conductive response with a short time constant and hence more likely a weak surficial source.

The anomalies discussed in Figures 1 and 2 have very similar characteristics on dB/dt X and Z and B-Field X and yet may reflect very different conductive sources, one being of potentially economic interest. The only distinguishing signature is offered by the B-Field Z-coil response. Be aware that these differences are not properly accounted for in the current anomaly selection and presentation process.

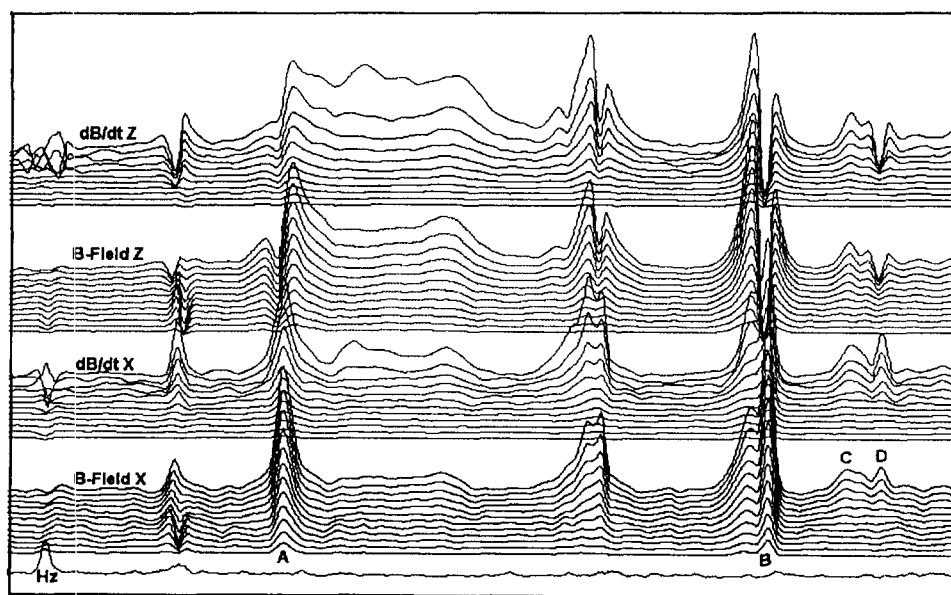
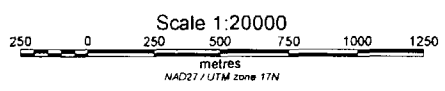
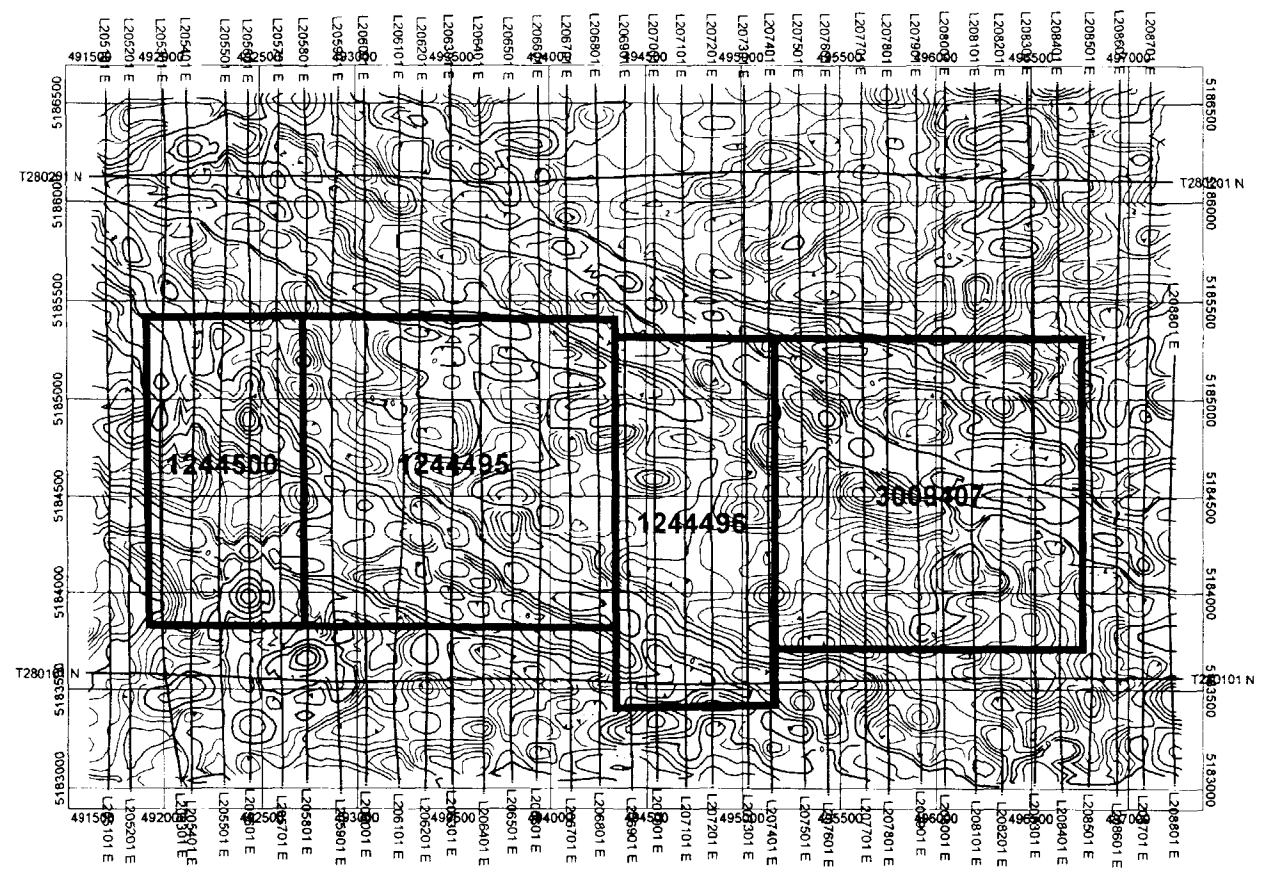


Figure 3

Figure 3 shows the importance of looking at the response with all components when evaluating the possible source of a conductive response. Anomalies identified as A and B look quite similar on the

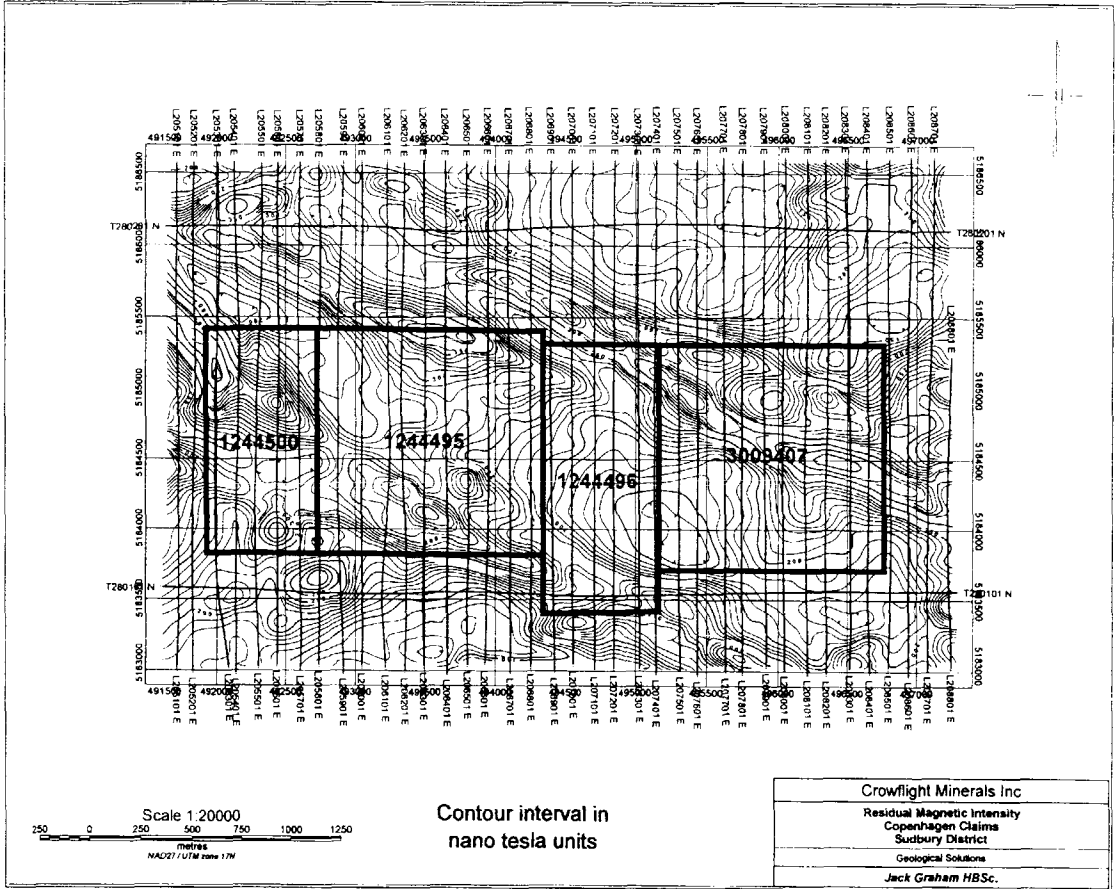
X-coil response and could both be interpreted as narrow, vertical conductors. However, looking at the response on the Z-coil clearly shows that anomaly A is the leading edge of a broad tabular body, better displayed on Z because of the enhanced coupling with the Z-coil, whereas anomaly B does reflect a narrow, near-vertical conductor. Anomalies C and D again look very similar on the response from the X-coil and could be interpreted as related to the same source. However, the response on the Z-coil indicates that the response at C is from a tabular or flat-lying source whereas the response at D is from a vertical source.

RESULTS



Contour interval in
nano tesla units

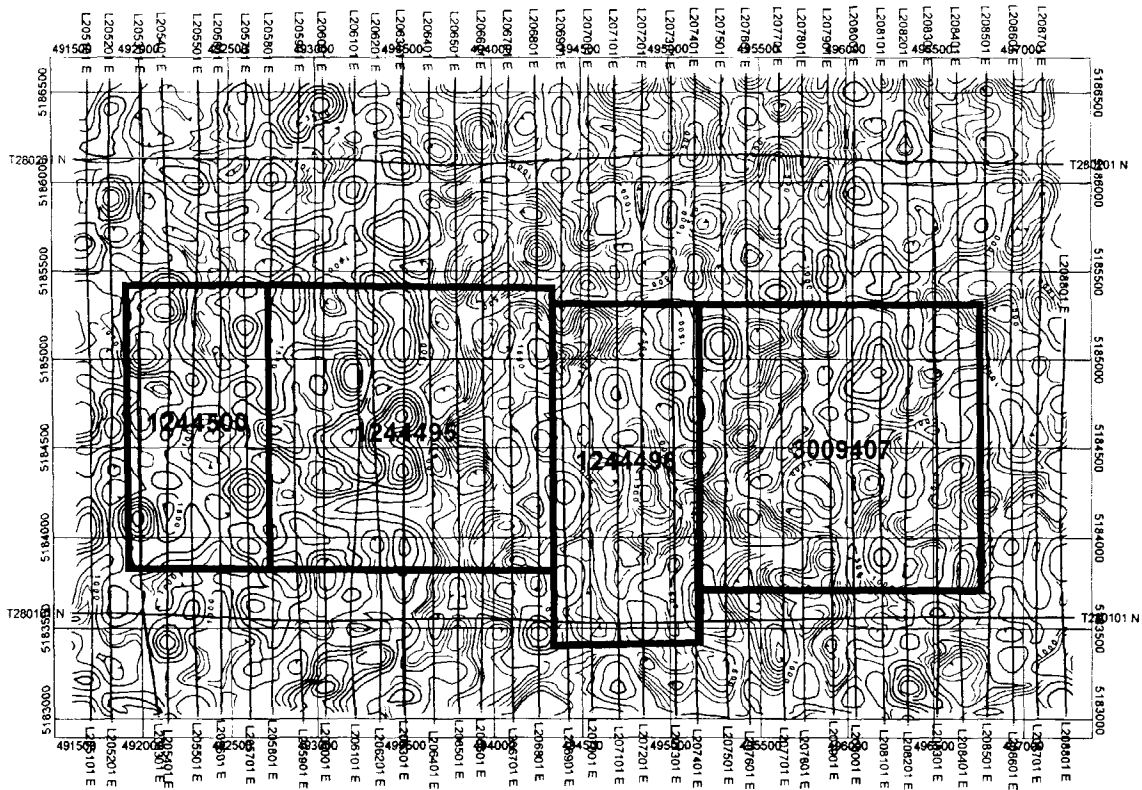
Crowflight Minerals Inc
Residual Magnetic Intensity: First Vertical Derivative Copenhagen Claims Sudbury District
Geological Solutions
Jack Graham HBSc.



Scale 1:20000
 250 0 250 500 750 1000 1250
 metres
 NAD27 / UTM zone 17N

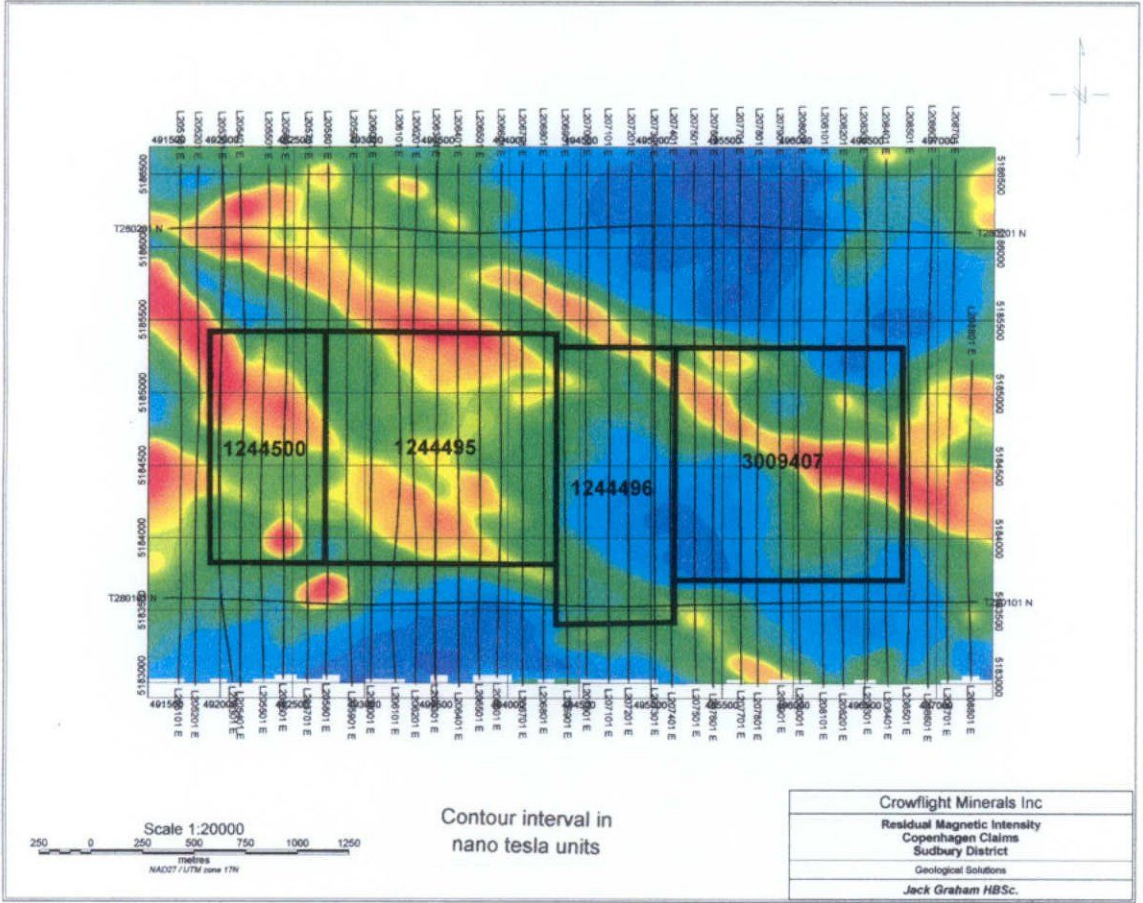
Contour interval in
 nano tesla units

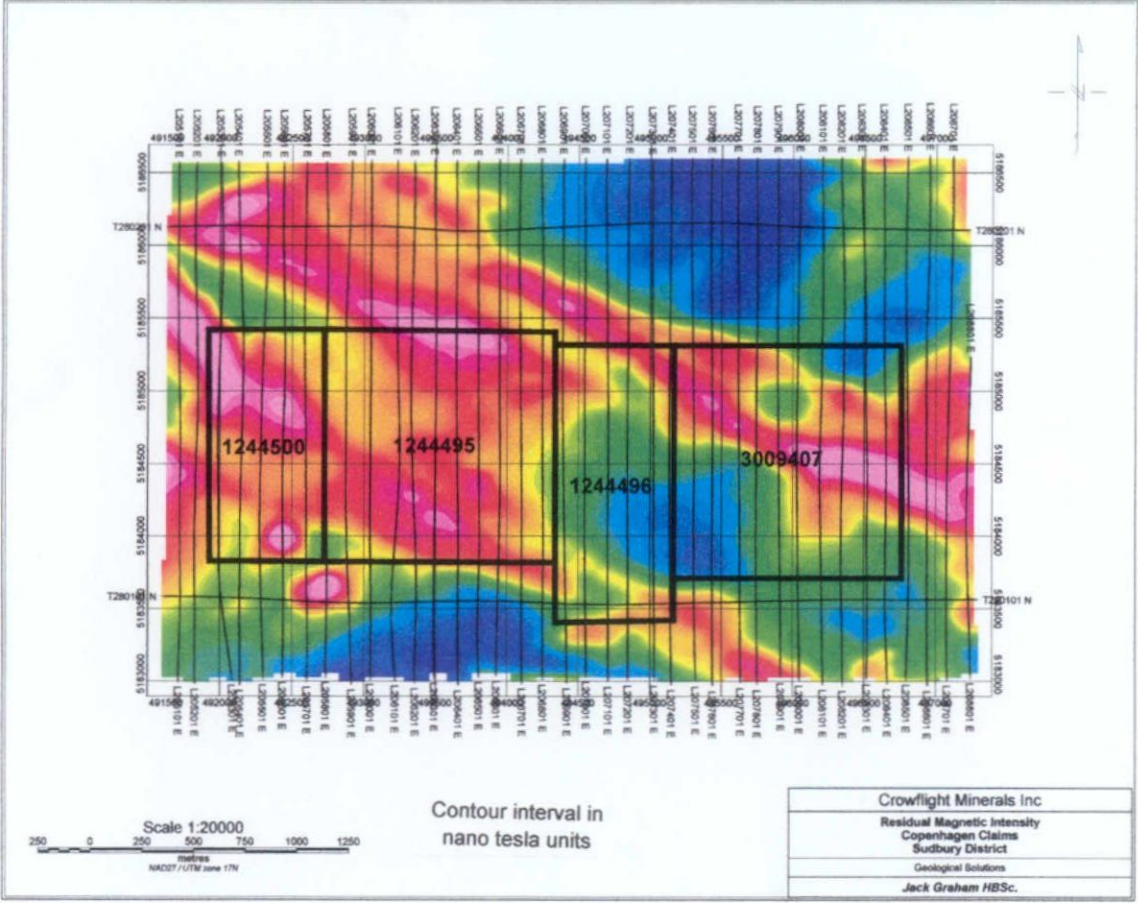
Crowflight Minerals Inc
Residual Magnetic Intensity
Copenhagen Claims
Sudbury District
Geological Solutions
Jack Graham H.B.Sc.



Contour interval in
femto tesla units

Crowflight Minerals Inc
Total Energy Envelope of the B-Field Copenhagen Claims Sudbury District
Geological Solutions
Jack Graham HBSc.

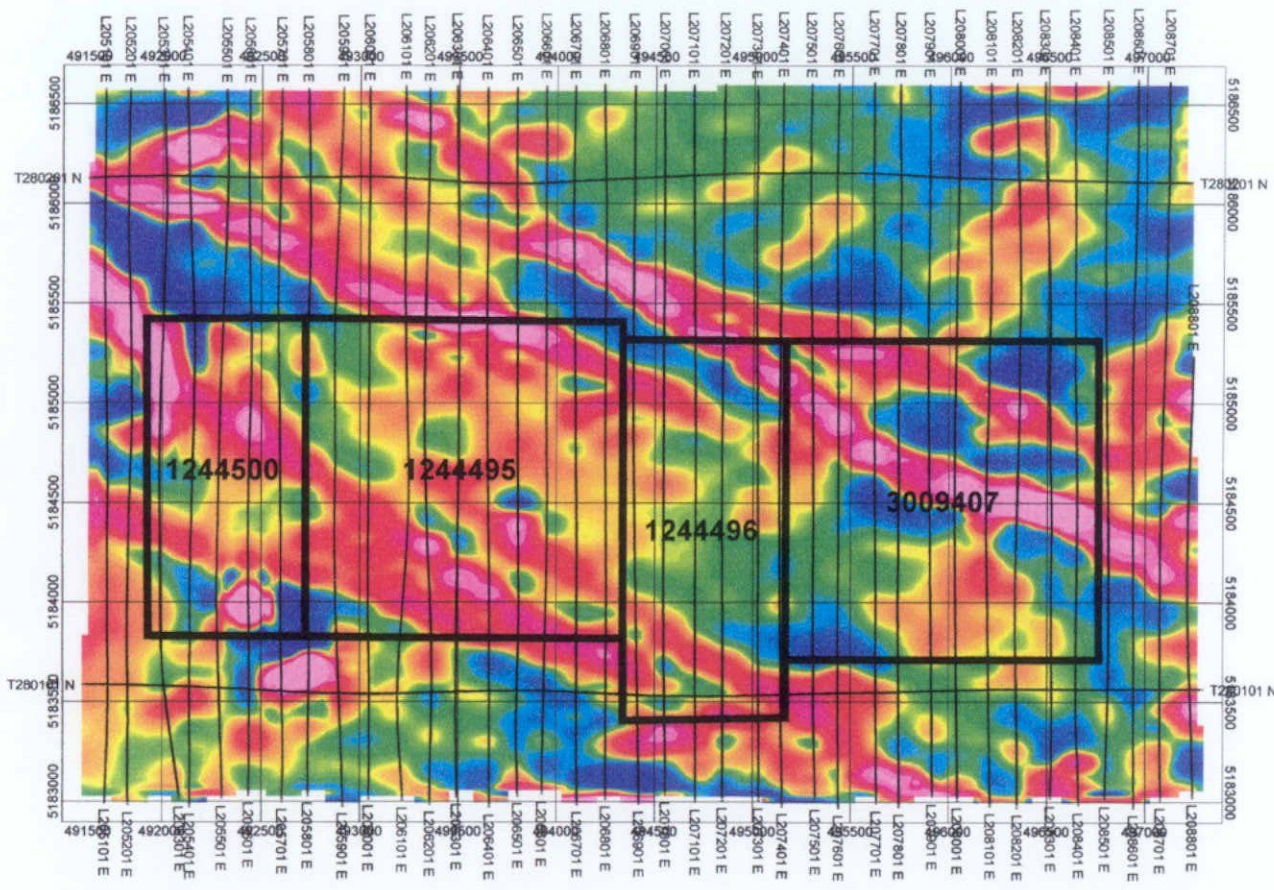




Scale 1:20000
 250 0 250 500 750 1000 1250
 metres
 NAD83 / UTM zone 17N

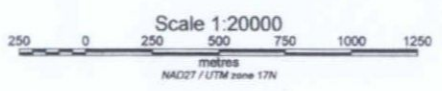
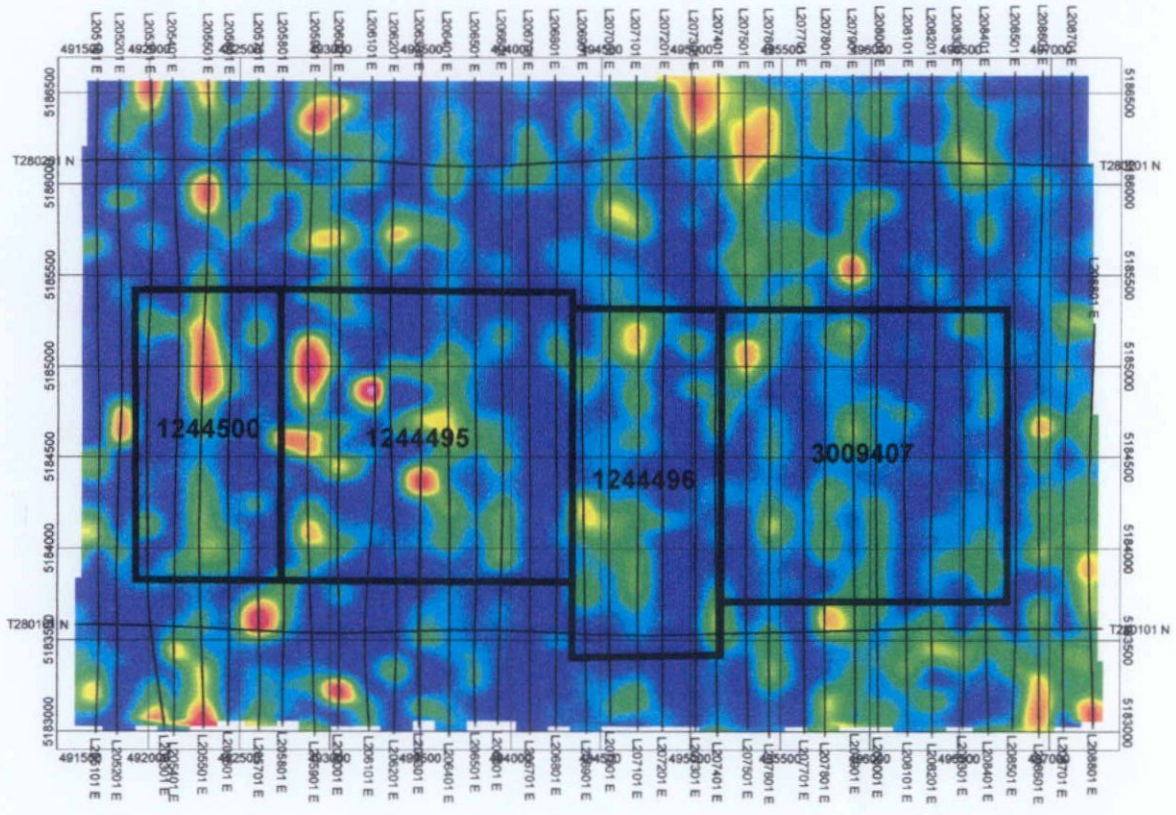
Contour interval in
 nano tesla units

Crowflight Minerals Inc
Residual Magnetic Intensity
Copenhagen Claims
Sudbury District
Geological Solutions
Jack Graham HBSc.



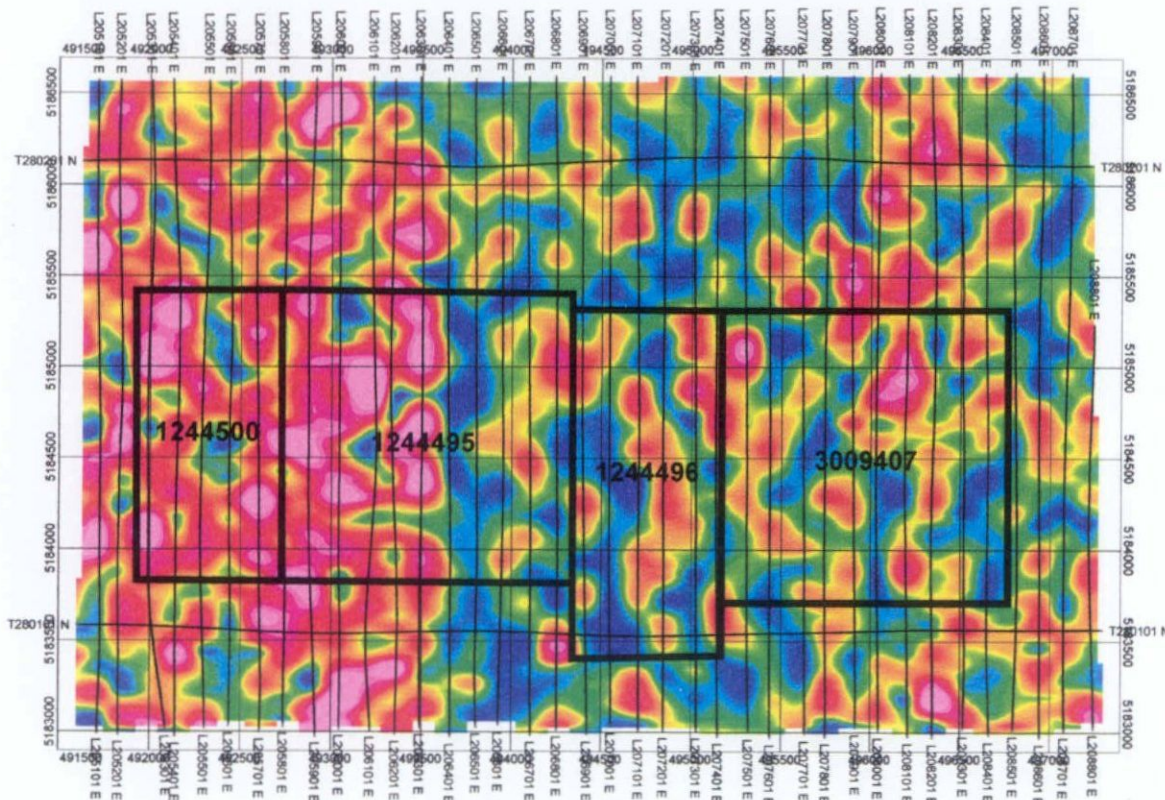
Contour interval in
nano tesla units

Crowflight Minerals Inc
Residual Magnetic Intensity: First Vertical Derivative Copenhagen Claims Sudbury District
Geological Solutions
Jack Graham HBSc.



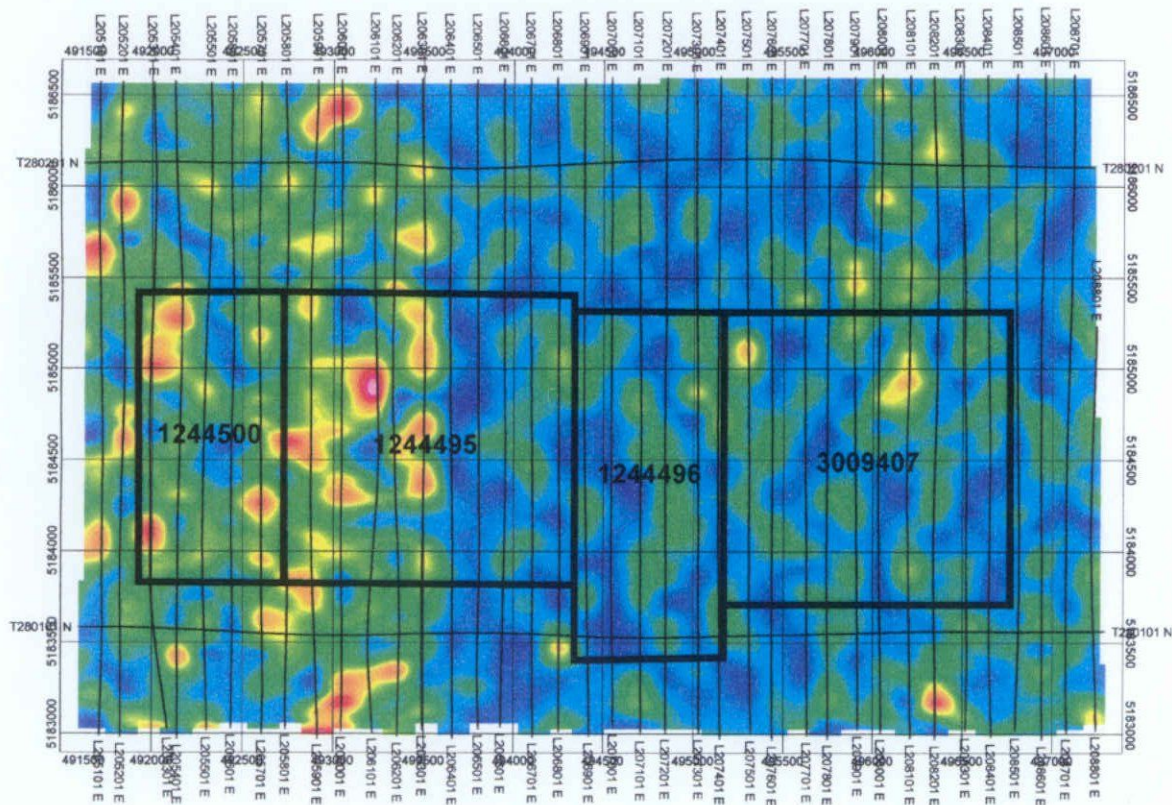
Contour interval in
femto tesla units

Crowflight Minerals Inc
Apparent Conductance Copenhagen Claims Sudbury District
Geological Solutions
Jack Graham HBSc.



Contour interval in femto tesla units

Crowflight Minerals Inc
Total Energy Envelope of the B-Field Copenhagen District Sudbury District
Geological Solutions
Jack Graham HBSc.



Contour interval in
femto tesla units

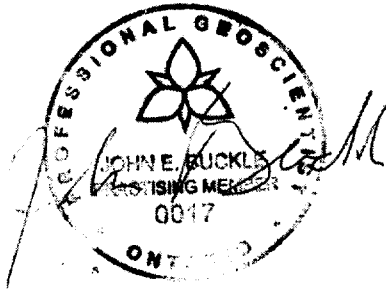
Crowflight Minerals Inc
Total Energy Envelope of the B-Field Copenhagen Claims Sudbury District
Geological Solutions
Jack Graham HBSc.

STATEMENT OF QUALIFICATIONS

I, John Buckle, hereby declare that:

1. I am a geoscientist with residence in Waterdown, Ontario
2. I am presently the principal of Geological Solutions of Waterdown Ontario.
3. I am a registered professional geoscientist with the Association of Professional Geoscientists of Ontario, member number 0017.
4. I have practiced my profession since 1972, in Canada, the United States, Chile, Argentina, Peru and Brazil.
5. The geophysical data that is the subject of this report was collected under my supervision.
6. I do not hold securities in Crowflight minerals nor do I have direct or indirect interest in this property.
7. I am the author of this report

Waterdown
September 27, 2004



Distribution of Assessment Work Credit

The following credit distribution reflects the value of assessment work performed on the mining land(s).

Date: 2005-JAN-25

Submission Number: 2.28573

Transaction Number: W0470.01587

Claim Number	Value of Work Performed
S 1244495	2,825.00
S 1244496	1,874.00
S 1244500	1,284.00
Total:	\$5,983.00

Date: 2005-JAN-25

GEOSCIENCE ASSESSMENT OFFICE
933 RAMSEY LAKE ROAD, 6th FLOOR
SUDBURY, ONTARIO
P3E 6B5

JOHN GREGORY BRADY
1227 HOLLAND ROAD
SUDBURY, ONTARIO
P3A 3R1 CANADA

Tel: (888) 415-9845
Fax: (877) 670-1555

Submission Number: 2.28573
Transaction Number(s): W0470.01587

Dear Sir or Madam

Subject: Approval of Assessment Work

We have approved your Assessment Work Submission with the above noted Transaction Number(s). The attached Work Report Summary indicates the results of the approval.

At the discretion of the Ministry, the assessment work performed on the mining lands noted in this work report may be subject to inspection and/or investigation at any time.

The value of work approved for this submission is \$5983.00 as outlined on the attached Work Report Summary.

If you have any question regarding this correspondence, please contact LUCILLE JEROME by email at lucille.jerome@ndm.gov.on.ca or by phone at (705) 670-5858.

Yours Sincerely,



Ron C. Gashinski
Senior Manager, Mining Lands Section

Cc: Resident Geologist

John Gregory Brady
(Claim Holder)

Assessment File Library

John Gregory Brady
(Assessment Office)



Date / Time of Issue: Fri Feb 18 15:22:09 EST 2005

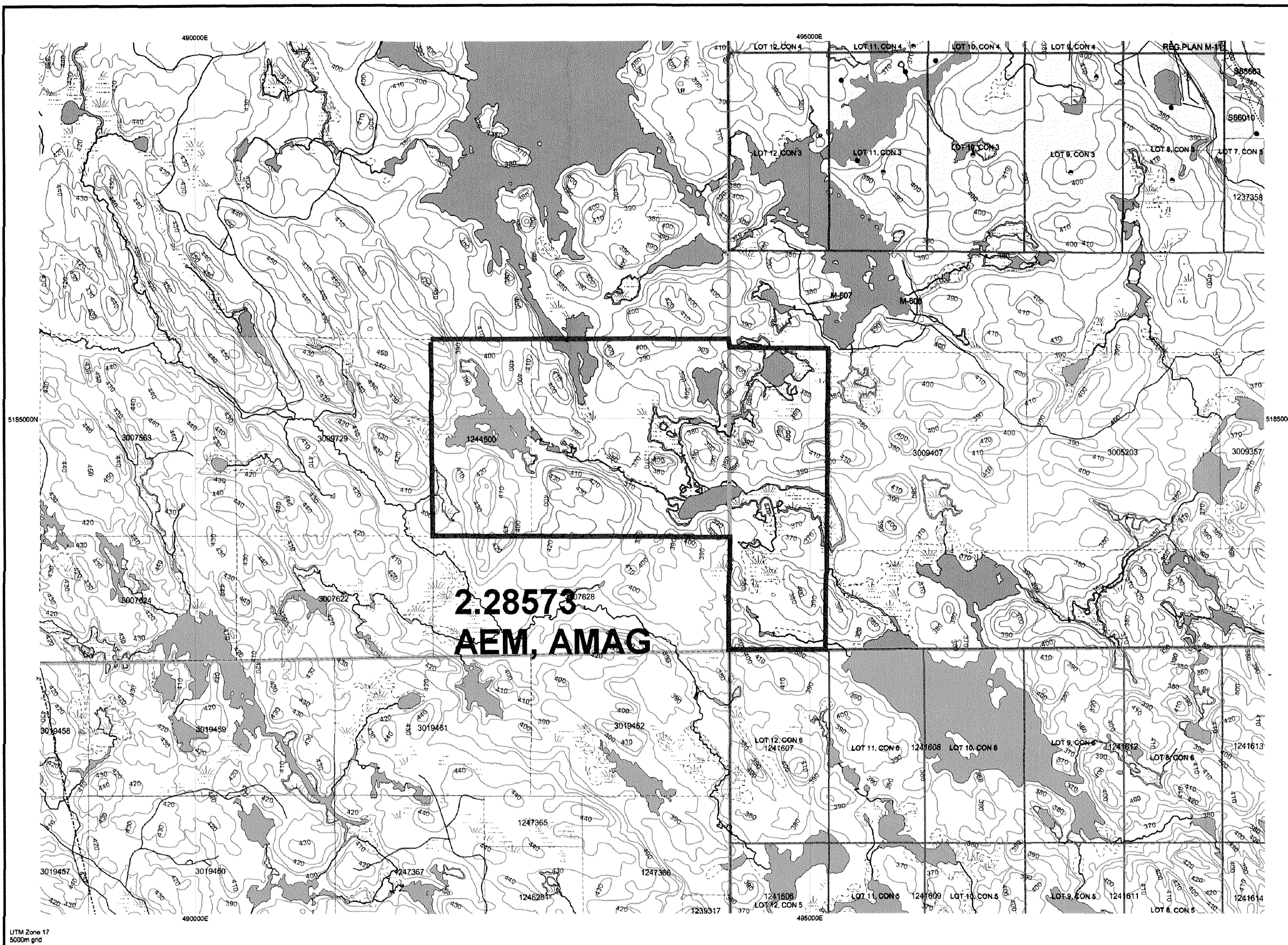
TOWNSHIP / AREA
KITCHENER

PLAN
G-4069

ADMINISTRATIVE DISTRICTS / DIVISIONS

Mining Division
Land Titles/Registry Division
Ministry of Natural Resources District

Sudbury
SUDBURY
SUDBURY



TOPOGRAPHIC

- Administrative Boundaries
- Township
- Concession Lot
- Provincial Park
- Indian Reserve
- Cliff, Pit & Pile
- Contour
- Mine Shafts
- Mine Headframe
- Railway
- Road
- Trail
- Natural Gas Pipeline
- Utilities
- Tower

Land Tenure

- Freehold Patent**
 - Surface And Mining Rights
 - Surface Rights Only
 - Mining Rights Only
- Leasehold Patent**
 - Surface And Mining Rights
 - Surface Rights Only
 - Mining Rights Only
- Licence of Occupation**
 - Uses Not Specified
 - Surface And Mining Rights
 - Surface Rights Only
 - Mining Rights Only
 - Land Use Permit
 - Order In Council (Not open for staking)
 - Water Power Lease Agreement

MINING CLAIM	FILED ONLY MINING CLAIMS
1234567	1234567
1234567	1234567

LAND TENURE WITHDRAWALS

- Areas Withdrawn from Disposition
- Mining Acts Withdrawal Types**
 - Surface And Mining Rights Withdrawn
 - Surface Rights Only Withdrawn
 - Mining Rights Only Withdrawn
- Order In Council Withdrawal Types**
 - Surface And Mining Rights Withdrawn
 - Surface Rights Only Withdrawn
 - Mining Rights Only Withdrawn

IMPORTANT NOTICES



Those wishing to stake mining claims should consult with the Provincial Mining Recorders' Office of the Ministry of Northern Development and Mines for additional information on the status of the lands shown hereon. This map is not intended for navigational, survey, or land title determination purposes as the information shown on this map is compiled from various sources. Completeness and accuracy are not guaranteed. Additional information may also be obtained through the local Land Titles or Registry Office, or the Ministry of Natural Resources.

The information shown is derived from digital data available in the Provincial Mining Recorders' Office at the time of downloading from the Ministry of Northern Development and Mines web site.

General Information and Limitations
 Contact Information:
 Provincial Mining Recorders' Office
 Willet Green Miller Centre 933 Ramsey Lake Road
 Sudbury ON P3E 6B5
 Home Page: www.mndm.gov.on.ca/MNDM/MINESLANDS/mismnpgp.htm

Toll Free
 Tel: 1 (888) 415-9845 ext 57
 Fax: 1 (877) 670-1444

Map Datum: NAD 83
 Projection: UTM (6 degree)
 Topographic Data Source: Land Information Ontario
 Mining Land Tenure Source: Provincial Mining Recorders' Office

This map may not show unregistered land tenure and interests in land including certain patents, leases, easements, right of ways, flooding rights, licences, or other forms of disposition of rights and interest from the Crown. Also certain land tenure and land uses that restrict or prohibit free entry to stake mining claims may not be illustrated.